Real time model predictive control of inverters and linear motor drive

Cao, Runzi

2009

Cao, R. (2009). Real time model predictive control of inverters and linear motor drive. Doctoral thesis, Nanyang Technological University, Singapore.

https://hdl.handle.net/10356/46937

https://doi.org/10.32657/10356/46937

REAL TIME MODEL PREDICTIVE CONTROL OF INVERTERS AND LINEAR MOTOR DRIVE

Cao Runzi

School of Electrical & Electronic Engineering

A thesis submitted to the Nanyang Technological University
in fulfillment of the requirement for the degree of
Doctor of Philosophy

2009

Statement of Originality

I hereby certify that the content of this thesis is the result of work done by me and has not been submitted for a higher degree to any other University or Institution.

Oct 15 2009
Date


Cao Runzi

Acknowledgment

I would like to express my gratefulness to my supervisor, Associate Professor Low Kay Soon for his guidance, patience, and support throughout the past few years. His enthusiasm for research and concern for my personal development has made working with him an enjoyable and very rewarding experience. My thanks also go to the students whom I have had the pleasure of working with in the Control Engineering laboratory, especially, Mr. Zhuang Hualiang and Mr. Deng Wu for their valuable discussions and encouragement.

I would also like to thank my co-supervisor Associate Professor Liu Ai Qun and his research group. I have never worked with such an intelligent and efficient group of individuals, each of whom was always willing to interrupt their work to help a fellow lab mate. I am grateful for the time and effort they devoted to me and my research.

I wish to acknowledge the scholarship provided by Nanyang Technological University. Last but not least, my thanks go to the laboratory technicians, Ms. Joanne Lim and Ms. Janet Tan for their assistance throughout the project.

Summary

This thesis addresses the control problems in linear motion system and parallel connected inverters system. Model Predictive Control (MPC) technique has been investigated to improve the control performance of inverters and linear motor drive. Based on the characteristics of the applications, suitable control structure and techniques are proposed and developed to solve specific problems.

In this research, a linear motion system with superior tracking ability is developed. Instead of using friction model based method, the repetitive control technique is incorporated into the conventional MPC structure to minimize the influence of friction force. In which, a finite impulse response (FIR) approximation of the system inverse is used to compensate the system phase delay. Wider learning range is achieved without introducing instability. Both simulation and experimental results have shown that the tracking performance is greatly improved by using this new MPC control approach. In this proposed control approach, the original structure of MPC is maintained. Thus, the complexity of implementation has not been greatly increased.

Besides the linear motion system, this thesis also studies the control method for parallel connected inverters system. Based on a multi-input multi-output (MIMO) inverter system model, a MPC controller is designed. By combining the objective of the voltage tracking and current sharing into one cost function, a MIMO control law is obtained. The stability and robustness of the parallel connected inverters system has been verified in simulation. The experimental results have shown that the proposed approach yields good performance under both static and dynamic loading conditions as well as hot-swap operations.

Table of Contents

ACKNOWLEDGMENT I

SUMMARY II

TABLE OF CONTENTS III

LIST OF FIGURES VI

LIST OF TABLES X

CHAPTER 1 1

INTRODUCTION 1

1.1 MOTIVATION 1

1.1.1 Linear Motor Drive Control 1

1.1.2 Parallel Connected Inverters Control 4

1.2 OBJECTIVE 7

1.3 MAJOR CONTRIBUTIONS OF THE THESIS 7

1.4 ORGANIZATION OF THE THESIS 9

CHAPTER 2 SYSTEM MODELING USING STATE SPACE PREDICTIVE CONTROL 11

2.1 INTRODUCTION 11

2.2 MODELING OF THE LINEAR MOTION SYSTEM 12

2.2.1 State Space Model of the Linear Motor Drive 13

2.2.2 Friction force 18

2.2.3 State Space Prediction Model 22

2.3 MODELING OF PARALLEL CONNECTED INVERTERS SYSTEM 25

2.3.1 Introduction 25

2.3.2 Topology of the parallel connected inverters system 25

2.3.3 State space prediction model 28

2.4 CONCLUSIONS 31

CHAPTER 3 MODEL PREDICTIVE CONTROL OF A LINEAR MOTION SYSTEM 32

3.1 INTRODUCTION 32

3.2 CONTROLLER DESIGN 34

3.2.1 Control Law Formulation 35

3.2.2 Observer Design 37

3.2.3 Overall control system and Parameter Tuning 41

3.3 STABILITY AND ROBUSTNESS ANALYSIS 43

3.4 FREQUENCY DOMAIN PROPERTIES ANALYSIS 44

3.5 POINT TO POINT TRACKING CONTROL 48

3.6 TRAJECTORY TRACKING PERFORMANCE 52

3.7 CONCLUSIONS 58

CHAPTER 4 REPETITIVE MODEL PREDICTIVE CONTROLLER 59

4.1 INTRODUCTION 59

4.2 REPETITIVE MODEL PREDICTIVE CONTROL 61

4.3 ROBUSTNESS STABILITY ANALYSIS 68

4.3.1 Stability Condition 69

4.3.2 Load Variation 71

4.3.3 Parameter Variation 72

4.4 RELATED RESEARCH WORKS 59

4.5 EXPERIMENTAL RESULTS 74

4.5.1 Dynamic Response 75

4.5.2 Effects of Filter Cutoff Frequencies on Tracking Performance .. 80

4.5.3 Comparison with P-type Repetitive controller 82

4.5.4 Tracking Performance under Different Loadings 83

4.5.5 Effects of Different Reference Trajectories on Tracking Performance 85

4.6 CONCLUSIONS 91

CHAPTER 5 MODEL PREDICTIVE CONTROL FOR PARALLEL CONNECTED INVERTERS SYSTEM 92

5.1 INTRODUCTION 92

5.2 CONTROL LAW FORMULATION 93

5.3 PERFORMANCE ANALYSIS 95

5.4 HOT SWAP DESIGN AND ITS ROBUSTNESS ANALYSIS 98

5.5 SIMULATION RESULT 102

5.6 EXPERIMENTAL RESULTS 110

5.7 CONCLUSIONS 117

CHAPTER 6 CONCLUSIONS AND RECOMMENDATIONS 118

6.1 CONCLUSIONS 118

6.2 RECOMMENDATIONS FOR FURTHER RESEARCH 120

PUBLICATIONS 121

REFERENCES 122

List of Figures

Fig. 2-1 The experimental linear motor drive system 12

Fig. 2-2 The *dq* reference frame PI current controller. 15

Fig. 2-3 The block diagram of the drive. 16

Fig. 2-4 Plot of (a) Coulomb friction and (b) Coulomb + Viscous friction versus velocity. 19

Fig. 2-5 Plot of static friction with Stribeck effect versus velocity. 20

Fig. 2-6 The experimentally captured friction-velocity map. 21

Fig. 2-7 Block diagram of parallel connected inverters 26

Fig. 3-1 Basic idea of model predictive control 33

Fig. 3-2 Schematics of the model predictive controller system 41

Fig. 3-3 Pole placement result of the MPC controller 43

Fig. 3-4 Nyquist plot of closed system with 300% load uncertainty (solid line-nominal system dash line-system with 300% load variation) 44

Fig. 3-5 Bode plot of the MPC controlled system (a) Without K_I (b) With K_I 46

Fig. 3-6 Step response with ideal condition (a) position response (b) control signal ... 49

Fig. 3-7 Simulation of step response with constraint 50

Fig. 3-8 Experimental Step Response 51

Fig. 3-9 Simulation of Step response with load variation 52

Fig. 3-10 Simulation result of trajectory tracking control response for a sinusoidal input (a) position response (b) tracking error 54

Fig. 3-11 experimental result of trajectory tracking response for a sinusoidal input (a) position response (b) tracking error 55

Fig.3-12 simulation result of trajectory tracking response for a triangle wave trajectory (a) position response (b) tracking error 56

Fig. 3-13 experimental result of trajectory tracking response for a triangle wave trajectory 57

Fig. 4-1 Block diagram of the proposed repetitive model predictive control system... 62

Fig. 4-2 Bode plot of system $F(z)$ without considering phase lead of $\mathbf{K}_1$ 66

Fig. 4-3 Impulse response of the feedback system 67

Fig. 4-4 Phase Cancellation result of the designed system 68

Fig. 4-5 Phase properties with 100% to 300% load variation..... 71

Fig. 4-6 The error contraction condition for designed repetitive control system with load variation..... 72

Fig. 4-7 The error contraction condition for designed repetitive control system with parameter L variation from 50% to 200% 73

Fig. 4-8 The error contraction condition for designed repetitive control system with parameter R variation from 50% to 200% 73

Fig. 4-9 The error contraction condition for designed repetitive control system with parameter K_e variation from 50% to 200%..... 74

Fig. 4-10 (a)Experimental result of tracking error of RMPC with sinusoidal trajectory (b)Zoom in View of tracking error at 1st, 2nd and 30th run.(c) Zoom in View of position reference and result at 1st, 2nd and 30th run. 76

Fig. 4-11(a) Control signal at 1st run and 30th run (b) Compensation signal at 30th run 77

Fig. 4-12 (a)Experimental result of tracking error of RMPC with Triangle Waveform (b) Zoom in View of tracking error at 1st, 2nd and 30th run. (c) Zoom in View of position reference and result at 1st, 2nd and 30th run. 79

Fig. 4-13 Experimental result of (a)Maximum tracking Error and (b) RMS tracking error..... 81

Fig. 4-14 Experimental result of P-type repetitive controller (a) Maximum tracking..83

Fig. 4-15 Experimental result with 100% to 300% load variation (a) maximum tracking error (b) rms tracking error 85

Fig. 4-16 Tracking performance under different reference frequencies 86

Fig. 4-17 Normalized converging rate comparison under different reference amplitudes 87

Fig. 4-18 Tracking performance of 100um amplitude sine wave (a) position tracking response (b) tracking error history (c) Control signal 89

Fig. 4-19 Tracking performance of 50um amplitude sine wave (a) position tracking response (b)tracking error history(c)control signal 90

Fig. 5-1 Closed-loop poles distribution (a) with α changes from 0.0001 to 1000. 96

Fig. 5-2 Bode plots of the system (a) with and without feed-forward gain (b) under load variation.....97

Fig. 5-3 Block diagram of the control system.....99

Fig. 5-4 Poles distribution when the inverter number changes. (a) One inverter removed from the nominal system (b) extra inverter added to the system.101

Fig. 5-5 (a)Two inverters in operation without current sharing control (b) Performance of the proposed multi-objective MPC controller(c) Performance of the proposed multi-objective MPC controller with 200% of the nominal load 104

Fig. 5-6 Simulation results of the system under(a) triac load (b) rectifier load.....105

Fig. 5-7 control diagram of the voltage droop method 106

Fig. 5-8 Two inverters in operation with virtual impedance method (a) nominal load condition (b) 200% load condition.....108

Fig. 5-9 Experimental results of the system under (a) 50 Ω load (b)triac load 111

Fig. 5-10 Harmonic distortion of the output voltage (a) 50 Ω load (b)triac load 112

Fig. 5-11 Experimental results of the system under R-L load 113

Fig. 5-12 Experimental results of the system under rectifier load 113

Fig. 5-13 Dynamic experimental response (a) load changes from null to full (b) load changes from full to null 114

Fig. 5-14 Experimental result of output voltage and current waveforms (a) Inverter 2 is isolated from the system (b) Inverter 2 is plugged into the system 116

List of Tables

Table 2-1 Linear motor's specifications 18

Table 2-2 Static friction parameters 22

Table 2-3 Parameters of electrical components 28

Table 5-1 Parameters of the parallel connected inverters systems 102

Table 5-2 Simulation result comparison with different operating conditions 109

Chapter 1

Introduction

1.1 Motivation

In this research, model predictive control technique is developed to solve problems in two research areas: one is the linear motor drive control; the other is the control of parallel connected inverters for uninterruptible power supply (UPS). In this section, the background of these two research topics will be introduced and the related research works on these two subjects will be described.

1.1.1 Linear Motor Drive Control

The linear motion systems, especially those that generate accurate coordinated multi-axis motion are of great importance in high precision machining applications [1-3]. For example, high speed machining [4, 5], semiconductor manufacturing [6], etc. As the world progresses and the competition becomes more intensive, the requirements on the system design have become more rigorous. To achieve high precision, it requires the effort in many areas such as advance control technique, metrology, calibration/error compensation, actuators/sensors design etc.

A linear motion system comes in various forms and types. The most common mechanism uses a rotary motor coupled to a long ballscrew. Such a design works well in the past due to less stringent requirements. As the requirements on velocity, length of travel, and

accuracy increase, direct drive motors are becoming more popular [7]. To realize a direct drive, many conventional motors such as the induction motor, the stepper motor and the permanent magnet synchronous motor (PMSM) have been redesigned for linear motion application [8-11]. The linear motor simplifies the mechanical structure, eliminating the contact-type nonlinearities caused by backlash, friction, and compliance. Without such constraints, high dynamic speed and acceleration become possible. Linear motors are frequently used in applications where accurate positioning and fast dynamics are needed [12]. The cost of this improvement is strong coupling between the machining process and servo control of the feed drive. Unlike rotational motors, permanent magnet linear motors are more sensitive to various disturbances because of the absent of gears [13]. Commercial machines usually use PID for feedback control, occasionally with additional velocity and acceleration feedforward compensation. The appeal of these types of control is that they can be tuned to obtain moderate control performance with little or no control knowledge. In recent years, more attention has been paid to the development of advanced control of the linear motor. In [12, 14], neural network based methods are proposed to suppress the mechanical vibration of a linear motor to achieve precision motion. Robust adaptive method is used to compensate disturbances to achieve better tracking [15]. Adapted inverse model [16] is used for adaptive position control of a linear motor.

In practice, the field engineers prefer a method that is robust against the variation of system parameters and ease of commissioning. Model predictive control (MPC) appears to be one of the suitable candidates. MPC can be considered as one of the most general way of posing control problem in the time domain [17]. As an advanced control technique, the MPC integrates the optimal control, the multivariable control and the robust control techniques together. Moreover, it can handle control constraints and

nonlinear plant. In a MPC scheme, the receding horizon strategy is used to make the closed-loop system more robust to modeling error and disturbances. Its excellent performance and reliability have been confirmed by various successful applications, such as arc welding and sheet/film process [18, 19], motion control [20, 21], single phase inverter [22], three-phase inverter [23], and surgical robot [24].

For ease of controller design, a motion control system is simplified as a linear mass-spring-damp system. The neglected nonlinear effect such as cogging force, Coulomb friction force can degrade the tracking performance significantly. Among these factors, the friction force gives the most significant influence on the system performance. In [25], a survey on friction characteristics and various friction compensation methods have been discussed. The most frequently used method is the model based friction compensation approach [26-28]. It is reasonable to use this method when an accurate parametric friction model is available. In practice, the modeling of nonlinear friction is not straightforward. The procedure of determining the friction parameters usually requires time-consuming tests. Moreover, the coefficients of a friction model might change with time, temperature and loading condition. This makes the modeling process more complicated. For this reason, several design methods without parametric model have been proposed [29-31]. However, the design procedure will be time-consuming. Thus, a fast and effective method that makes the drive to track accurately regardless of environment changes is desired.

In many industrial applications, the tasks are typically repetitive. Repetitive control (RC) has been proven to be an effective approach in motion control applications to eliminate deterministic errors, regardless of whether they are due to periodic disturbances, or

modelling error [32]. A repetitive controller can achieve perfect tracking or disturbance rejection for systems subject to any periodic reference or disturbance with a known period. Applications of RC range from robots performing periodic tasks [33-36], to vibration isolation [37-39], control of rotating machinery [40, 41], computer disk drives [42-44], and nonlinear load compensation of inverter control in power electronics [45-47]. In this thesis, a novel approach is proposed to incorporate RC into the conventional MPC formulation to improve the dynamic performance for repetitive tasks.

1.1.2 Parallel Connected Inverters Control

As modern society continues to increase its reliance on electrical and electronic equipment, there is a growing demand for a clean and reliable AC power to keep these devices operating regardless of weather, location or other conditions adverse to nominal utility power supply. Uninterruptible power supply (UPS) is the most commonly used equipment to provide reliable and well regulated AC voltages for critical loads such as computer server, air traffic control system, medical and communication equipments etc, where an unexpected power disruption could cause injuries, fatalities, serious business disruption, or data loss [48].

In many installations, it is found that higher capacity UPS is needed to replace the existing UPS as the system load grows over time. Such a situation could be solved by using a large UPS unit or using a modularized small capacity UPS that are available with parallel operation capability [49-56]. The former approach may be undesirable because of higher initial cost, installation difficulties, and reliability. In contrast, parallel operation can easily expand the system power capability by adding more modules. Parallel

connected UPS also has the advantage in terms of cost and maintenance as compared to the single higher power UPS. Moreover, it has effectively no single point of failure in the system thereby offering significantly higher level of availability.

As one of the major component of UPS, the parallel operation of inverters has attracted a lot of research effort in recent years. One of the technical challenges involved in paralleling UPS units is to ensure that the load is shared equally among the inverters. To achieve this objective, suitable control technique must be developed. Due to the component tolerances and the non-uniformity of the units, circulating current between modules might appear in the system. Under unbalanced operating condition, the circulating current might deteriorate the power quality, or even destroying the components. Thus, there are two key control objectives for the parallel connected inverters system. One is tracking the voltage reference; the other is sharing the current equally among the inverters. In this thesis, a new control approach for parallel operation of inverters will be investigated.

To connect inverters in parallel, the simplest method is to employ a coupled inductor at the output end of the inverter [57]. The coupled inductor can reasonably balance the output currents among the inverters. However, the low working frequency would lead to a bulky inductor and greatly increases the weight and cost of the system. If harmonics exist in the system, the output voltage will be strongly distorted by the inductors. In addition, it is inconvenient to add more inverters to the system. To achieve the desired performance and attain good robustness with respect to load disturbances or parameter variations, an advanced control scheme that could be realized in real time is desired to perform tight closed loop control. Various control techniques have been reported in

literature to control single phase parallel connected inverters. The most frequently used method is the frequency and voltage droop method [58-61]. The advantage of this method is its simplicity. Because no extra interconnections among the inverters are required, high modularity and good reliability can easily be achieved. However, this method achieves power sharing by making a compromise between voltage regulation and transient response. In addition, the harmonic currents cannot be shared properly. To have good performance on both the control objectives, instantaneous current sharing control schemes have been proposed to overcome the weakness of the droop method. For examples, the master slave current sharing method [62, 63], circular-chain current sharing method [64], average current sharing method [53, 65]. Since the output currents are regulated at every switching interval, instantaneous current sharing method promises good performances in both voltage tracking and current sharing. However, additional interconnections among inverters are usually needed and the complexity compromises its dealing with failure. Different from most methods that designed the controller based on transfer function approach, a state space model based MPC controller is proposed and developed in this thesis to systematically control the current and voltage. By optimizing the objectives of voltage tracking and current sharing at the same time, a control law suitable for parallel operation can be formulated. In [66], the use of the model predictive control (MPC) scheme to control an inverter has been reported. In this thesis, we will further develop the approach to control multiple inverters connected in parallel for an UPS.

1.2 Objective

The objectives of this research have two goals: One is to develop a motion control system that can achieve high tracking precision. For the investigated linear motion system, the focus is on minimizing the influence of friction force. The other is the development of a reliable and robust parallel connected inverters system. The focus is the realization of a control structure that is suitable for hot-swap operation and achieves superior performance under various loading conditions. In these two applications, the problems are addressed by utilizing the model predictive control technique. The development of control oriented predictive models of the system and suitable control algorithms is required to achieve these objectives.

1.3 Major Contributions of the Thesis

This thesis presents new approaches for performance improvement of linear motors drive and inverters. In these two applications, state space based model predictive control technique has been investigated and developed to achieve better performance. The contributions of this research are summarized as follows:

- A linear motor drive is designed with model predictive control technique to achieve precise motion control. The characteristics of the system are analyzed in frequency domain. The MPC provides a unified procedure to design the motion control system, which offers good performances against disturbances and uncertainty. Experimental study has validated its good performance.

- A repetitive model predictive control (RMPC) scheme is proposed to achieve better performance in periodic tracking tasks. For the proposed approach, the phase compensated tracking error history is used to achieve wider learning frequency range. Extensive simulation and experimental studies on trajectory tracking performance have been conducted. From the results, it is observed that good performance is obtained in minimizing the influence of phase delay and friction force. Furthermore, the long term learning stability and robustness against parameter variations have also been verified in the experiment.

- Based on the characteristics of the parallel connected inverters, the control problem is formulated as a multi-input multi-output (MIMO) state space system. Model predictive control law is formulated with two control objectives namely the voltage tracking and current sharing. They are optimized at the same time for the multi-inverter system. Frequency domain analysis of the system verifies that the proposed approach is robust. Various loading conditions, modularity, and hot-swap ability of the system have been investigated in both the simulation and experimental studies. The results show that the proposed control scheme achieves good performance on both voltage reference tracking and current sharing. The experimental results show that the designed system performs well under various loading conditions and permits hot-swap operation.

1.4 Organization of the thesis

The thesis is organized as follows:

Chapter 2 introduces the linear motion system and parallel connected inverters system used in this thesis. Their state space models are first developed. Suitable prediction models are then derived for these two systems that will be used in the subsequent chapters.

Chapter 3 mainly deals with the model predictive controller design and analysis for the linear motor drive. Based on the prediction model constructed in Chapter 2, a linear motion control system using the MPC is designed. The system is then analyzed using the frequency domain approach. Finally, the system tracking performance is evaluated in both simulation and experimental studies.

Chapter 4 proposed a repetitive model predictive controller, which augments the MPC controlled system with repetitive tracking ability. A phase cancellation based method is incorporated into the MPC controller. By repetitively updating the new tracking trajectory, a learning controller is achieved. The proposed control algorithm effectively minimizes the influence of friction force. Good tracking performance has been achieved as observed in the experimental study.

Chapter 5 proposes the MPC approach for controlling a parallel connected inverters system. The control system achieves the objective of voltage tracking and current sharing

in one control law. The performance under various loading conditions and the hot-swap ability are examined in both simulation and experiment.

Chapter 6 summarises the research and recommends future works.

Chapter 2

System Modeling Using State Space Predictive Control

2.1 Introduction

In this thesis, we seek to improve the system performance of a linear motor drive and parallel connected inverters system with model predictive control technique. Achievement of these goals implicitly requires the development of control oriented models of the systems. As introduced in Chapter 1, there are some critical issues in these two applications need to be resolved, In particular, the fiction effect in the motion control and circulating current in the parallel connected inverters system. In this chapter, the basics of the linear motion system and parallel connected inverters system will be introduced. Based on the system dynamics, state space models for both systems are formulated. By repeated use of the state space model, the prediction model is then formulated. It is presented in the form of the predictions of the system output at future time instants in a finite horizon. The system model will be used in subsequent chapters for the design of controllers.

2.2 Modeling of the Linear Motion System

Fig. 2-1 shows the experimental setup of the 3-phase PMSM linear motor used in this thesis. The linear motor is a thrust tube type motor [67] based on the PMSM (permanent magnet synchronous motor) concept. It is driven by a standard three phase inverter circuit consists of six insulated gate bipolar transistors (IGBT). The IGBT is controlled by a driver circuit via opto-coupler with a 25 kHz PWM switching signal generated from a DSP based controller. To facilitate position measurement and provide accurate commutation logic, a position encoder [68] with a resolution of 0.1um has been used. In the experimental system, the DSPACE 1104 controller board [69] with a sampling period of 1ms has been used. This controller board consists of a main processing unit MPC8240 using a PowerPC 603e microprocessor and a slave DSP subsystem using TMS320F240DSP.

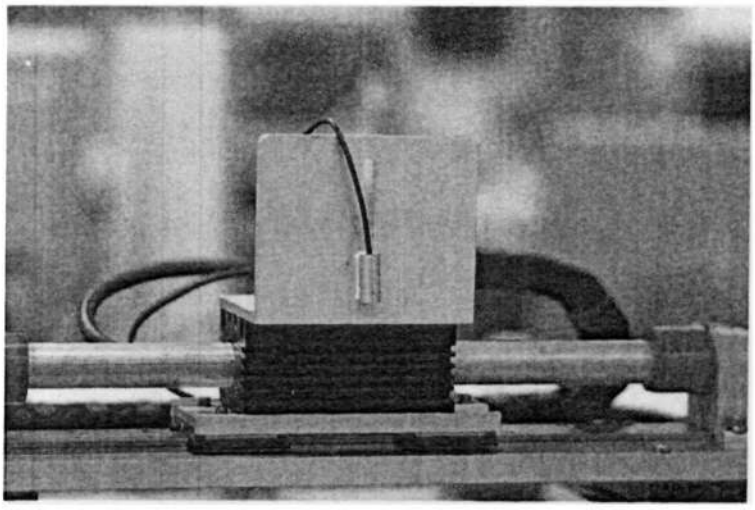

Fig. 2-1 The experimental linear motor drive system

2.2.1 State Space Model of the Linear Motor Drive

The dynamics of a PMSM linear motor is similar to a rotary motor, where the mechanical and electrical relationship can be mapped directly. Consequently, vector control method [70-75] that is used to drive the rotary AC motor can be similarly applied to linear motor. The vector control based upon the field orientation principle uses the analogy between the AC (induction or synchronous) motor and DC motor. After park transformation, the dynamic model of a synchronous machine can be expressed in a rotating reference frame that moves at synchronous speed ω. The time varying parameters are eliminated and all variables are expressed in orthogonal of mutually decoupled d and q axes. The active and reactive currents are decoupled, which in turn determine the thrust and magnetic flux respectively.

Let M, D, p, k_e, R, L_q and L_d be the mass, viscous friction coefficient, number of pole-pairs, back EMF constant, winding resistance, inductance in the quadrature and direct axis respectively. Moreover, let F_r be the frictional force acting on the system. Then the linear motor can be modelled as [28]

$$\dot{\mathbf{x}}(t) = \mathbf{h}\left(\mathbf{x}(t)\right) + \mathbf{g}\left(\mathbf{x}(t)\right)\boldsymbol{\Gamma}(t) \tag{2.1}$$

where the state variables of the system is $\boldsymbol{x} = [d \quad v \quad i_q \quad i_d]^{\mathrm{T}}$ representing the linear position, linear speed, quadrature and direct current respectively. Moreover, the functions $\mathbf{h}(\mathbf{x})$, $\mathbf{g}(\mathbf{x})$ and $\Gamma(t)$ in (2.1) are defined as

$$\mathbf{h}(\mathbf{x}) = \begin{bmatrix} v \\ \left(\frac{3pk_e}{2M}\right) i_q + \left(\frac{3p\left[L_d - L_q\right]}{2M}\right) i_q i_d - \frac{F_r}{M} - \frac{D}{M} v \\ -\frac{pk_e}{L_q} v - \frac{R}{L_q} i_q - \frac{pL_d}{L_q} v i_d \\ -\frac{R}{L_d} i_d + \frac{pL_q}{L_d} v i_q \end{bmatrix} \tag{2.2}$$

$$\mathbf{g}(\mathbf{x}) = \begin{bmatrix} 0 & 0 \\ 0 & 0 \\ \frac{1}{L_q} & 0 \\ 0 & \frac{1}{L_d} \end{bmatrix} \quad \text{and} \quad \mathbf{\Gamma}(t) = \begin{bmatrix} v_q \\ v_d \end{bmatrix} \tag{2.3}$$

The force produced by the linear motor is a function of the q-axis current and d-axis current. Moreover, the force is also affected by the q-axis inductance, d-axis inductance, the number of pole-pairs and back EMF constant. It is expressed as

$$F = \frac{3}{2} p\left(K_e i_q + \left(L_d - L_q\right) i_d i_q\right) \tag{2.4}$$

Since the d and q-axes inductances are almost the same for the motor under consideration, the reluctance force will be neglected. This will simplify the design of the current control loop. Moreover, the d-axis current i_d is regulated to be near zero in the control system design. Consequently, the desired force in (2.4) is dependent on i_q as follows:

$$F = K_f i_q \tag{2.5}$$

where K_f is known as the force constant of the linear motor.

With the d-axis current properly regulated, the force is controlled to be proportional to the q-axis current. The block diagram of the current control loops that are used to provide the necessary force is shown in Fig. 2-2. As shown in the figure, two PI controllers in the

d and q reference frames are used. The bandwidth of the current loop is set to at least 10 times the bandwidth of the position loop to ensure the dynamics of the current loop has negligible effect on the performance in the outer loop.

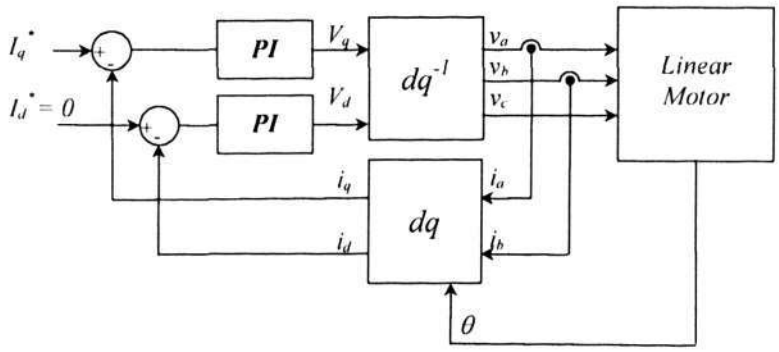

Fig. 2-2 The dq reference frame PI current controller.

In Fig. 2-2, the dq and dq^{-1} blocks represent the dq and inverse dq transformation. Let S represents the current or voltage quantity to be transformed, then the dq transformation matrix is

$$\begin{bmatrix} S_d \\ S_q \\ S_0 \end{bmatrix} = \sqrt{\frac{2}{3}} \begin{bmatrix} \cos\theta & \cos\left(\theta - \frac{2}{3}\pi\right) & \cos\left(\theta + \frac{2}{3}\pi\right) \\ \sin\theta & \sin\left(\theta - \frac{2}{3}\pi\right) & \sin\left(\theta + \frac{2}{3}\pi\right) \\ \frac{1}{\sqrt{2}} & \frac{1}{\sqrt{2}} & \frac{1}{\sqrt{2}} \end{bmatrix} \begin{bmatrix} S_a \\ S_b \\ S_c \end{bmatrix} \tag{2.6}$$

where the subscripts a, b, c are the notation of the phases and d, q, o are the direct, quadrature and zero sequence respectively.

The corresponding inverse matrix is

$$\begin{bmatrix} S_a \\ S_b \\ S_c \end{bmatrix} = \sqrt{\frac{2}{3}} \begin{bmatrix} \cos\theta & \sin\theta & \frac{1}{\sqrt{2}} \\ \cos\left(\theta - \frac{2}{3}\pi\right) & \sin\left(\theta - \frac{2}{3}\pi\right) & \frac{1}{\sqrt{2}} \\ \cos\left(\theta + \frac{2}{3}\pi\right) & \sin\left(\theta + \frac{2}{3}\pi\right) & \frac{1}{\sqrt{2}} \end{bmatrix} \begin{bmatrix} S_d \\ S_q \\ S_0 \end{bmatrix} \tag{2.7}$$

For the current control loop, the DSP samples the phase currents i_a and i_b by means of current sensors. The phase currents will be transformed into i_d and i_q using (2.6). The sampling time is typically set at 200μsec. In each interrupt, the digital PI controllers implemented in the DSP first compute the errors between i_q^* and i_q, i_d^* and i_d. Subsequently, the two voltage outputs V_d and V_q are determined with PI controllers. The two voltages are then transformed into the phase voltages V_a, V_b and V_c using (2.7) and finally converted to the respective three-phase PWM outputs. The computational time is approximately 45 μsec. The PI gains are tuned using the Nichols-Zeigler step response tuning method [76].

Consider that the d-axis current is properly regulated, then the force is controlled to be proportional to the q-axis current. Thus, we can further simplify the model of the drive for position/speed loop design by neglecting the d-axis current control loop. Fig. 2-3 shows the block diagram of the simplified current control system represented in the Laplace transform domain.

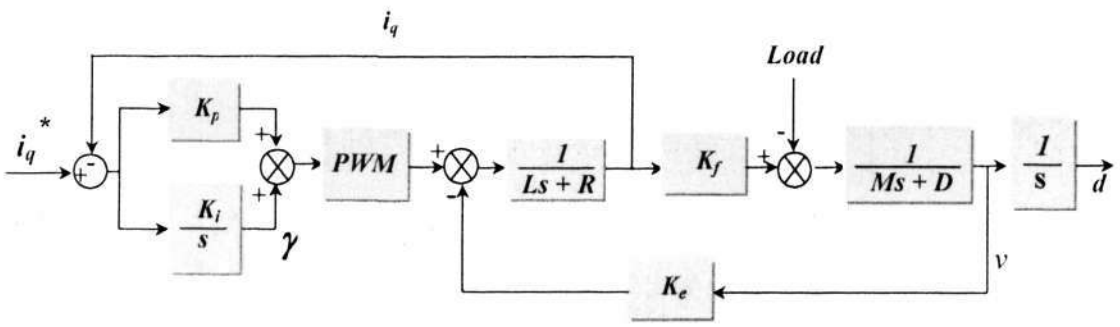

Fig. 2-3 The block diagram of the drive.

To derive the model of the drive, we define the state variables and the output of the system as

$$\mathbf{Z} = \begin{bmatrix} d & v & i_q & \gamma \end{bmatrix}^T \tag{2.8}$$

where d, v, i_q and γ are the measured position, speed, q-axis current and integral voltage respectively. Then the motor dynamics can be described using the following state space equation based on the block diagram in Fig. 2-3 as

$$\dot{\mathbf{Z}} = \mathbf{A}\mathbf{Z} + \mathbf{B}i_q + \mathbf{E}F_L \tag{2.9}$$

$$Y = \bar{\mathbf{C}}\mathbf{Z} \tag{2.10}$$

where

$$\mathbf{A} = \begin{bmatrix} 0 & 1 & 0 & 0 \\ 0 & -\dfrac{D}{M} & \dfrac{K_f}{M} & 0 \\ 0 & \dfrac{-K_e}{L} & -\dfrac{R+K_p}{L} & \dfrac{1}{L} \\ 0 & 0 & -K_i & 0 \end{bmatrix}$$

$$\mathbf{B} = \begin{bmatrix} 0 & 0 & \dfrac{K_p}{L} & K_i \end{bmatrix}^T$$

$$\bar{\mathbf{C}} = \begin{bmatrix} 1 & 0 & 0 & 0 \end{bmatrix}$$

$$\mathbf{E} = \begin{bmatrix} 0 & -\dfrac{1}{M} & 0 & 0 \end{bmatrix}^T$$

In (2.9), F_L is the unknown disturbance. It includes the nonlinear frictional force and the load.

In the model (2.9)-(2.10), most of the parameters are either available in the datasheet or can be experimentally measured.

Table 2-1 lists the parameters of the linear motor used in this research.

Nominal Specifications	Symbols	Values	Units
Electrical Resistance	R	3	Ω (line-to-line)
Back EMF constant	K_e	18	$V_{pk}/msec^{-1}$ (line-to-line)
Force Constant	K_f	22	N/A_{rms}
Mass	M	5.8	Kg
Viscous constant	D	20	$N/msec^{-1}$
Pole pair	P	1	
Inductance	L	1.95	mH

Table 2-1 Linear motor's specifications

2.2.2 Friction force

In section 2.2.1, the friction force is often modeled as a linear function varying with speed. In reality, friction force has highly nonlinear dynamics. To better understand the control problem in our investigated system, the dynamics associated with friction force will be briefly introduced in this section.

The physics behind the friction phenomenon and the compensation techniques of dealing with it has been extensively discussed in the literature [25, 77-86]. Fig. 2-4(a) shows the classical Coulomb friction model and Fig. 2-4 (b) shows the coulomb plus viscous friction model.

Fig. 2-4 Plot of (a) Coulomb friction and (b) Coulomb + Viscous friction versus velocity

As shown in Fig. 2-4(a), a constant friction force α is opposing the motion when the object velocity is not zero. As long as the driving force is smaller than the static friction force, the static friction will vary with respect to the driving force to keep the object stationary and the velocity will remain zero. Let F_r be the friction force, then the Coulomb friction model can be described by the following equation

$$F_r(v) = \alpha \operatorname{sgn}(v) \tag{2.11}$$

where $\operatorname{sgn}(v) = \begin{cases} 1 & v \geq 0 \\ -1 & v < 0 \end{cases}$

Because of its simplicity, the model (2.11) has been used for friction compensation in many applications [81-86]. As the velocity gradients increase, a force caused by viscosity of lubricants will grow in proportional. This force is called viscous friction, which is often combined with the Coulomb friction as show in Fig. 2-4(b). The combined model is represented as

$$F_r(v) = \alpha \operatorname{sgn}(v) + \alpha_2 v \tag{2.12}$$

where α_2 is the viscous constant.

In this research, high quality linear guides that have insignificant asymmetries are used in the system. For this setup, the parameters α and α_2 in (2.12) can be assumed to be constant for both positive and negative velocities.

One important phenomenon that is neglected in model (2.12) is the Stribeck effect [87, 88]. When the system breaks away from stationary, the friction force will decrease exponentially until it reaches about 60% of the breakaway force. Subsequently, it increases linearly with the velocity. This downward bends occurs at velocities closed to zero. The friction force as a function of velocity for constant velocity motion is called the Stribeck curve. This is illustrated in Fig. 2-5.

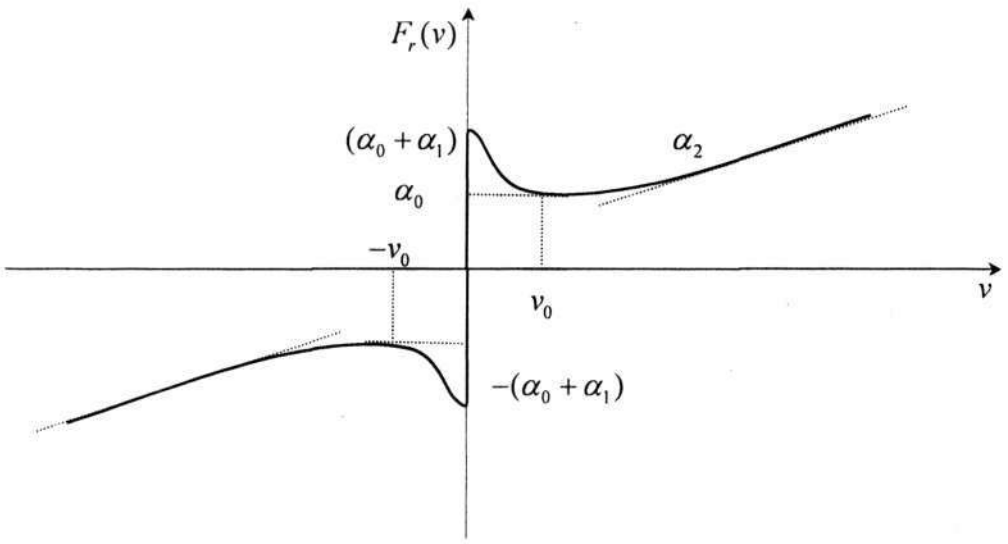

Fig. 2-5 Plot of static friction with Stribeck effect versus velocity.

In the figure, the parameters α_0 is the coulomb friction and $(\alpha_0+\alpha_1)$ is the breakaway force. v_0 is called the Stribeck velocity. Thus, the static friction is characterized by four parameters $\alpha_0, \alpha_1, \alpha_2$ and v_0. The mathematical expression for the static friction model with Stribeck effect can be defined [87] as

$$F_r(v) = \left(\alpha_0 + \alpha_1 e^{-(v/v_0)2}\right)\mathrm{sgn}(v) + \alpha_2 v \tag{2.13}$$

For this research, various experiments have been conducted to construct the friction-velocity map as in the Fig. 2-5 to determine (2.13). For the experiments, a PI velocity controller has been implemented on the prototype system. The reference velocity is set in the range from 0.0 to ±0.2 m/sec. For each velocity, the experiment is repeated for 10 times. The input control signal and control output are then averaged to reduce the noise. Using curve-fitting method [89], the approximated friction model is obtained. Fig. 2-6 shows the experimentally captured friction-velocity map.

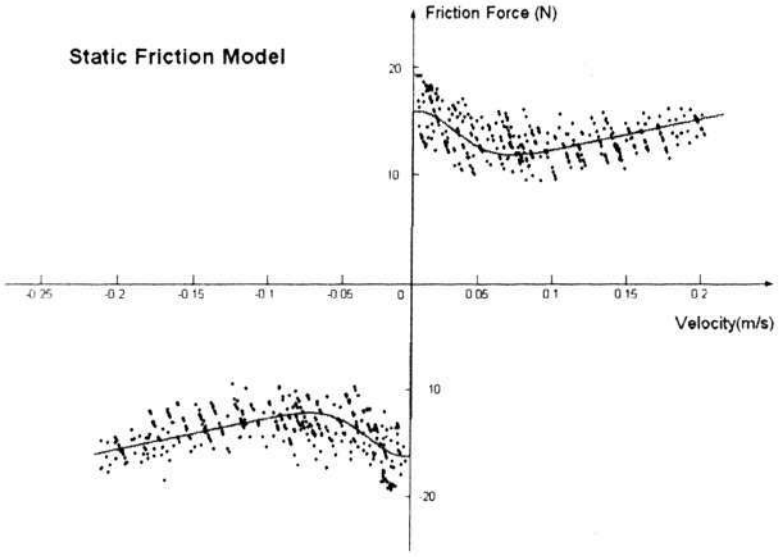

Fig. 2-6 The experimentally captured friction-velocity map.

From Fig. 2-6, the Stribeck effect can be clearly observed. Furthermore, the Coulomb and viscous fiction can be estimated respectively. The breakaway force is approximately 16 N. Thus, the parameters of the basic static friction model can be determined. They are listed in Table 2-2.

	Estimated values
α_0	12 N
α_1	4 N
α_2	20 N msec^{-1}
v_0	0.06 msec^{-1}

Table 2-2 Static friction parameters

It should be noted that this friction model is an approximation of the real nonlinear friction forces. There are other nonlinear effects that are position dependent or operating condition dependent such as cogging force[90] , end effect [91] of the linear motor have not been modeled. These will have influences on the designed motion control system.

2.2.3 State Space Prediction Model

To design a MPC controller, a state space prediction model is needed. In this section, we will derive the prediction model with the state space model obtained in section 2.2.1. As described in (2.9), the system is subject to external disturbances. Thus, the prediction of future movement will deteriorate if the disturbance is not modeled adequately.

To achieve bias free prediction, the incremental model is developed in the following such that an integrator can be added into the control loop. Furthermore, we assume that the input disturbance in (2.9) is varying slowly with respect to the sampling time T. The discrete time equivalent of the state space model of the motor can be expressed as:

$$\Delta \mathbf{Z}(kT+T) = \bar{\mathbf{G}}\Delta \mathbf{Z}(kT) + \bar{\mathbf{H}}\Delta i_q(kT) \tag{2.14}$$

$$\Delta Y(kT) = \bar{\mathbf{C}}\Delta \mathbf{Z}(kT) \tag{2.15}$$

where $\bar{\mathbf{G}} = e^{\mathbf{A}T}$, $\bar{\mathbf{H}} = (\int_0^T e^{\mathbf{A}\lambda} d\lambda)\mathbf{B}$

In (2.14), k is the discrete time index and Δ is the difference operator such that

$$\Delta \mathbf{Z}(kT) = \mathbf{Z}(kT) - \mathbf{Z}(kT-T) \tag{2.16}$$

$$\Delta i(kT) = i_q(kT) - i_q(kT-T) \tag{2.17}$$

$$\Delta Y(kT) = Y(kT) - Y(kT-T) \tag{2.18}$$

Combine (2.10), (2.14) and (2.15), we have a new state variable

$$\mathbf{X}(kT) = \begin{bmatrix} \Delta \mathbf{Z}(kT) \\ Y(kT-T) \end{bmatrix} \tag{2.19}$$

Using (2.9) and (2.14), the system can be augmented as

$$\begin{bmatrix} \Delta \mathbf{Z}(kT+T) \\ Y(kT) \end{bmatrix} = \begin{bmatrix} \bar{\mathbf{G}} & \mathbf{0} \\ \bar{\mathbf{C}} & 1 \end{bmatrix} \begin{bmatrix} \Delta \mathbf{Z}(kT) \\ Y(kT-T) \end{bmatrix} + \begin{bmatrix} \bar{\mathbf{H}} \\ 0 \end{bmatrix} \Delta i_q(kT) \tag{2.20}$$

Substitute (2.19) into (2.20), we have

$$\mathbf{X}(kT+T) = \mathbf{G}\mathbf{X}(kT) + \mathbf{H}\Delta i_q(kT) \tag{2.21}$$

$$Y(kT) = \mathbf{C}\mathbf{X}(kT) \tag{2.22}$$

where

$$\mathbf{G} = \begin{bmatrix} \bar{\mathbf{G}} & \mathbf{0} \\ \bar{\mathbf{C}} & 1 \end{bmatrix}, \quad \mathbf{H} = \begin{bmatrix} \bar{\mathbf{H}} \\ 0 \end{bmatrix}, \quad \mathbf{C} = \begin{bmatrix} 1 & 0 & 0 & 0 & 1 \end{bmatrix}$$

Using (2.21)-(2.22) and by repeated substitution, the predictive model of the system that is represented in the form of the predictions of the system output at future time instants in a finite horizon can be formulated as follows.

$$\begin{cases} \mathbf{X}(kT+T) = \mathbf{G}\mathbf{X}(kT) + \mathbf{H}\Delta i_q(kT) \\ \mathbf{X}(kT+2T) = \mathbf{G}^2\mathbf{X}(kT) + \mathbf{G}\mathbf{H}\Delta i_q(kT) \\ \vdots \quad \vdots \quad \vdots \quad \vdots \quad \vdots \\ \mathbf{X}(kT+nT) = \mathbf{G}^n\mathbf{X}(kT) + \mathbf{G}^{n-1}\mathbf{H}\Delta i_q(kT) + \cdots + \mathbf{H}\Delta i_q(kT+nT-T) \end{cases} \tag{2.23}$$

$$\begin{cases} \mathbf{Y}(kT+T) = \mathbf{C}\left[\mathbf{G}\mathbf{X}(kT) + \mathbf{H}\Delta i_q(kT)\right] \\ \mathbf{Y}(kT+2T) = \mathbf{C}\left[\mathbf{G}^2\mathbf{X}(kT) + \mathbf{G}\mathbf{H}\Delta i_q(kT) + \mathbf{H}\Delta i_q(kT+T)\right] \\ \vdots \quad \vdots \quad \vdots \quad \vdots \quad \vdots \\ \mathbf{Y}(kT+nT) = \mathbf{C}\left[\mathbf{G}^n\mathbf{X}(kT) + \mathbf{G}^{n-1}\mathbf{H}\Delta i_q(kT) + \mathbf{G}^{n-2}\mathbf{H}\Delta i_q(kT+T) + \cdots \right. \\ \qquad \left. + \mathbf{H}\Delta i_q(kT+(n-1)T)\right] \end{cases} \tag{2.24}$$

Define $\mathbf{Y}_p$ as the predicted motor position vector over the prediction horizon as

$$\mathbf{Y}_p(kT) = \begin{bmatrix} \mathbf{Y}(kT+T) \\ \mathbf{Y}(kT+2T) \\ \vdots \\ \mathbf{Y}(kT+N_yT) \end{bmatrix} \tag{2.25}$$

Moreover, we define an incremental input control signal vector as

$$\Delta\mathbf{I}_p(kT) = \begin{bmatrix} \Delta i_q(kT) \\ \Delta i_q(kT+T) \\ \vdots \\ \Delta i_q(kT+N_yT-T) \end{bmatrix} \tag{2.26}$$

then from (2.23) and (2.24), the future prediction up to a horizon N_y can be formulated as follows:

$$\mathbf{Y}_p(kT) = \mathbf{\Phi}\mathbf{X}(kT) + \mathbf{R}\Delta\mathbf{I}_p(kT) \tag{2.27}$$

where

$$\mathbf{\Phi} = \begin{bmatrix} \mathbf{C}\mathbf{G} \\ \mathbf{C}\mathbf{G}^2 \\ \vdots \\ \mathbf{C}\mathbf{G}^{N_y} \end{bmatrix} \qquad \mathbf{R} = \begin{bmatrix} \mathbf{C}\mathbf{H} & \mathbf{0} & \cdots & \mathbf{0} \\ \mathbf{C}\mathbf{G}\mathbf{H} & \mathbf{C}\mathbf{H} & \vdots & \vdots \\ \vdots & \ddots & \ddots & \mathbf{0} \\ \mathbf{C}\mathbf{G}^{N_y-1}\mathbf{H} & \cdots & \mathbf{C}\mathbf{G}\mathbf{H} & \mathbf{C}\mathbf{H} \end{bmatrix}$$

According to (2.27), the motor position sequence in the future instants is decided by the future control sequence once the system model and present state vector are available.

Therefore, it is possible to find an appropriate control sequence to minimize the tracking error of the future position over the prediction horizon. If the sampling time is constant, the predictive horizon N_y will decide the length of the prediction range in the future. A larger N_y will result in a longer predictive range. The design and optimization of a control law for the linear motion system will be presented in details in Chapter 3.

2.3 Modeling of Parallel Connected Inverters System

2.3.1 Introduction

With the advances in power electronic devices and processors, high-capacity PWM inverters that can deliver upto 100 kVA and beyond are now available [92-94]. As with the improvement in electronics technology, better performance is continually being sought. The demand for compact, reliable and efficient UPS with high dynamic performance has increased steadily. To satisfy this demand, several issues such as the parallel-ability of inverters, the circulating current between modules, hot-swap ability of the system etc. need to be investigated. It is desirable to use a parallel architecture with standardized modules [95, 96] to reduce the cost and improve the system performance. This has greatly brought up the research interest in parallel operation of inverter system.

2.3.2 Topology of the parallel connected inverters system

The topology of the parallel connected inverters system is shown in Fig. 2-7. This power conversion system consists of a DSP based digital controller and several standalone inverters that have DC source, bridge inverter and LC filter. For simplicity, the fault

detection, synchronization and switching over modules of the UPS are not shown. The bridge inverter converts the DC input voltage into PWM voltage according to the modulation signal. After the LC filter, the high frequency components in the PWM voltage are removed and the DC voltage is converted to the desired AC voltage. The switching sequences of the inverters are determined by the digital signal processor, such that the resultant output voltage tracks the reference waveform.

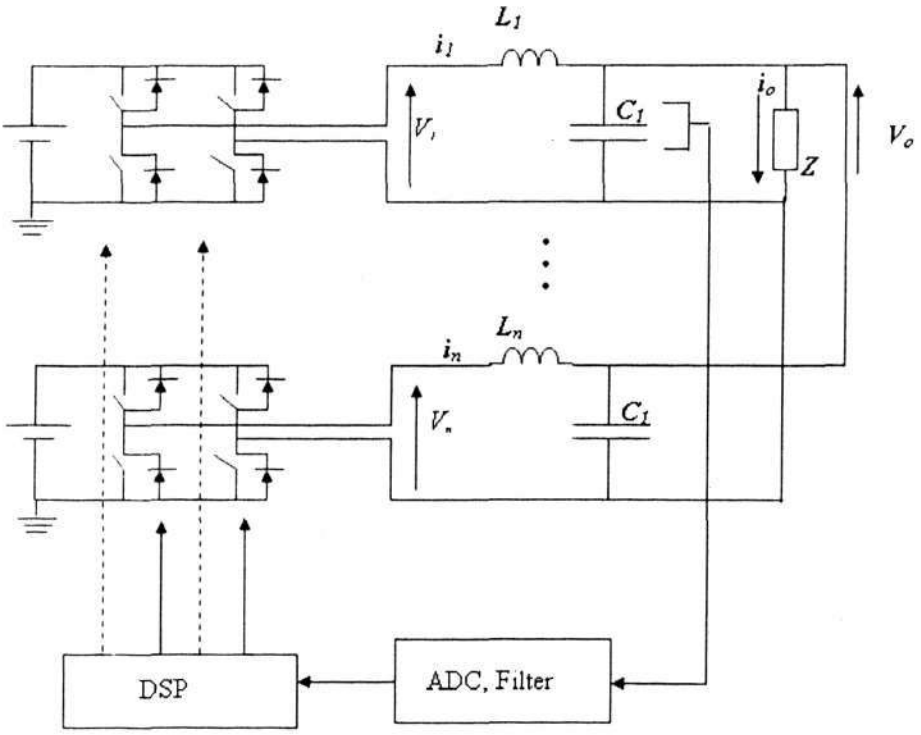

Fig. 2-7 Block diagram of parallel connected inverters

Consider the general case that there are n inverters connected in parallel with the simplified model as shown in Fig. 2-7. Define r as the equivalent series resistor (ESR) of the inductor and neglect the ESR of the capacitor, as it is very small. Based on the Kirchhoff's voltage law, we obtain the following equations are obtained:

$$\begin{aligned} V_1 &= L_1 \frac{di_1}{dt} + r_1 i_1 + V_0 \\ V_2 &= L_2 \frac{di_2}{dt} + r_2 i_2 + V_0 \\ &\vdots \\ V_n &= L_n \frac{di_n}{dt} + r_n i_n + V_0 \end{aligned} \tag{2.28}$$

where $V_1, V_2, ..., V_n$ are the output voltages of the inverters, $i_1, i_2, ..., i_n$ are the currents flowing through the inductors, and V_0 is the output voltage of the parallel connected inverters.

Define $i_{c1}, i_{c2}, ..., i_{cn}$ as the currents flowing into the capacitors, then

$$\begin{aligned} i_{c1} &= C_1 \frac{dV_0}{dt} \\ i_{c2} &= C_2 \frac{dV_0}{dt} \\ &\vdots \\ i_{cn} &= C_n \frac{dV_0}{dt} \end{aligned} \tag{2.29}$$

Define i_0 as the output current, From the Kirchhoff's current law

$$i_1 + i_2 + \cdots + i_n = i_0 + i_{c1} + i_{c2} + \cdots + i_{cn} \tag{2.30}$$

Substituting (2.29) into (2.30),

$$\frac{dV_0}{dt} = \frac{1}{\sum_{j=1}^{n} C_j} \left(\left(\sum_{k=1}^{n} i_k \right) - i_0 \right) \tag{2.31}$$

From (2.28), we have the following equations

$$\begin{aligned} \frac{di_1}{dt} &= -\frac{1}{L_1}(r_1 i_1 + V_0 - V_1) \\ \frac{di_2}{dt} &= -\frac{1}{L_2}(r_2 i_2 + V_0 - V_2) \\ &\vdots \\ \frac{di_n}{dt} &= -\frac{1}{L_n}(r_n i_n + V_0 - V_n) \end{aligned} \tag{2.32}$$

Based on Ohm's law, we have

$$V_o = R \cdot i_o \tag{2.33}$$

As the parameters of the parallel connected inverters system are standard electronic components that can be obtained from experiment easily, a relative accurate system model is available as nominal system for control system design. In this thesis, the parameters given in Table 2-3 are used for the system modeling.

Input Inductor L_n	1 mH
Equivalent series resistor r_n	1.7 Ω
Output Capacitor C_n	4.7μH
Nominal Load R	50 Ω

Table 2-3 Parameters of electrical components

2.3.3 State space prediction model

Define the state variables as the output voltage V_0 and the currents from the inverters $i_1, i_2, \cdots, i_n$ i.e.,

$$\mathbf{Z}(t) = \begin{bmatrix} V_0 & i_1 & i_2 & \cdots & i_n \end{bmatrix}^T \tag{2.34}$$

The system in Fig. 2-7 can be modeled as a discrete time MIMO state space model using (2.31) and (2.32)

$$\dot{\mathbf{Z}}(t) = \mathbf{A}\mathbf{Z}(t) + \mathbf{B}\mathbf{u}(t) \tag{2.35}$$

where $\mathbf{A} = \begin{bmatrix} -\frac{1}{R\cdot\sum_{j=1}^{n} C_j} & \frac{1}{\sum_{j=1}^{n} C_j} & \frac{1}{\sum_{j=1}^{n} C_j} & \cdots & \frac{1}{\sum_{j=1}^{n} C_j} \\ -\frac{1}{L_1} & -\frac{r_1}{L_1} & 0 & \cdots & 0 \\ -\frac{1}{L_2} & 0 & -\frac{r_2}{L_2} & \cdots & 0 \\ \vdots & \vdots & \cdots & \ddots & \vdots \\ -\frac{1}{L_n} & 0 & 0 & \cdots & -\frac{r_n}{L_n} \end{bmatrix}$, $\mathbf{B} = \begin{bmatrix} 0 & 0 & \cdots & 0 \\ \frac{1}{L_1} & 0 & \cdots & 0 \\ 0 & \frac{1}{L_2} & \cdots & 0 \\ \vdots & \vdots & \ddots & \vdots \\ 0 & 0 & \cdots & \frac{1}{L_n} \end{bmatrix}$,

$$\mathbf{u}(t) = \begin{bmatrix} V_1 \\ V_2 \\ \vdots \\ V_n \end{bmatrix}$$

With the state space model (2.35), a prediction model can be developed for the parallel connected inverters system similar to the linear motor drive as described in section 2.2.3. The incremental state space model of the system can be expressed as

$$\Delta\mathbf{Z}(kT+T) = \bar{\mathbf{G}}\Delta\mathbf{Z}(kT) + \bar{\mathbf{H}}\Delta\mathbf{u}(kT) \tag{2.36}$$

where $\bar{\mathbf{G}} = e^{\mathbf{A}T}$, $\bar{\mathbf{H}} = \left[\int_0^T e^{\mathbf{A}\tau} d\tau\right]\mathbf{B}$ and Δ is the difference operator, such that

$$\Delta\mathbf{Z}(kT) = \mathbf{Z}(kT) - \mathbf{Z}(kT-T)$$

$$\Delta\mathbf{u}(kT) = \mathbf{u}(kT) - \mathbf{u}(kT-T)$$

As the current sharing is one of the control objectives, the current difference between adjacent inverters are chosen as the output variables for simplicity of control design. Under optimal condition, the current differences are expected to be zero. With the Output Voltage, the state is defined as

$$\mathbf{Y}(kT)=\begin{bmatrix} V(kT) \\ i_1(kT)-i_2(kT) \\ \vdots \\ i_{n-1}(kT)-i_n(kT) \end{bmatrix} \tag{2.37}$$

Hence, the MIMO system in minimal realization after augmentation can be expressed as

$$\begin{bmatrix} \Delta\mathbf{Z}(kT+T) \\ \mathbf{Y}(kT) \end{bmatrix}=\begin{bmatrix} \bar{\mathbf{G}} & \mathbf{0} \\ \mathbf{C}_1 & \mathbf{C}_2 \end{bmatrix}\begin{bmatrix} \Delta\mathbf{Z}(kT) \\ \mathbf{Y}(kT-T) \end{bmatrix}+\begin{bmatrix} \bar{\mathbf{H}} \\ \mathbf{0} \end{bmatrix}\Delta\mathbf{u}(kT) \tag{2.38}$$

where

$$\mathbf{C}_1=\begin{bmatrix} 1 & 0 & 0 & \cdots & 0 \\ 0 & 1 & -1 & \ddots & 0 \\ \vdots & & \ddots & & \vdots \\ 0 & \cdots & 0 & 1 & -1 \end{bmatrix}_{n\times(n+1)}, \quad \mathbf{C}_2=\begin{bmatrix} 1 & 0 & \cdots & 0 \\ 0 & 1 & \ddots & \vdots \\ \vdots & \ddots & \ddots & 0 \\ 0 & \cdots & 0 & 1 \end{bmatrix}_{n\times n}.$$

Define a new state vector as

$$\mathbf{X}(kT)=\begin{bmatrix} \Delta\mathbf{Z}(kT) \\ \mathbf{Y}(kT-T) \end{bmatrix} \tag{2.39}$$

then (2.38) can be rewritten as the following state space equation:

$$\mathbf{X}(kT+T)=\mathbf{G}\mathbf{X}(kT)+\mathbf{H}\Delta\mathbf{u}(kT) \tag{2.40}$$

$$\mathbf{Y}(kT)=\mathbf{C}\mathbf{X}(kT) \tag{2.41}$$

where

$$\mathbf{G}=\begin{bmatrix} \bar{\mathbf{G}} & \mathbf{0} \\ \mathbf{C}_1 & \mathbf{C}_2 \end{bmatrix}, \quad \mathbf{H}=\begin{bmatrix} \bar{\mathbf{H}} \\ \mathbf{0} \end{bmatrix}, \quad \mathbf{C}=[\mathbf{C}_1 \quad \mathbf{C}_2].$$

Using (2.40)-(2.41) and by repeated substitution, we have the following prediction model:

$$\mathbf{Y}_p(kT)=\mathbf{\Phi}\mathbf{X}(kT)+\mathbf{R}\Delta\mathbf{U}_p(kT) \tag{2.42}$$

where

$$\mathbf{Y}_p(kT) = \begin{bmatrix} \mathbf{Y}(kT+T) \\ \mathbf{Y}(kT+2T) \\ \vdots \\ \mathbf{Y}(kT+N_y T) \end{bmatrix}, \quad \Delta\mathbf{U}_p(kT) = \begin{bmatrix} \Delta\mathbf{u}(kT) \\ \Delta\mathbf{u}(kT+T) \\ \vdots \\ \Delta\mathbf{u}(kT+N_y T-T) \end{bmatrix},$$

$$\mathbf{\Phi} = \begin{bmatrix} \mathbf{CG} \\ \mathbf{CG}^2 \\ \vdots \\ \mathbf{CG}^{N_y} \end{bmatrix}, \quad \mathbf{R} = \begin{bmatrix} \mathbf{CH} & \mathbf{0} & \cdots & \mathbf{0} \\ \mathbf{CGH} & \mathbf{CH} & \vdots & \vdots \\ \vdots & \ddots & \ddots & \mathbf{0} \\ \mathbf{CG}^{N_y-1}\mathbf{H} & \cdots & \mathbf{CGH} & \mathbf{CH} \end{bmatrix}.$$

With this incremental prediction model, a model predictive controller will be developed and investigated in Chapter 5.

2.4 Conclusions

In this chapter, the basic characteristics of a linear motion system and a parallel connected inverters system are described and analyzed. For the linear motion system, a suitable state space prediction model has been developed. Likewise, a MIMO state space model has also been derived for the parallel connected inverters system based on the analysis of the system electrical characteristics. However, problems in different aspect need to be solved. For the linear motion system, the influence of friction needs to be minimized to achieve a better tracking performance. On the other hand, the flexibility to add-in and remove inverter units and reliability during hot-swap operation are the most important design criterion for the parallel connected inverters system. Approaches for solving these issues will be proposed and described in Chapters 3 to 5.

Chapter 3

Model Predictive Control of a Linear Motion System

3.1 Introduction

Model predictive control (MPC) originated in the late seventies and has developed considerably since then [97]. The term MPC does not designate a specific control strategy but rather an ample range of predictive control methods with abbreviation like IDCOM [98], DMC [99], GPC [100], IMC [101], RHC [102], which make explicit use of a model of the process to obtain the control signal by minimizing an objective function. Theoretical and practical issues associated with MPC technology are summarized in several recent publications. In [103], Rawlings gives an introduction to the MPC technology aiming at the potential MPC users. Qin and Badgewell [17] present the history of MPC technology development and a survey of industrial applications that focused primarily on those employing linear models. The issues related to closed-loop nominal stability and feasibility of the MPC over the last decade has been extensively addressed by Mayne and J. H. Lee [104, 105]. Several recently published books [97, 106-108]also provide more detailed explanation on MPC.

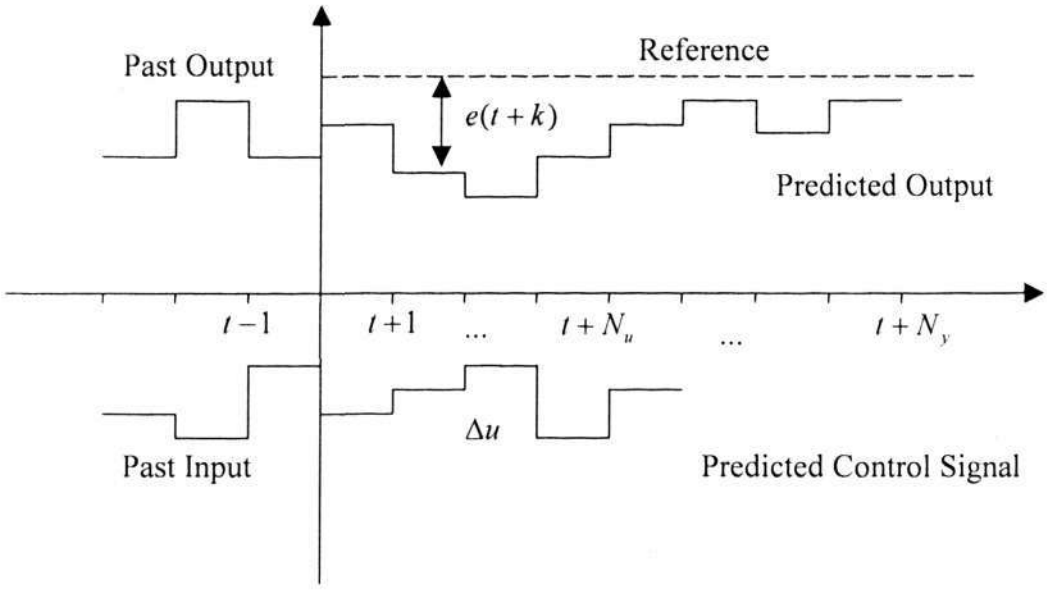

Fig. 3-1 Basic idea of model predictive control

Fig. 3-1 shows the basic idea of a model predictive control. MPC is typically based upon the following steps: output prediction, control calculation, and feedback implementation. The parameter N_y and N_u in Fig. 3-1 are the finite horizons of system output and input prediction respectively. The future behavior of the system output is predicted based on the system model and available historical data. The future control signal is then calculated by minimizing a cost function, which enables the predicted output to be as close as possible to the desired future output. The first two steps are performed in open-loop to minimize the error between the projected output and reference point. The loop is then closed by applying the calculated control signal to the system.

Although there are many variants of the predictive control schemes, the controllers have practically the same structure under the same design philosophy. The common characteristics of all these methods can be summarized as follows:

1. The MPC strategies use a dynamic model to predict the system output over a range of future time;
2. The strategies assume that the future set point is known and they calculate a set of future control signals by minimizing a objective function.

The MPC scheme uses a receding horizon strategy. In this strategy, it involves the application of the first control signal of the sequence calculated at each step, so that at each instant the horizon is displaced toward the future.

In this chapter, a state space model predictive controller is designed for the linear motion control system. With the prediction model developed in Chapter 2, the control law is formulated. The characteristics of the MPC controller are analyzed using frequency domain. The performance of the system is evaluated through both simulation and experimental study.

3.2 Controller Design

For the investigated linear motion system, precise position trajectory control is the major objective. The control signal of a MPC controller is to be obtained by minimizing a general cost function *J*. The aim is to minimize the difference between the future output on the considered horizon and the target trajectory. At the same time, the control effort should be penalized. The general expression for such an objective for position control can be formulated as

$$J = \sum_{j=1}^{Ny} \left\| Y^*(kT + jT) - \hat{Y}(kT + jT|kT) \right\|^2 + \lambda \sum_{j=1}^{Nu} \left\| \Delta i_q(kT + jT - T) \right\|^2 \qquad (3.1)$$

where $Y^*(\cdot)$ and $\hat{Y}(\cdot)$ are the reference of motor position Y and the predicted position respectively.

Moreover, it is assumed that control increments are zero beyond the control horizon, that is

$$\Delta i_q(kT + jT - T) = 0 \qquad \forall\, j > N_u. \tag{3.2}$$

The parameter N_y in (3.1) is known as the prediction horizon. It is defined as the interval over which the tracking error is minimized. The parameter N_u is called the control horizon. It defines the degree of freedom available for optimization. The control weighting factor λ is used to penalize excessive control activity and to ensure a numerically well-conditioned algorithm.

3.2.1 Control Law Formulation

The cost function (3.1) can be expressed in a vector form as

$$\mathbf{J} = (\mathbf{Y}^* - \hat{\mathbf{Y}})^T(\mathbf{Y}^* - \hat{\mathbf{Y}}) + \lambda \Delta \mathbf{I}_p{}^T \Delta \mathbf{I}_p \tag{3.3}$$

where $\mathbf{Y}^*$ is the reference output vector or the set points at sampling time kT. It can be expressed as follows

$$\mathbf{Y}^*(kT) = \begin{bmatrix} Y^*(kT+T) \\ Y^*(kT+2T) \\ \vdots \\ Y^*(kT+N_yT) \end{bmatrix} \tag{3.4}$$

The cost function is to be minimized with respect to the available future input signals $\Delta \mathbf{I}$. From the condition (3.2), we have the available control input vector for optimization as

$$\Delta \mathbf{I} = \left[\Delta i_q(kT) \quad \cdots \quad \Delta i_q(kT + N_u T - T) \right]^T$$

If we perform partial differentiation of (3.3) with respect to $\Delta \mathbf{I}$, we have

$$\frac{\partial \mathbf{J}}{\partial \Delta \mathbf{I}} = -2 \frac{\partial \hat{\mathbf{Y}}}{\partial \Delta \mathbf{I}} \left(\mathbf{Y}^* - \hat{\mathbf{Y}} \right) + 2\lambda \frac{\partial \Delta \mathbf{I}_p}{\partial \Delta \mathbf{I}} \Delta \mathbf{I}_p \tag{3.5}$$

The relationship between $\Delta \mathbf{I}$ and $\Delta \mathbf{I}_p$ can be expressed as

$$\Delta \mathbf{I}_p = \mathbf{M} \Delta \mathbf{I} \tag{3.6}$$

where M is a $N_y \times N_u$ matrix defined as

$$\mathbf{M} = \begin{bmatrix} 1 & 0 & \cdots & 0 \\ 0 & 1 & & 0 \\ \vdots & & \ddots & \vdots \\ 0 & \cdots & 0 & 1 \\ 0 & \cdots & \cdots & 0 \\ \vdots & & & \vdots \\ 0 & \cdots & \cdots & 0 \end{bmatrix}_{N_y \times N_u} \tag{3.7}$$

Differentiate (3.6), we obtain

$$\frac{\partial \Delta \mathbf{I}_p}{\partial \Delta \mathbf{I}} = \mathbf{M}^T \tag{3.8}$$

Differentiate $\hat{\mathbf{Y}}$ with respect to $\Delta \mathbf{I}$ yields

$$\frac{\partial \hat{\mathbf{Y}}}{\partial \Delta \mathbf{I}} = \mathbf{M}^T \mathbf{R}^T \tag{3.9}$$

Substitute (3.8) and (3.9) into (3.5), and after some algebraic manipulation yields

$$\Delta \mathbf{I} = \left(\mathbf{M}^T \mathbf{R}^T \mathbf{R} \mathbf{M} + \lambda \mathbf{M}^T \mathbf{M} \right)^{-1} \left[\mathbf{M}^T \mathbf{R}^T \mathbf{Y}^* - \mathbf{M}^T \mathbf{R}^T \mathbf{\Phi} \mathbf{X}(kT) \right] \tag{3.10}$$

As the control law uses the receding horizon scheme, the control signal of the first element is obtained as

$$\Delta i_q(kT) = \begin{bmatrix} 1 & 0 & \cdots & 0 \end{bmatrix}_{1 \times N_u} \Delta \mathbf{I} \tag{3.11}$$

Hence, the final state space predictive control law can be formulated by substituting (3.10) into (3.11) as follows

$$\Delta i_q(kT) = \mathbf{K}_1 \mathbf{Y}^*(kT) + \mathbf{K}_2 \mathbf{X}(kT) \tag{3.12}$$

where

$\mathbf{K}_1 = \mathbf{K}\mathbf{M}^T\mathbf{R}^T$,

$\mathbf{K}_2 = -\mathbf{K}\mathbf{M}^T\mathbf{R}^T\mathbf{\Phi}$,

$\mathbf{K} = \begin{bmatrix} 1 & 0 & \cdots & 0 \end{bmatrix}_{1\times N_u} (\mathbf{M}^T\mathbf{R}^T\mathbf{R}\mathbf{M} + \lambda\mathbf{M}^T\mathbf{M})^{-1}$.

3.2.2 Observer Design

The control law development in last section is based on the assumption that all system states are available for feedback. In practice, only the position measurement is available. Thus, a state observer is required for reconstructing the system state vector using the available input signals.Consequently, the control law (3.12) should be written as follows

$$\Delta i_q(kT) = \mathbf{K}_1 \mathbf{Y}^*(kT) + \mathbf{K}_2 \hat{\mathbf{X}}(kT) \tag{3.13}$$

where $\hat{\mathbf{X}}$ is the estimated state vector

Based on the system model and the measurement of the system inputs and outputs, a state observer can be designed as an auxiliary dynamic system that reconstructs the system state vector. In this study, the observer is designed based on the receding horizon methodology. The basic principle behind receding horizon estimation is the formulation of an optimization problem where a quadratic objective function is minimized to provide an optimal estimation of state variables and disturbances [109]. The objective function is composed of model errors over a horizon of control history. It is well known that if and

only if the system is completely observable, the state vector can be estimated using the available input/output signals [110]. Hence, the observability of the linear drive system should be examined. The observability matrix of the system is $[\mathbf{C};\mathbf{CG};\mathbf{CG}^2;\mathbf{CG}^3;\mathbf{CG}^4]$ that has a rank of 5. As it equals to the dimension of the matrix, the system is completely observable.

From the state equation (2.21), we have

$$\begin{cases} \hat{\mathbf{X}}(kT-N_eT+T)=\hat{\mathbf{X}}(kT-N_eT+T) \\ \hat{\mathbf{X}}(kT-N_eT+2T)=\mathbf{G}\hat{\mathbf{X}}(kT-N_eT+T)+\mathbf{H}\Delta i_q(kT-N_eT+T) \\ \hat{\mathbf{X}}(kT-N_eT+3T)=\mathbf{G}^2\hat{\mathbf{X}}(kT-N_eT+T)+\mathbf{GH}\Delta i_q(kT-N_eT+T) \\ \qquad\qquad +\mathbf{H}\Delta i_q(kT-N_eT+2T) \\ \qquad\vdots \qquad\qquad\qquad \vdots \qquad\qquad\qquad \vdots \\ \hat{\mathbf{X}}(kT)=\mathbf{G}^{N_e-1}\hat{\mathbf{X}}(kT-N_eT+T)+\mathbf{G}^{N_e-2}\mathbf{H}\Delta i_q(kT-N_eT+T) \\ \qquad\qquad \mathbf{G}^{N_e-3}\mathbf{H}\Delta i_q(kT-N_eT+2T)+\cdots+\mathbf{H}\Delta i_q(kT-T) \end{cases} \tag{3.14}$$

where the estimation horizon N_e determines the number of past samples of output signals used in reconstructing the state vector. Multiply both sides of the above equations by $\mathbf{C}$ and arrange them in matrix form yields

$$\bar{\mathbf{Y}}=\mathbf{M}_e\hat{\mathbf{X}}+\mathbf{PU} \tag{3.15}$$

where

$$\mathbf{M}_e=\begin{bmatrix} \mathbf{CG}^{Ne-1} \\ \mathbf{CG}^{Ne-2} \\ \vdots \\ \mathbf{C} \end{bmatrix},\quad \mathbf{P}_e=\begin{bmatrix} \mathbf{CH} & \mathbf{CG}^{N_v-1}\mathbf{H} & \cdots & \mathbf{CG}^{N_v-1}\mathbf{H} \\ 0 & \mathbf{CH} & \cdots & \mathbf{CG}^{N_v-1}\mathbf{H} \\ 0 & 0 & \ddots & \vdots \\ \vdots & \vdots & \ddots & \mathbf{CH} \\ 0 & 0 & \cdots & 0 \end{bmatrix}$$

Define $\mathbf{Y}_e$ as the position measurement vector and $\mathbf{I}_e$ as the system input command vector as

$$\mathbf{Y}_e = \begin{bmatrix} Y(kT) & Y(kT-T) & \cdots & Y(kT-N_eT+T) \end{bmatrix}^T \tag{3.16}$$

$$\mathbf{I}_e = \begin{bmatrix} \Delta i_q(kT-T) & \Delta i_q(kT-2T) & \cdots & \Delta i_q(kT-N_eT+T) \end{bmatrix}^T \tag{3.17}$$

Similar to the controller design, the observer can be derived by minimizing the following cost function:

$$J_e = \sum_{j=0}^{N_e-1} \left\| Y(kT-jT) - \mathbf{C}\hat{\mathbf{X}}(kT-jT) \right\|^2 \tag{3.18}$$

with respect to $\hat{\mathbf{X}}\big(kT-(N_e-1)T\big)$, where N_e is termed as the estimation horizon.

The cost function can be expressed in vector form as

$$\mathbf{J}_e = (\mathbf{Y}_e - \bar{\mathbf{Y}})^T (\mathbf{Y}_e - \bar{\mathbf{Y}}) \tag{3.19}$$

where

$$\bar{\mathbf{Y}} = \begin{bmatrix} \mathbf{C}\hat{\mathbf{X}}(kT) \\ \mathbf{C}\hat{\mathbf{X}}(kT-T) \\ \vdots \\ \mathbf{C}\hat{\mathbf{X}}(kT-N_eT+T) \end{bmatrix}$$

To minimize $\mathbf{J}_e$ in (3.19), we perform partial differentiation of (3.19) and set it to 0. This yields the following equation

$$\frac{\partial \mathbf{J}_e}{\partial \hat{\mathbf{X}}(k-N_e+1)} = -2\frac{\partial \bar{\mathbf{Y}}}{\partial \hat{\mathbf{X}}(k-N_e+1)}\left(\mathbf{Y}_e - \bar{\mathbf{Y}}\right) = 0 \tag{3.20}$$

Substituting (3.15) into (3.20) and rearrange the equation into expression of $\hat{\mathbf{X}}(k)$, we have the following state observer

$$\hat{\mathbf{X}}(k) = \mathbf{E}_y \mathbf{Y}_e + \mathbf{E}_I \mathbf{I}_e \tag{3.21}$$

where

$$\mathbf{E}_y = \mathbf{G}^{N_e-1}(\mathbf{M}_e^T \mathbf{M}_e)^{-1}\mathbf{M}_e^T$$

$$\mathbf{E}_t = \begin{bmatrix} \mathbf{H} & \mathbf{HG} & \cdots & \mathbf{H}^{N_e-2}\mathbf{G} \end{bmatrix} - \mathbf{E}_y \mathbf{P}_e$$

It is noted that for the minimization of the cost function to have a solution, there exists a minimum setting of N_e for $(\mathbf{M}_e^T \mathbf{M}_e)^{-1}$ to exist in (3.21). It can be proved that the necessary condition for the existence of $(\mathbf{M}_e^T \mathbf{M}_e)^{-1}$ is $N_e \geq n$, where n is the system dimension. It is obvious that if $N_e = n$, $\mathbf{M}_e$ will have the same rank as the system observability matrix.

With a longer estimation horizon, a longer data history is included in the optimization. Thus, a stronger averaging effect can be expected with increased estimation horizon [111]. Ideally, we would like to use all available historical data to obtain an optimal state estimate, but the optimization problem grows in size at every instant and the computational effort increases linearly with time. The tradeoff between robustness and accuracy must be made by choosing an appropriate estimation horizon [112]. Here, we choose N_e as 7.

3.2.3 Overall control system and Parameter Tuning

Based on the discussion in section 3.2.1 and 3.2.2, the structure of the whole system is shown in Fig. 3-2.

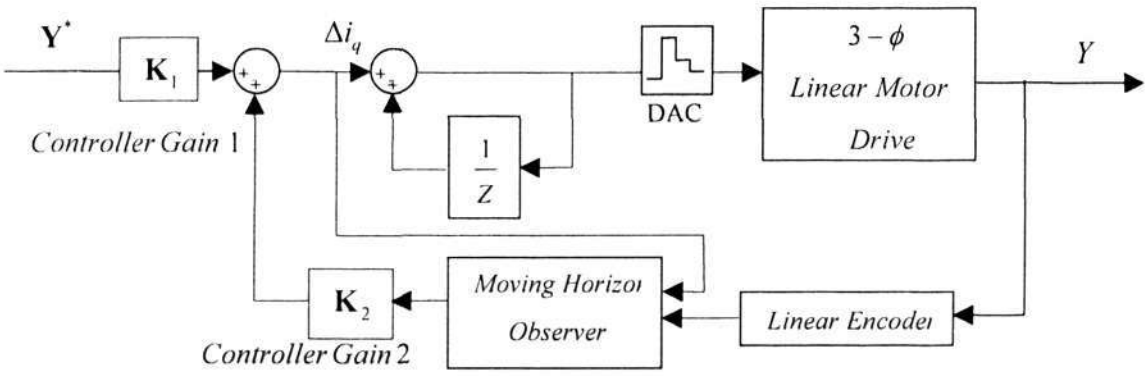

Fig. 3-2 Schematics of the model predictive controller system

In the figure, the observer block estimates the state variables using the previous input signal and previous output position history. The output of the feedback signal is obtained from the multiplication of the estimated state variables $\hat{\mathbf{X}}$ and the feedback gain vector $\mathbf{K}_2$. Similarly, the output of the feedforward signal is obtained from the multiplication of the input profiles $\mathbf{Y}^*$ and the feedforward gain vector $\mathbf{K}_1$. The signal Δi_q is then updated by adding the output of the feedforward and feedback signals according to (3.13). The symbol $1/z$ in Fig. 3-2 represents a unit delay of the accumulated input signal and is added to Δi_q, which is reflecting the use of incremental control structure. In this way, a digital integrator is included in this structure. The calculated input signal i_q is then applied to the system. In practical implementation, a constraints needs to be imposed on the controller. This issue will be discussed in later experimental study.

For the MPC controller, there are three design parameters: prediction horizon, control horizon and input weighting factor [106, 113, 114]. The input weighing factor sets a constraint on the control effort. The prediction horizon and control horizon are the finite horizons of the system output and control input predictions. They are essentially the constraints on the length of prediction and control history. From the controller formulation (3.12), it is observed that the dimension of controller gain $\mathbf{K}_2$ should not be smaller than the system states dimension. Thus, the possible range of prediction horizon is given as

$$N_y \geq 5 \tag{3.22}$$

As the control horizon available for optimization is up to the prediction horizon, a N_u smaller than N_y should be used to make the optimization meaningful. So we have

$$N_y \geq N_u \geq 1 \tag{3.23}$$

Besides the constraints, the controller parameters should be appropriately selected to achieve the desired performance. The control horizon is the available control signal changes at future sampling intervals. If a long prediction horizon N_y is chosen, a better response arises where more control changes are allowed in transients and hence the open-loop predictions can be close to the desired closed-loop behavior. Unsurprisingly, a larger N_u results in better closed-loop performance. However, the system's robustness against noise and unknown disturbances will deteriorate. Because the optimization will emphasize more on the current input signal, excessive control action will be expected. Thus, a relatively long prediction horizon and a short control horizon should be used to achieve robustness with respect to noise and transient disturbances. For motion control system, the controller should be designed to have good disturbance rejection ability as well as robustness to system uncertainty. Setting high gain will lead to instability and

sometimes uncontrollable oscillations. The goal is to tune the system for maximum responsiveness with the minimum instability. With these considerations, the parameters for the system used in this study are set as $N_y = 20,\ N_u = 2$. The pole placement result is shown in Fig. 3-3. In simulation, the weighting factor is tuned to have the critical poles (circled) placed at damping ratio near 0.7. The weighting factor λ on the control signal used in both simulation and experiment is 1e-5.

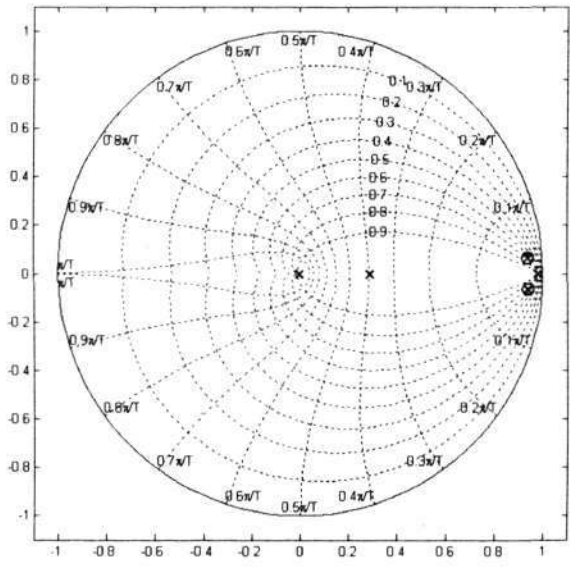

Fig. 3-3 Pole placement result of the MPC controller

3.3 Stability and Robustness Analysis

The stability of the control system can be examined through the pole distribution. As demonstrated earlier in Fig. 3-3, the designed motion control system is nominally stable. Its stability is guaranteed by placing all the closed-loop poles inside the unity circle. However, its stability under system uncertainties should also be examined to ensure good

performance. Thus, the robustness of MPC to maintain the system in satisfactory performance in the context of a varying load will be investigated in the following.

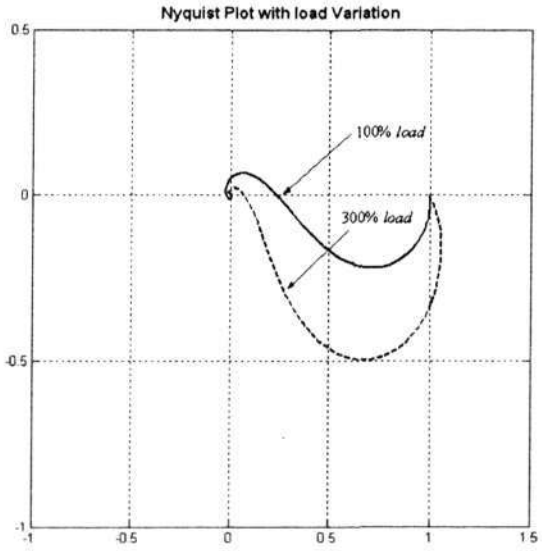

Fig. 3-4 Nyquist plot of closed system with 300% load uncertainty (solid line-nominal system dash line-system with 300% load variation)

The load variation can be considered as pure parametric uncertainty [115]. Suppose some pay load is added to the system, the system Mass M is increased to 300% of its original value, Fig. 3-4 shows the Nyquist plot of the closed loop system. As shown in Fig. 3-4, the system remains stable with 300% load variation. In the whole frequency range, the system keeps away from the point $(-1,0)$. Thus, the robustness of the system is guaranteed.

3.4 Frequency Domain Properties Analysis

The designed MPC controlled system can be viewed as a SISO system. By combining (2.27) and (3.12), the controlled system can be described using the following state space model

$$\mathbf{X}(kT+T) = (\mathbf{G} + \mathbf{H} \cdot \mathbf{K}_2)\mathbf{X}(kT) + \mathbf{H} \cdot \mathbf{K}_1 \cdot \mathbf{Y}^*(kT) \tag{3.24}$$

$$Y(kT) = \mathbf{C}\mathbf{X}(kT) \tag{3.25}$$

If the designed MPC controller is viewed as a two-degree of freedom (2DF) controller, it can be separated into two parts: a feedback controller and a feed-forward controller. $\mathbf{K}_1\mathbf{Y}^*(kT)$ is the control input to the system after the desired trajectory $\mathbf{Y}^*(kT)$ going through a set of feedforward controller gain $\mathbf{K}_1$. $\mathbf{K}_2$ serves as the feedback controller to stabilize the whole system.

From (3.24)-(3.25), the magnitude and phase properties of the system can be determined. The system characteristics without considering the feedforward controller $\mathbf{K}_1$ is shown in Fig. 3-5(a). From the figure, it can be observed that certain degree of phase delay resides in the system dynamics. The bode-plot of the control system with $\mathbf{K}_1$ is shown in Fig. 3-5(b). The controller gain $\mathbf{K}_1$ can be considered functioning as a FIR filter on the desired trajectory. As all the poles of the FIR filter are located at the origin and thus are located within the unit circle, it has no influence on the system stability. As shown in the figure, it provides an attenuation effect on the reference signals. Moreover, it provides phase lead to cancel the phase lag of the feedback control system in the frequency range 0Hz-10Hz.

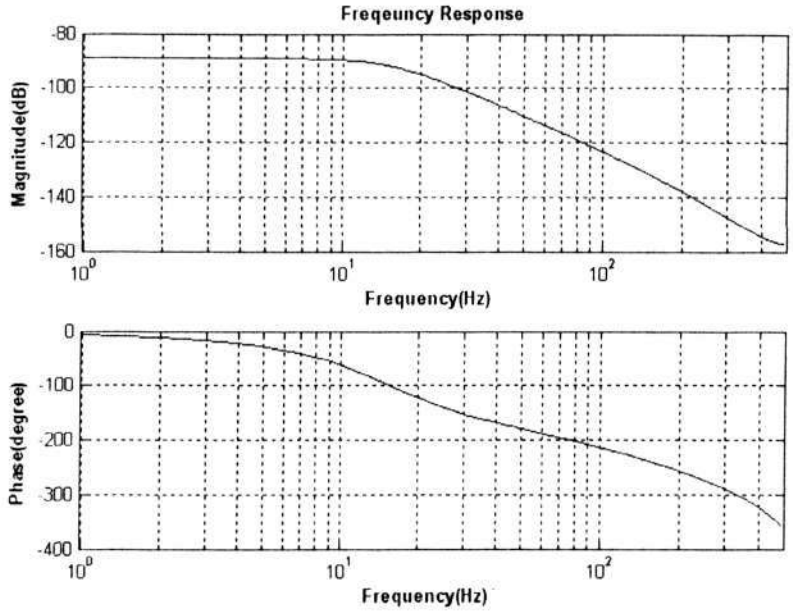

(a)

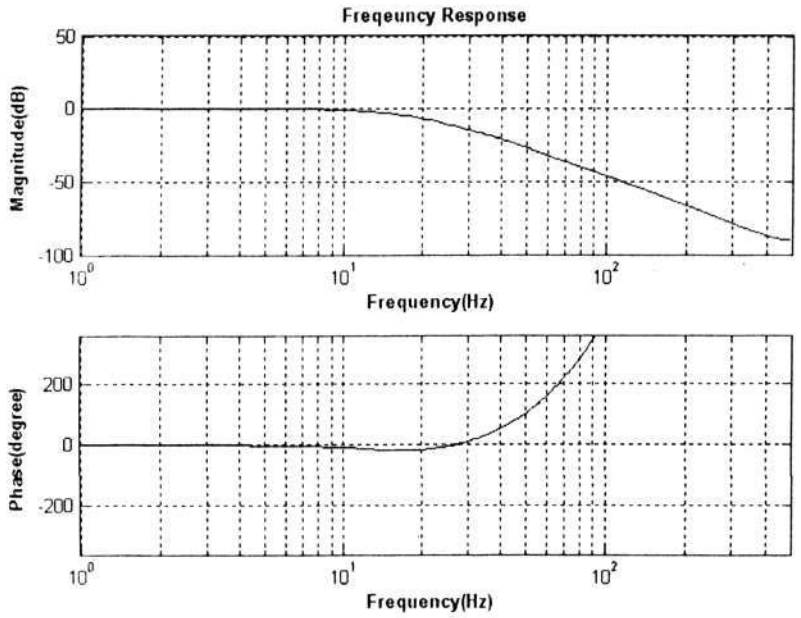

(b)

Fig. 3-5 Bode plot of the MPC controlled system (a) Without K_1 (b) With K_1

As the parameter change of $\mathbf{K}_1$ will not influence the stability of the system, the stability of the system is determined by the controller gain $\mathbf{K}_2$ only. The discrete-time DC gain of the system can be obtained from (3.24)-(3.25) as follows

$$DC_{feedback} = \mathbf{C}(\mathbf{I} - (\mathbf{G} + \mathbf{H} \cdot \mathbf{K}_2))^{-1}\mathbf{H} \tag{3.26}$$

Let $\mathbf{\Psi} = \mathbf{G} + \mathbf{H} \cdot \mathbf{K}_2$, we can obtain the following

$$\mathbf{\Omega} = \mathbf{\Gamma}^{-1} = (\mathbf{I} - (\mathbf{G} + \mathbf{H} \cdot \mathbf{K}_2))^{-1}$$

$$= \begin{bmatrix} 1-\Psi_{11} & -\Psi_{12} & -\Psi_{13} & -\Psi_{14} & -\Psi_{15} \\ -\Psi_{21} & 1-\Psi_{22} & -\Psi_{23} & -\Psi_{24} & -\Psi_{25} \\ -\Psi_{31} & -\Psi_{32} & 1-\Psi_{33} & -\Psi_{34} & -\Psi_{35} \\ -\Psi_{41} & -\Psi_{42} & -\Psi_{43} & 1-\Psi_{44} & -\Psi_{45} \\ -1 & 0 & 0 & 0 & 0 \end{bmatrix}^{-1}$$

$$= \begin{bmatrix} 0 & 0 & 0 & 0 & \Omega_{15} \\ \Omega_{21} & \Omega_{22} & \Omega_{23} & \Omega_{24} & \Omega_{25} \\ \Omega_{31} & \Omega_{32} & \Omega_{33} & \Omega_{34} & \Omega_{35} \\ \Omega_{41} & \Omega_{42} & \Omega_{43} & \Omega_{44} & \Omega_{45} \\ \Omega_{51} & \Omega_{52} & \Omega_{53} & \Omega_{54} & \Omega_{55} \end{bmatrix}$$

Substitute $\mathbf{\Omega}$ into (3.26), the DC gain of the feedback system can be described as

$$DC_{feedback} = \mathbf{C\Omega H} = \Omega_{51} \cdot \bar{H}_{11} + \Omega_{52} \cdot \bar{H}_{21} + \Omega_{53}\bar{H}_{31} + \Omega_{54}\bar{H}_{41} \tag{3.27}$$

where $\Omega_{5n} = \dfrac{M_{n5}}{\det(\mathbf{\Gamma})}$, (n = 1, 2, 3, 4) and M_{n5} are the minors of the matrix $\mathbf{\Gamma}$.

The determinants of $\mathbf{\Gamma}$ can be calculated as

$$\det(\mathbf{\Gamma}) = -\sum_{n=1}^{4} M_{n5} \cdot \Psi_{n5} = -\sum_{n=1}^{4} M_{n5} \cdot H_{n1} \cdot \mathbf{K}_2(5) \tag{3.28}$$

Thus, the DC gain of the system can be calculated as

$$DC_{feedback} = \frac{\sum_{n=1}^{4} M_{n5} \cdot H_{n1}}{-\sum_{n=1}^{4} M_{n5} \cdot H_{n1} \cdot \mathbf{K}_2(5)} = -\frac{1}{\mathbf{K}_2(5)}$$

It is easy to verify that $\mathbf{\Phi}_{n5}$ of $\mathbf{\Phi}$ in (2.27) equals to 1. As $\mathbf{K}_2 = -\mathbf{K}_1 \cdot \mathbf{\Phi}$, we obtain the relationship

$$\mathbf{K}_2(5) = -\sum_{n=1}^{N_v} \mathbf{K}_1(n) \tag{3.29}$$

Hence, the DC gain of the feed-forward controller equals to

$$DC_{feedforward} = \sum_{n=1}^{N_y} \mathbf{K}_1(n) = \frac{1}{DC_{feedback}} \tag{3.30}$$

The relationship (3.30) guarantees that the whole system has a unity DC gain with regards to different parameter tuning and parameter variation. This is also manifested in Fig. 3-5. As shown in Fig. 3-5(b), the DC gain of feed-forward controller has a reciprocal relationship with the DC gain of the feedback system. This ensures that the whole system maintains a unity DC gain.

3.5 Point to Point Control

To evaluate the performance of the MPC controller, the step response is first investigated with simulation and experimental study. For the step response, the system overshoot, settling-time, and rise-time are the key transient performance characteristics.

Fig. 3-6 shows the step response of the system with nominal payload for a command of 1cm movement. As can be seen from Fig. 3-6, the motion control system achieves a slightly under damped step response, which agrees with the damping ratio selection as 0.7 in section 3.2.3 . The overshoot is within 5% of the desired moving distance. It may be noted that the set-point change starts from 0.35s (red dash line). Because of the prediction of MPC, the controller starts to move from 0.15s (with 20 prediction horizon and 0.001s sampling time). The phase advance induced at high frequency range of the model predictive controller (Fig. 3-5(b)) is manifested. The rise time is around 0.04s and the system settles within 0.1s. For application where pre-movement is not desired, offset can be added into the trajectory.

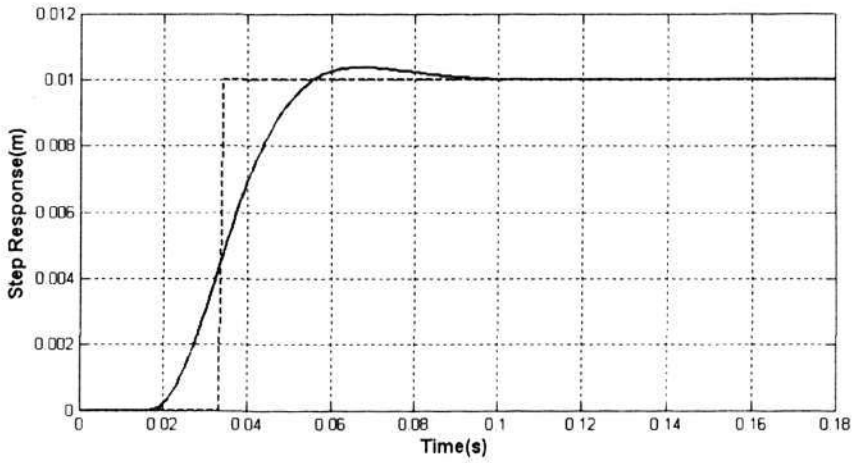

(a)

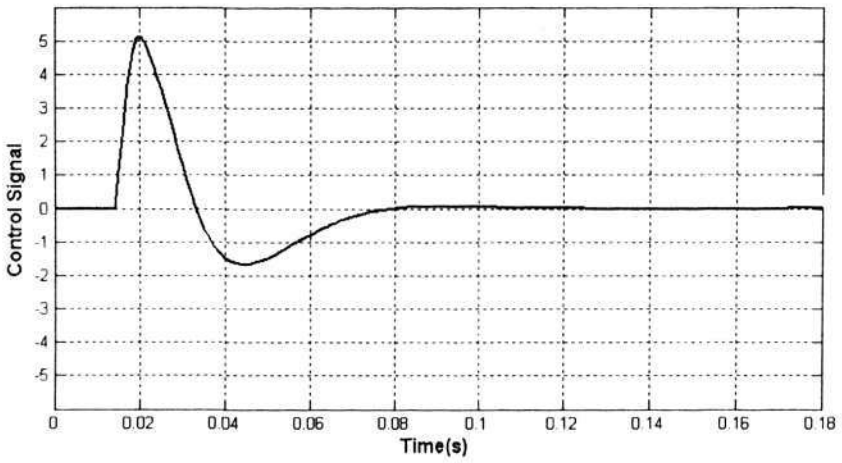

(b)

Fig. 3-6 Step response with ideal condition (a) position response (b) control signal

Next, the system's performance under constraints is examined. For the motor drive, there is a physical limit on the control signal, i.e the current that can be supplied to the motor. To verify the system's performance, a ±4 A constraint is applied on the input signal. The system response is shown in Fig. 3-7.

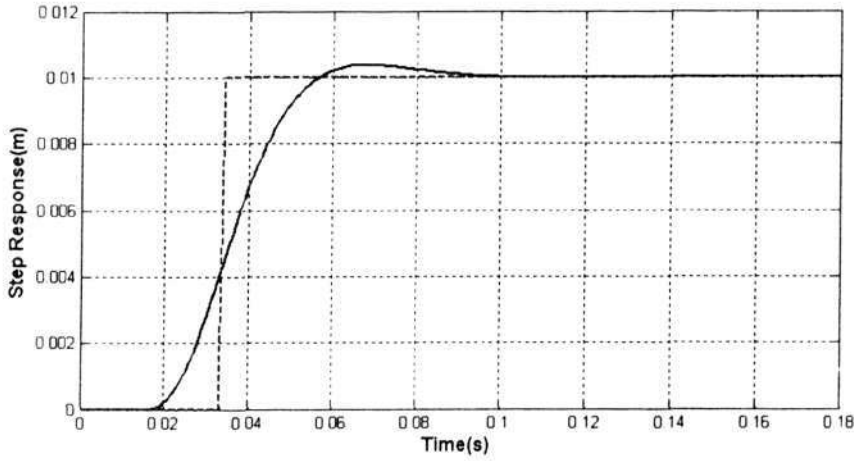

(a)

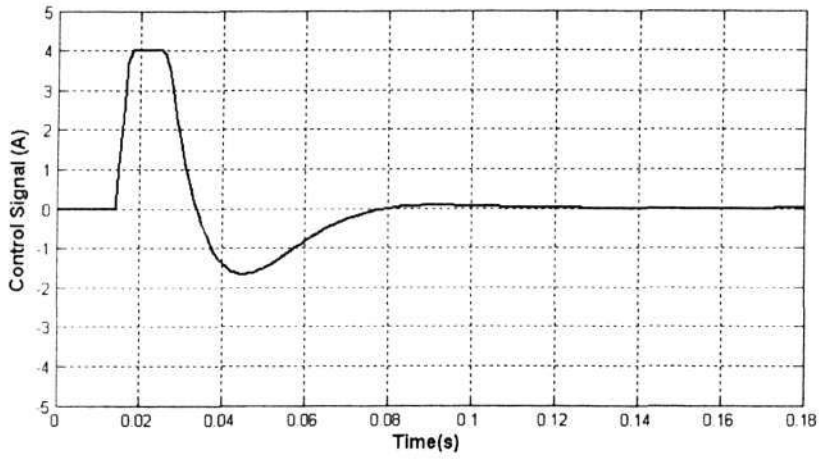

(b)

Fig. 3-7 Simulation of step response with constraint

As shown in Fig. 3-7, the performance under the constraints condition remains good. Although the hard constraint on the control signal is reached, the system performance does not deviate from the desired response. The motor moved swiftly to the desired position within 0.1s. The overshoot is confined within 5%. Compared with the ideal condition, the performance is almost the same. The incremental formulation of the control signal as in (3.12) precludes the possibility of winding up that usually occurs in simple PID controller for constrained system.

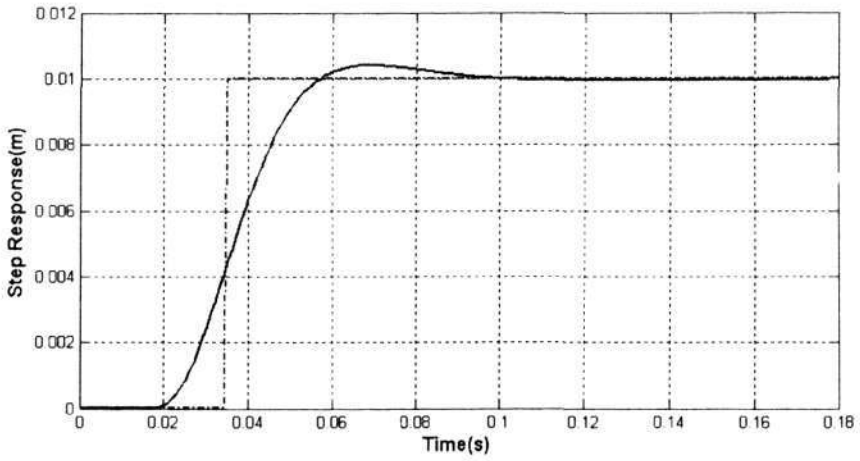

(a)

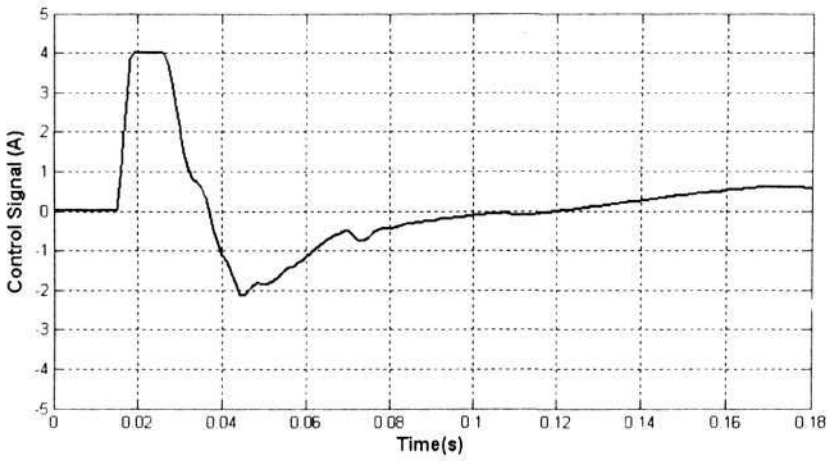

(b)

Fig. 3-8 Experimental Step Response

Fig. 3-8 shows the corresponding experimental result with a constraint of ±4 A placed on the control signal. Fig. 3-8(a) shows that the system output position approaches $1\,cm$ with a small overshoot and reaches the steady state in 0.1 second. Similarly, the system has hit the constraints during the transient. However, the controller is able to maintain a proper step response. This result is consistent with the simulation result. Fig. 3-8 (b) shows that the steady state control signal is not zero, which is different from the simulation result.

For the experiment, a counter force is required to overcome the influence from cogging force and cable spring effect.

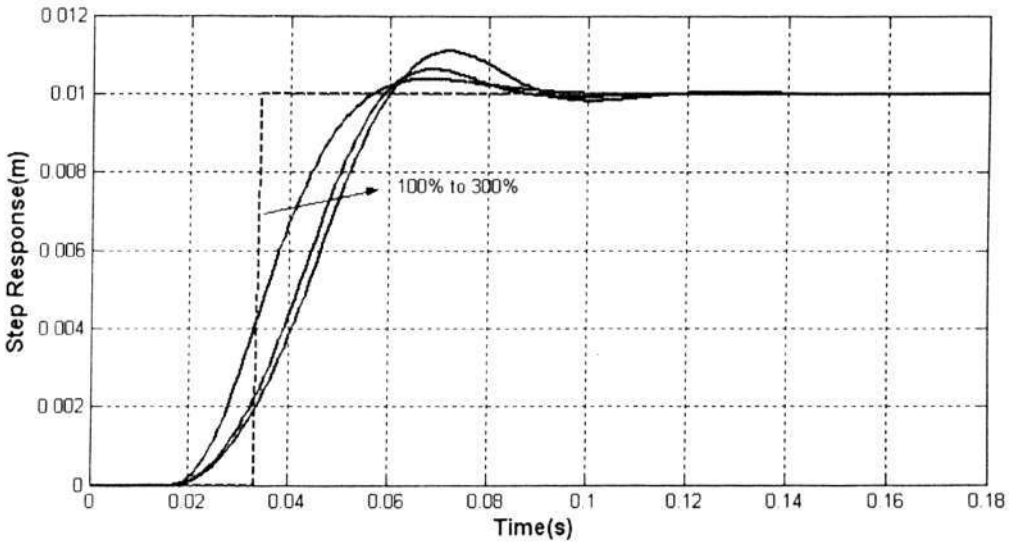

Fig. 3-9 Simulation of Step response with load variation

Simulation is also conducted to study the performance of the drive under the influence of load variation. For the simulation, different payload ranging from the nominal 100% to 300% have been used. The step response results are shown in Fig. 3-9. As can be seen from the figure, the motion control system maintains its stability and satisfactory performance with system load variation.

3.6 Trajectory Tracking Performance

In section 3.5, the system's point to point control ability has been investigated. It has been shown that the model predictive controller can provide good tracking properties and maintain good performance under constrained condition. In this section, the trajectory

tracking (path following) control property will be investigated. The same set of controller gain vector has been used for the experimental prototype.

Different from point to point control, which concerns with moving the control object from one point to another, the control object must be moved along the desired trajectory in tracking control over the entire operating cycle with prescribed accuracy. The tracking problem in control theory has been well researched, largely due to its broad engineering applications. For instance, automated chip inspection, robot spray painting, pick-and-place etc.[116-119].

Fig. 3-10 shows the simulation result of the designed system tracking a 1cm amplitude and 2 Hz frequency sinusoidal wave. The corresponding experimental result is shown in Fig. 3-11. As shown in Fig. 3-10(a) and Fig. 3-11(a), similar good tracking response is obtained. The linear motion system follows the trajectory tightly. The corresponding tracking error is illustrated in Fig. 3-10 (b) and Fig. 3-11(b). It is observed that the phase delay and column friction force at velocity reversal point has significant influence on the tracking performance.

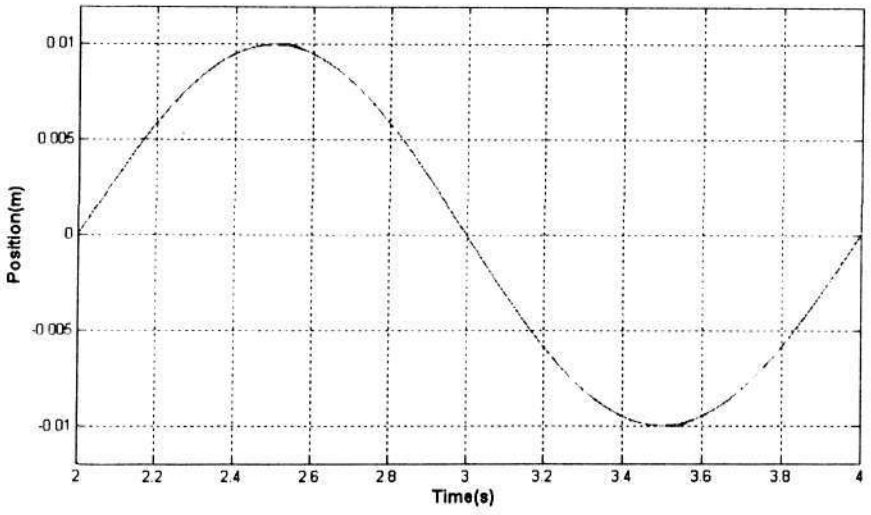

(a)

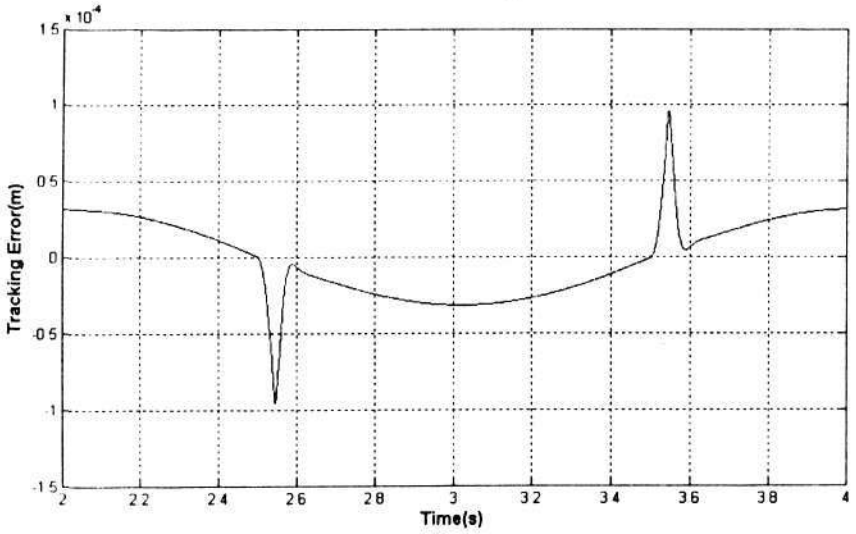

(b)

Fig. 3-10 Simulation result of trajectory tracking control response for a sinusoidal input (a) position response (b) tracking error

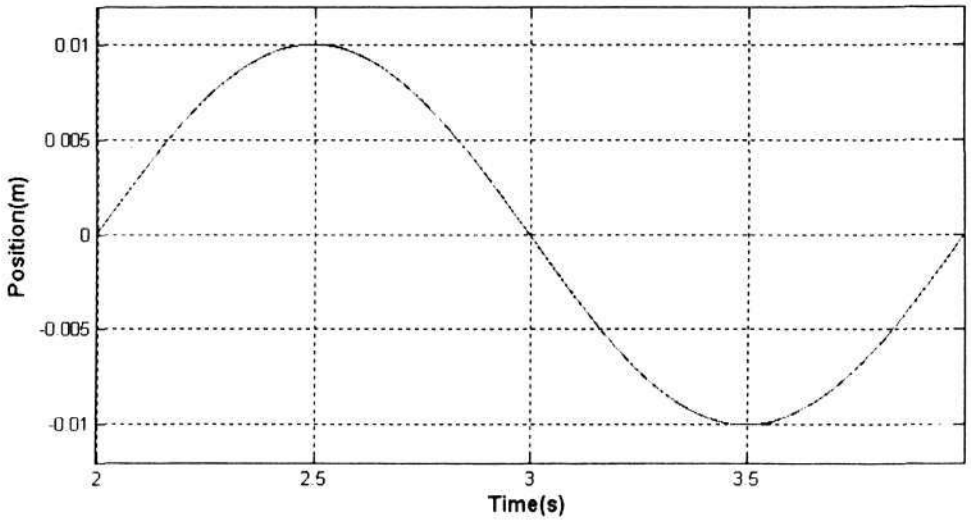

(a)

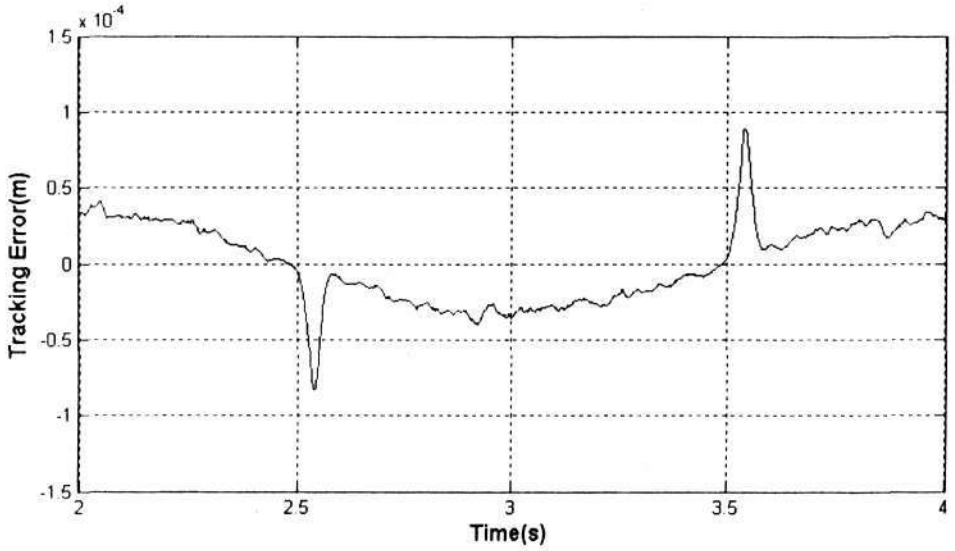

(b)

Fig. 3-11 experimental result of trajectory tracking response for a sinusoidal input (a) position response (b) tracking error

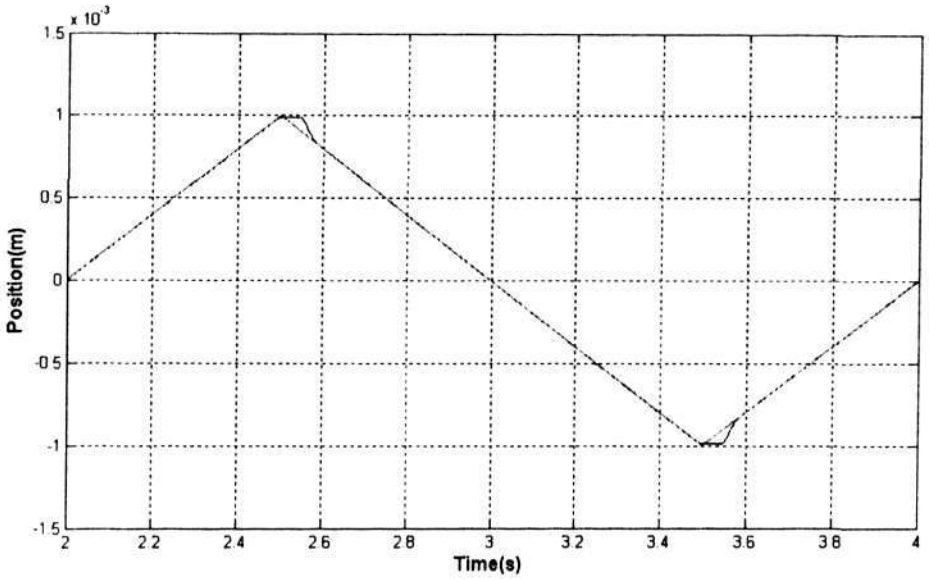

(a)

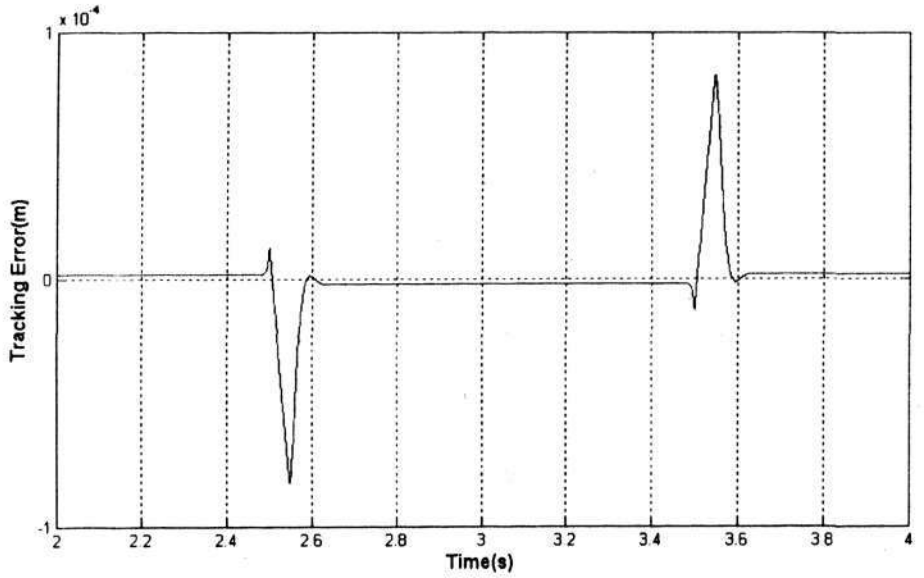

(b)

Fig.3-12 simulation result of trajectory tracking response for a triangle wave trajectory (a) position response (b) tracking error

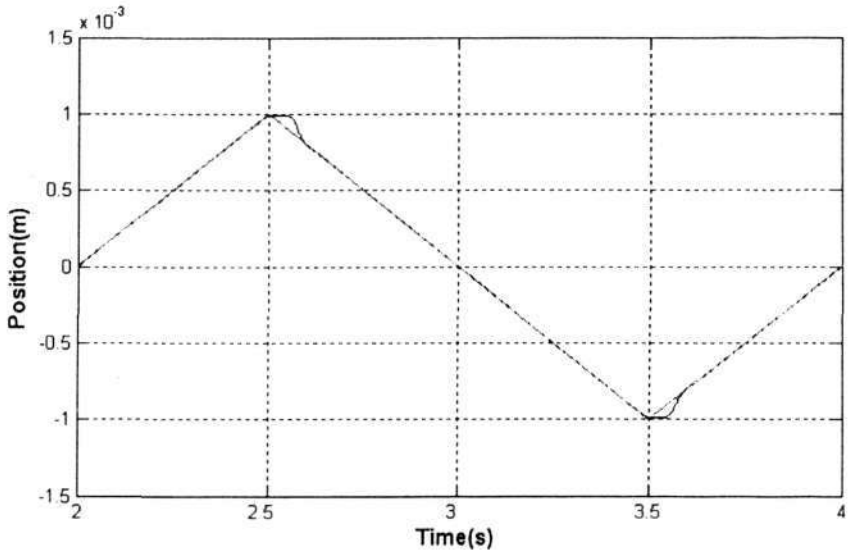

(a)

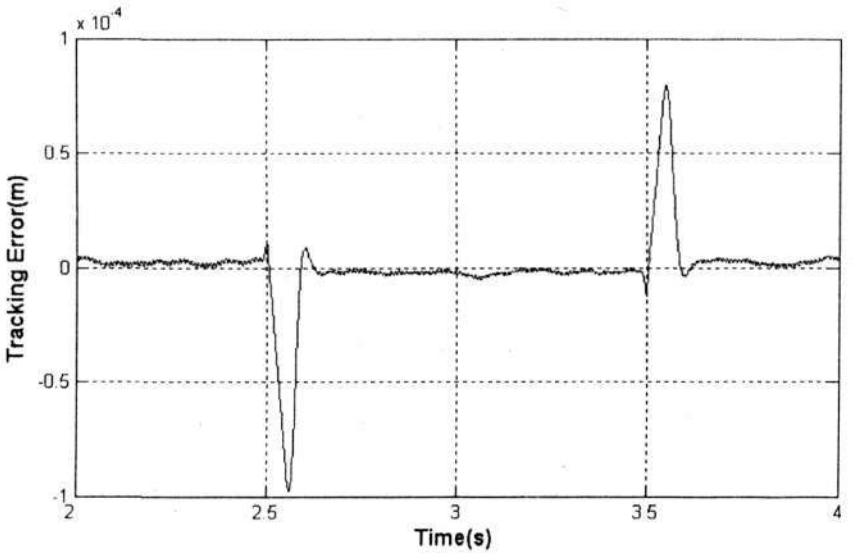

(b)

Fig. 3-13 experimental result of trajectory tracking response for a triangle wave trajectory (a) position response (b) tracking error

To further investigate the response of the system under sudden velocity reference change, a 1mm amplitude 2 Hz triangle waveform is used as the position reference trajectory. Both simulation and experiment have been carried out to examine the system performance. The results are shown in Fig.3-12 and Fig. 3-13. The position tracking response is shown in Fig.3-12(a) and Fig. 3-13(a), and the corresponding tracking error is shown in Fig.3-12(b) and Fig. 3-13(b). From the results, it can be concluded that the

MPC controller tracks the references accurately. However, it is observed that the influence of friction on the tracking error becomes more significant as compared to the sinusoidal reference trajectory at the speed reversal point. When a triangle-wave is used, the system will experience larger trajectory change before the system break away from stiction. This will result in more significant tracking error. Solutions to improve the tracking ability at the speed reversal will be proposed and developed in the next chapter.

3.7 Conclusions

In this chapter, the design of a model predictive controller for the linear motion system is presented. With the prediction model developed in Chapter 2, a state space model predictive controller with receding horizon observer is designed for the linear motion system. The stability and robustness of the designed controller have been examined through frequency domain study. With the developed controller, the system point to point and trajectory tracking control ability has been investigated. Good tracking performance is obtained in both the simulation and experimental study. As illustrated by the simulation and experimental result, the system is robust to parametric variation. However, the friction force has great influence on the system tracking precision when the system experiences a velocity reversal. An effective method needs to be introduced to further improve the system tracking precision. In next Chapter, repetitive tracking technique will be introduced to minimize the tracking error for periodic tasks.

Chapter 4

Repetitive Model Predictive Controller

4.1 Introduction

As presented in chapter 3, the MPC controller gives good performance in point to point and trajectory tracking. However, the influence of Coulomb friction force at the velocity reversal point could not be overcome. This deteriorates the system tracking performance. In this chapter, a new model predictive control (MPC) approach suitable for high precision linear motion drive operating with repetitive tracking tasks is presented. For the proposed predictive controller, the feedforward controller of the conventional MPC has been modified to provide zero phase learning property. This is achieved by augmenting the reference trajectory with a phase compensated term that is updated with the historical tracking error. The proposed approach attempts to combine the merits of both the conventional MPC and repetitive control schemes. Experimental results have demonstrated that the system reduces the tracking error from the periodic disturbance caused by the friction effectively. Its performance under varying reference conditions and different loadings shows that the system is robust.

4.2 Related Research Works

The learning control design scheme for model predictive control has been studied by several researchers. In many applications, model predictive control provides a good control design solution to achieve good tracking performance. However, the tracking

error resulting from periodic disturbances can further be minimized. It is desirable to incorporate idea of learning control into the conventional MPC formulation to achieve better tracking performance.

i) In [120], G. Bone presented a way to combine iterative learning control and generalized predictive control. The algorithm is implemented on a PUM-762 robot to carry out an edge following task. In his work, averaged tracking error history is combined with prediction horizon. It can be viewed as a P-type learning controller with an averaging filter. This method might give extra rejection performance to measurement error and uncertainties. Correspondingly, the learning speed and tracking accuracy is compromised by the averaging filter.

ii) A MPC controller with learning ability is also described in [24, 121]. In their work, a separate GPC controller is formulated for disturbance rejection. The disturbance information of previous run is used in the next run as reference signal. However, critical convergence analysis is not provided. Theoretically, it is equivalent to the method used in [120]. This algorithm is used in a robotized surgery to cancel out the repetitive motion of an artificial ventilation machine. However, the long term learning stability is not discussed. This method is useful if a stopping action can be taken. The tracking error will diverge, when an always-on learning control is required.

iii) In [122-126], Jay H. Lee etc's put forth an extension for repetitive control and iterative learning control. The extension is geared specifically to handle process control problems. These controllers are developed using the state-space

formulation of MPC and a linear time-invariant or even time-varying descriptions of the plants. In these applications, steady-state control is considered and no distinction is made between a periodic output disturbance or a periodically varying reference. This method uses a recurring optimization, with a fixed-size horizon moving constantly forward in time. However, when implemented in fast response systems. The horizon size may end up being very large. In spite of the versatility of this kind of algorithm, the characteristics inhibit its implementation for motion control system.

4.3 Repetitive Model Predictive Control

For applications that are repetitive in nature such as control of inverter, harddisk drive and automated process etc, the system can be designed with a repetitive controller to achieve better performance as the disturbance exists in the system is periodic [41, 44, 127]. In this chapter, a new model predictive controller that possesses the repetitive control property is proposed. The proposed repetitive MPC (RMPC) controller attempts to combine the merits of MPC and repetitive control. The repetitive control law has been augmented into the reference trajectory for the feedforward gain vector of MPC. In this way, the proposed control law is consistent with the conventional MPC structure. Different from the related work introduced in section 4.2, the augmentation uses frequency domain method. FIR filtering is used to achieve phase cancellation. In this way, wider compensation frequency range is obtained, so that good tracking performance is achieved.

As shown in Fig. 3-5, the system phase lag can not be perfectly cancelled by the feed-forward controller gain $\mathbf{K}_1$. The system phase lag at frequency larger than 50 Hz is out of the converging bound [-90°, 90°]. A learning controller applied in this frequency range is equivalent to changing the sign of the correction. When the phase lag reaches 180°, the learning control signal will give counteractive effect [128]. Thus, the original system phase properties can only provide limited learning frequency range. To extend the learning ability of the controller, a compensator which cancels the phase difference is desired. By utilizing phase compensation method, we seek to provide zero phase learning property for the whole frequency range. The block diagram of the proposed repetitive model predictive control is shown in Fig. 4-1.

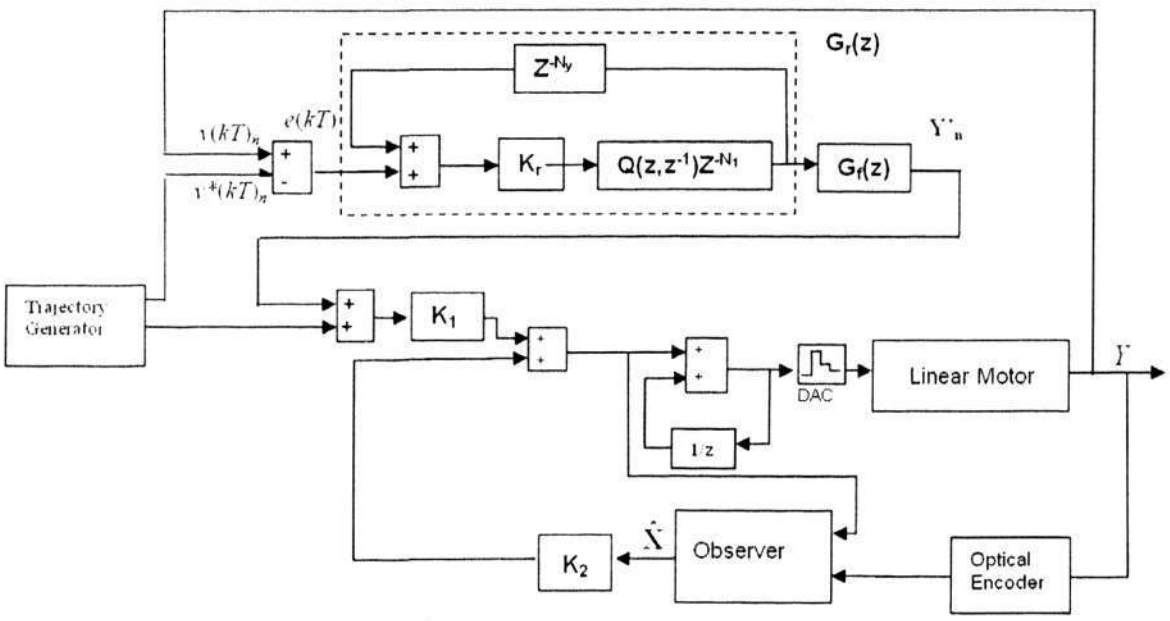

Fig. 4-1 Block diagram of the proposed repetitive model predictive control system

In this thesis, it is proposed to modify the conventional MPC control law given in (3.13) as follows

$$\Delta i_q(kT) = \mathbf{K}_1 \cdot \{\mathbf{Y}^*(kT) + \mathbf{Y}_\mathbf{n}^*\} + \mathbf{K}_2 \cdot \mathbf{X}(kT) \tag{4.1}$$

where $\mathbf{Y}_\mathbf{n}^*$ is an adjustment term to the reference trajectory. As shown in Fig. 4-1, it is formulated as

$$\mathbf{Y}_\mathbf{n}^* = G_r(z)G_f(z)e(kT)_n \tag{4.2}$$

where $e(kT)_n$ is the tracking error at current sampling time from previous run, n is the present run number. As shown in Fig. 4-1, the function $G_r(z)$ can be express as:

$$G_r(z) = \frac{k_r z^{-N_1} Q(z)}{1 - Q(z)z^{-N}} \tag{4.3}$$

where $N = T_s/T$ is the number of sample per cycle, $N_1 = N - N_y$ is the number of known pure time delay, T_s is the signal period, k_r is the repetitive gain which is tuned to have a 0.7 DC gain of the system, and $Q(z,z^{-1})$ is a zero phase low pass filter.

Although the influence of parametric uncertainty can be shown to be small on the repetitive controller, the influence of dynamic uncertainty can not be neglected. As a simplified model is used, some unknown system dynamics might exist at high frequencies, such as the stochastic disturbances and noises. Similar to other repetitive controller design, a zero-phase low pass filter $Q(z,z^{-1})$ is utilized in this investigation to relax the error convergence condition at high frequency range. Since the tracking error for the last run is known beforehand, the non-causal zero-phase low Pass FIR filter $Q(z,z^{-1})$ can be constructed as follows:

Firstly, a causal low pass FIR filter is constructed with a specified number of filter term m+1, and cut-off frequency,

$$f_{FIR}(z^{-1}) = \alpha_0 + \sum_{i=1}^{m} \alpha_i z^{-i} \tag{4.4}$$

The coefficients $\alpha_i (i = 0, 1, ..., m)$ in (4.4) can be determined by using MATLAB function "FIR1". In simulation and experiment, m is chosen as 10.

Thus, the zero phase counter part $Q(z, z^{-1})$ is expressed as [129]

$$Q(z, z^{-1}) = \frac{\sum_{i=0}^{m} \alpha_i z^i + \sum_{i=1}^{m} \alpha_i z^{-i}}{\alpha_0 + 2\sum_{i=1}^{m} \alpha_i} \tag{4.5}$$

Let $z = e^{j\omega}$, the frequency response of equation (4.5) can be described as

$$Q(j\omega) = \frac{\sum_{i=0}^{m} \alpha_i e^{j(i\omega)} + \sum_{i=1}^{m} \alpha_i e^{-j(i\omega)}}{\alpha_0 + 2\sum_{i=1}^{m} \alpha_i} \tag{4.6}$$

Using Euler's identity, $e^{j\omega} = \cos(\omega) + j\sin(\omega)$, the equation (4.6) can be further expressed as

$$\begin{aligned} Q(j\omega) &= \frac{\sum_{i=0}^{m} \alpha_i (\cos(i\omega) + j\sin(i\omega)) + \sum_{i=1}^{m} \alpha_i (\cos(i\omega) - j\sin(i\omega))}{\alpha_0 + 2\sum_{i=1}^{m} \alpha_i} \\ &= \frac{\alpha_0 + 2\sum_{i=1}^{m} \alpha_i \cos(i\omega)}{\alpha_0 + 2\sum_{i=1}^{m} \alpha_i} \end{aligned} \tag{4.7}$$

As can be seen in equation (4.7), the imaginary part is cancelled. Thus the $Q(z, z^{-1})$ has zero phase property. Considering a DC (zero Hz) input signal of equation (4.7) ($\omega = 0$), we have the DC gain of $Q(z, z^{-1})$ to be 1.

The FIR filters $Q(z, z^{-1})$ are inherently stable, any bounded input results in a bounded output. Thus, all the open-loop poles of Q are inside the unit circle. The inclusion of Q in (4.3) helps to enhance the robustness of the system and preclude the instability that might be induced by parasitic poles [128]. This compensation will cut off the frequencies in the stop band that might excite the unknown system dynamics but minimize the errors associated with frequencies in the pass band. Thus, there is a trade-off between the tracking precision and system robustness [127]. When a lower cut-off frequency is used, the system will be more robust to high frequency disturbance and noise, but the tracking precision will be sacrificed. This will be further explained in later experimental study in this section.

The feedback system (3.24) and (3.25) presented in chapter 3 can be viewed as a causal filter $F(z)$ with magnitude characteristic $N(\omega)$ and phase angle $\theta(\omega)$. As explained in section 3.4, The convolution of controller gain $\mathbf{K_I}$ and N_y sample ahead prediction trajectory is fed into the feedback control loop. As shown in Fig. 3-5, the system phase delay is partially compensated by the phase lead from the prediction. The gains of $\mathbf{K_I}$ are fixed weighting coefficient for future set-points. If the set-point at current sampling time is viewed as the input signal, we can view this system as a FIR filter. In this section, $\mathbf{K_I}$ is treated as a causal FIR filter (without phase lead) gain array. Thus, the finite impulse response of the system can be approximated as the convolution of the finite impulse responses of the feedback system and a causal FIR filter. The magnitude and phase properties of system $F(z)$ can be obtained as Fig. 4-2.

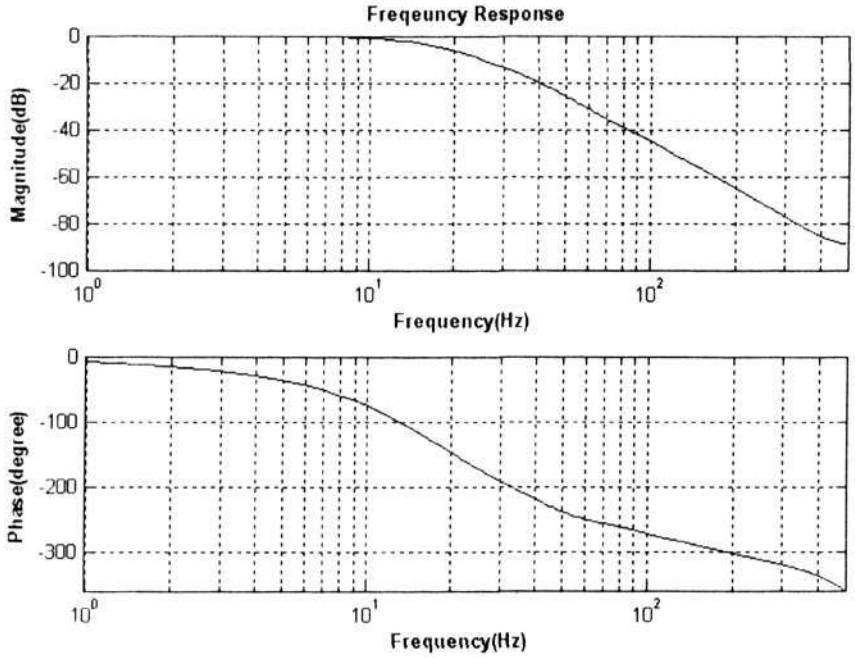

Fig. 4-2 Bode plot of system $F(z)$ without considering phase lead of $\mathbf{K_1}$

The impulse response of the system (3.24) and (3.25) can be represented as

$$F(z) = \sum_{k=0}^{\infty} b_k z^{-k} \tag{4.8}$$

where b_k , $k = 0, 1, \ldots$ are the Markov parameters (impulse response history). Assume there is a unity input at k = 0, the Markov parameters can easily be found by direct calculation using (3.24) and (3.25). Thus, the filter gain of (4.8) can be summarized as follow

$$b_k = \begin{cases} 0, & k = 0 \\ \sum_{i=0}^{k} \mathbf{K}_1(i) \cdot \left[\mathbf{C}(\mathbf{G} + \mathbf{H} \cdot \mathbf{K}_2)^{k-i} \mathbf{H} \right] & k > 0 \end{cases} \tag{4.9}$$

where $\mathbf{K}_1(i)$ is the parameters of the controller gain $\mathbf{K}_1$ (K_1= 0, if $i > N_y$).

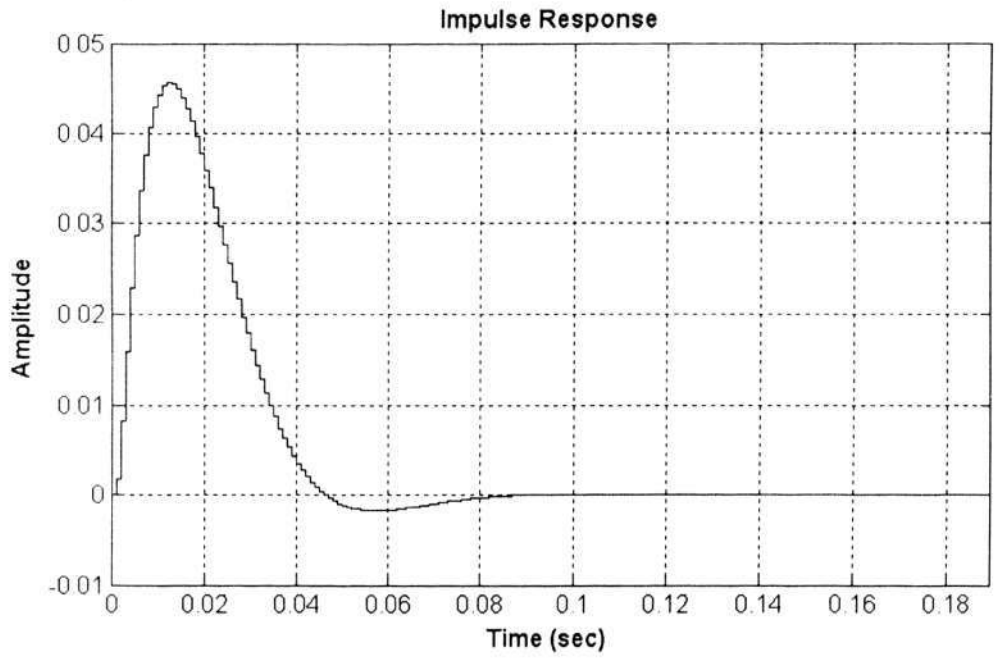

Fig. 4-3 Impulse response of the feedback system

The impulse response of the feedback system (3.24) and (3.25) is shown in Fig. 4-3. As can be observed from Fig. 4-3, the impulse response attenuates to 0 after 0.09s. The system's response can approximated with the truncated length ℓ of the impulse response of $F(z)$. In our design, the number of filter terms ℓ is chosen as 90.

By replacing z with z^{-1} in $F(z)$, denoted as $F(z^{-1})$, we obtain its non-causal counterpart, which has the reversed phase property of $F(z)$ [130]. The phase lead of the non-causal filter $F(z^{-1})$ is $-\theta(\omega)$, while its magnitude characteristics are the same as $H(z)$. Thus its inversed phase counterpart can be approximated with a FIR filter as

$$G_f(z) = F(z^{-1}) = \sum_{k=0}^{90} b_k z^k \tag{4.10}$$

The combination of $G_f(z)$ and $F(z)$ will produce zero phase properties. The phase cancellation result is shown in Fig. 4-4, the phase lead filter $G_f(z)$ has perfectly canceled

the phase lag of the system at most of the frequency range. The truncation has neglectable influence on the system, near perfect zero-phase is obtained at full frequency range.

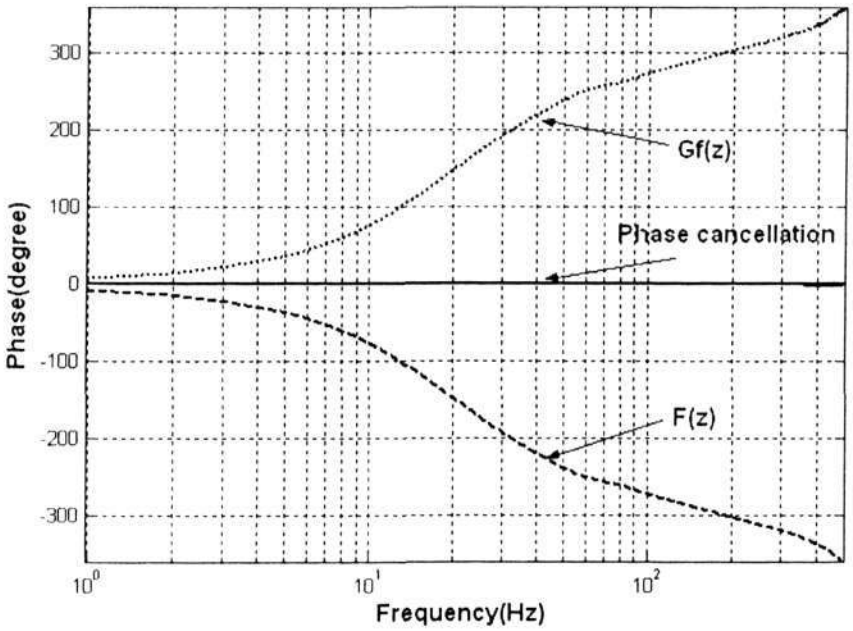

Fig. 4-4 Phase Cancellation result of the designed system

The design steps of the proposed control system can be summarized as:

1. obtain the impulse response of the controlled feedback system (equation 4.7)
2. use truncation to approximate the inverse of the system(equation 4.8 and Fig 4.3)
3. Set Cut-off frequency and term number m of filter $Q(z,z^{-1})$, obtained the parameters by using equation (4.4) and equation (4.5).
4. with the original MPC controller system, the repetitive MPC is obtained as shown in Fig 4.1

4.4 Robustness Stability Analysis

With the proposed controller and the nominal system model, a nearly perfect phase cancellation controller can be achieved. In practice, there exists model uncertainty. Thus,

the robustness against parameter variation needs to be examined. For the linear motion system, the load variation is one of the major factors that may influence the system performance. The stability and learning properties of the designed motion system under system uncertainties will be investigated in this section.

4.4.1 Stability Condition

In the basic MPC controller design, the stability is examined through the pole distribution in Chapter 3. As demonstrated in Fig. 3-3, all the closed-loop poles are placed inside the unity circle. The system is nominally stable. With the proposed learning control design method, the system stability condition is still determined by the feedback system (3.24), which remains the same. For repetitive controller design, the error contraction condition [131, 132] has been used by many researchers in designing a stabilizing controller.

With the control system described in Fig. 4-1, the transfer function for the repetitive control system can be obtained by viewing $y^*(kT)_n$ as the system input, Y as the system output. In which $y^*(kT)_n$ is the latest set-point to the system from the MPC controller

$$\frac{Y(Z)}{Y^*(Z)} = \frac{G_r(z)G_f(z)F(z)}{1+G_r(z)G_f(z)F(z)} = \frac{k_r Z^{-N} Q(z,z^{-1})G_f(z)F(z)}{1-Z^{-N}Q(z,z^{-1})(1-k_r G_f(z)F(z))} \tag{4.11}$$

Setting the denominator in (4.11) to 0, we have the characteristic equation of the repetitive control system as

$$1-Z^{-N}Q(z,z^{-1})(1-k_r G_f(z)F(z)) = 0 \tag{4.12}$$

For the system to have no enclosure of point $(-1, j0)$ by the Nyquist diagram of $-Z^{-N}Q(z,z^{-1})(1-k_r G_f(z)F(z))$, as z goes over the Nyquist path in the z-plane, we should have

$$\left|Z^{-N}Q(z,z^{-1})(1-k_rG_f(z)F(z))\right|<1 \tag{4.13}$$

As $\left|Z^{-N}\right|=1$,the regeneration spectrum $R(z)$ [133] should be smaller than 1

$$R(z)=|Q(z,z^{-1})(1-k_rG_f(z)F(z))|<1 \tag{4.14}$$

The equation (4.14) is also known as the error contraction condition for repetitive control.

The relationship of regeneration spectrum to the absolute stability of the system is established by the amplitude-phase method of stability analysis, which is essentially an application of Nyquist criterion to time-delayed systems [134].

$$N=Z-P \tag{4.15}$$

Equation (4.14) guarantees no enclosure of point $(-1, j0)$ by the Nyquist diagram , so $N = 0$. As the original system without repetitive control is stable, there are no poles of the characteristic equation that are out side the unit circle. So we can have P = 0. Thus, the number of zeros of the characteristic equation that outside the unit circle

$$Z=N-P=0 \tag{4.16}$$

So the system (4.11) is stable for all values of the time delay. Thus, the stability conditions of the whole system are

(1) All the poles of system resides in the unit circle

(2) $\left|Q(z,z^{-1})(1-k_r\cdot G_f(z)\cdot F(z))\right|<1$

According to the stability condition 2 (error contraction condition), the designed repetitive control system needs to satisfy both magnitude and phase properties. It can be further interpreted as the magnitude at all frequency needs to be smaller than 2, which also means the phase of the compensated system should remain within $(-90^\circ, 90^\circ)$ [32]. Only the frequency components that satisfy condition (4.14) will create monotonic decay of error for these components.

4.4.2 Load Variation

To examine the robustness of the repetitive control system, the stability of the system with load variation is examined. Assume there is a 100% to 300% load variation of the Mass M in Table 2-1, the influence of load variation on the phase properties is demonstrated in Fig. 4-5. For a nominal system, the designed control system provides zero phase learning properties. When the system load changes, the phase properties of the designed system will be different. As shown in Fig. 4-5, extra phase delay will be introduced at high frequency range. As long as the phase difference is within the interval [-90°,90°], the output error can be used to correct the input [128, 135]. A suitable learning gain k_r small enough to satisfy (4.14) can always be found [136].

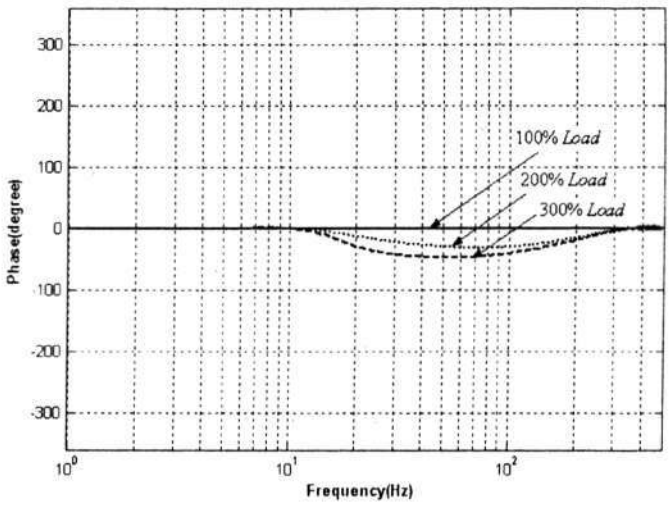

Fig. 4-5 Phase properties with 100% to 300% load variation

The error contraction condition with different loads at different frequency is shown in Fig. 4-6. The error contraction condition will be slightly influenced when the load changes, assuming there is a 100% to 300% load variation. In this simulation, a full pass filter is used (Q = 1). As demonstrated in Fig. 4-6, no violation is observed in the whole frequency range.

This error contraction condition can be understood in a simpler way. The tracking error history can be decomposed into a combination of harmonics, which can be viewed as the control result of the input signal at different frequencies. If the magnitude is larger than 1, the system will produce positive feedback instead of negative feedback [32]. The output error that used for correction will make the error larger. In another word, the system is unstable from a steady-state frequency response point of view [128].

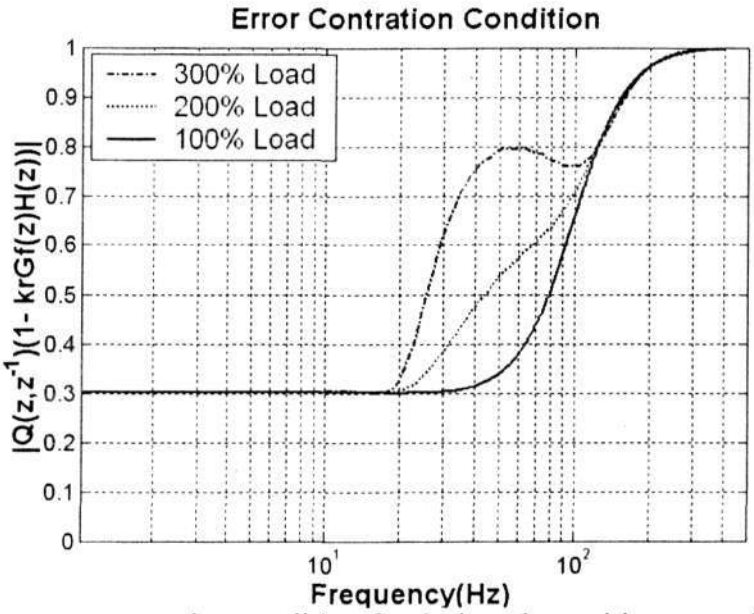

Fig. 4-6 The error contraction condition for designed repetitive control system with load variation

4.4.3 Parameter Variation

To study the long term learning stability of the proposed controller, the effects of parameter variation is studied in this section. As shown in Fig. 4-7, the error contraction condition is slightly influenced when the system inductance L changes from 50% to 200%. Similar results are obtained in Fig. 4-8 and Fig. 4-9, when the system resistance R

and force constant K_f changes from 50% to 200%. The error contraction condition (4.14) is not violated under these parameter variations.

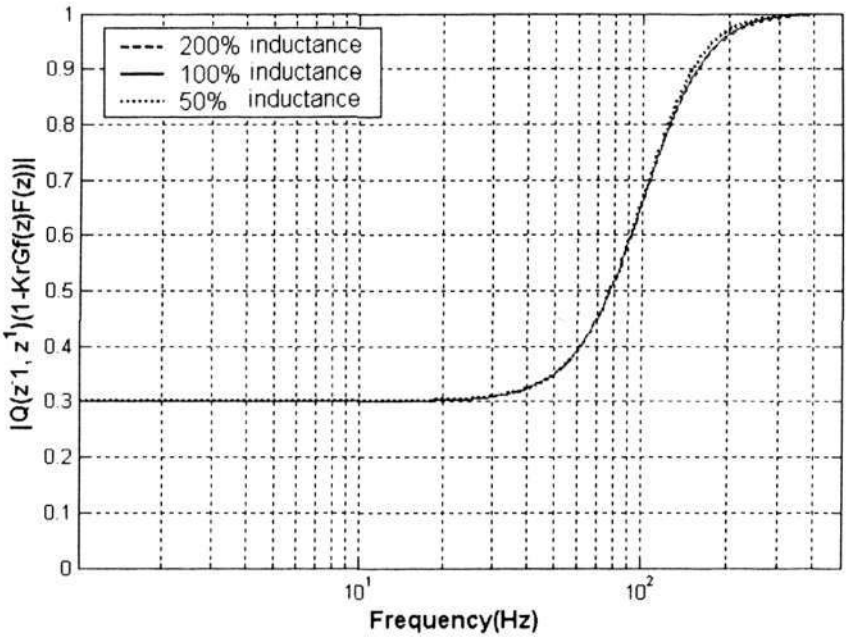

Fig. 4-7 The error contraction condition for designed repetitive control system with parameter L variation from 50% to 200%

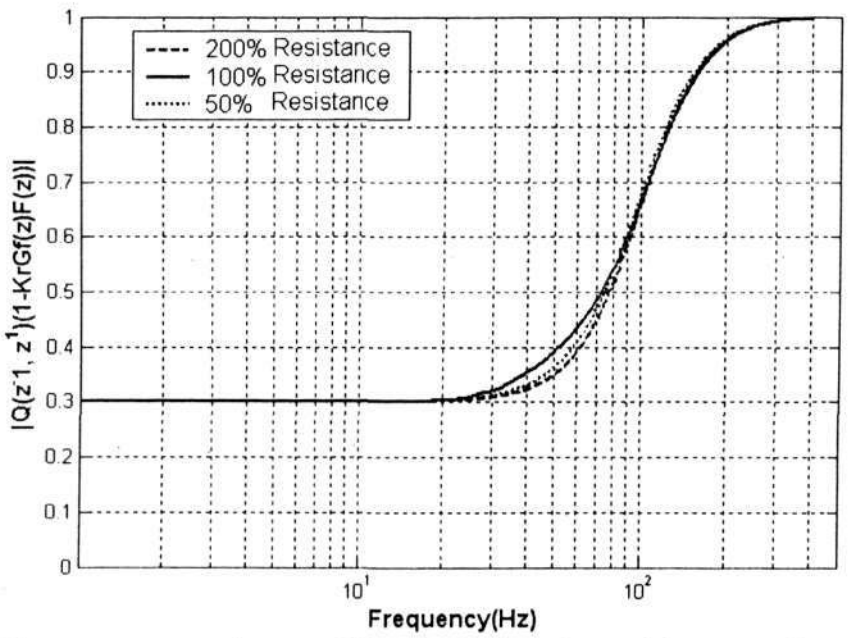

Fig. 4-8 The error contraction condition for designed repetitive control system with parameter R variation from 50% to 200%

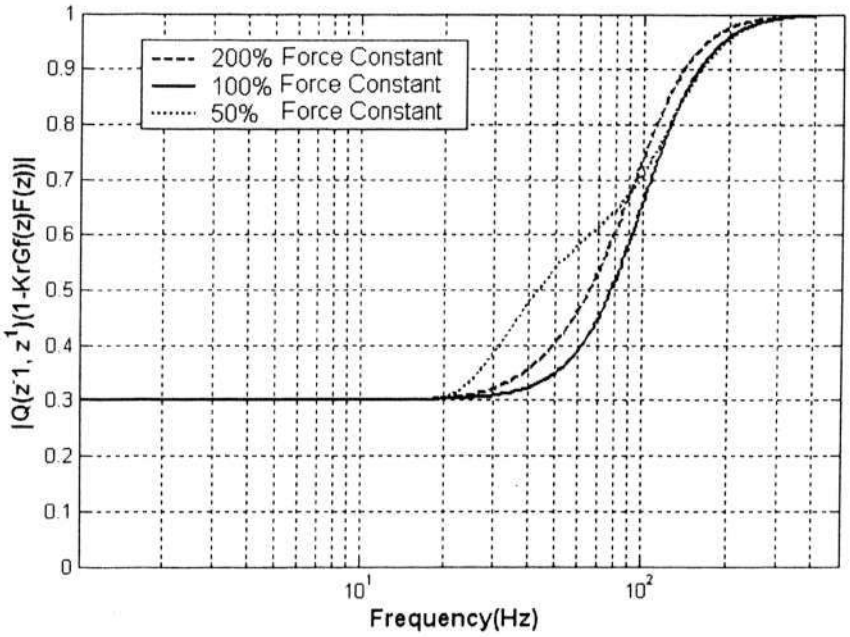

Fig. 4-9 The error contraction condition for designed repetitive control system with parameter K_e variation from 50% to 200%

As shown in Fig. 4-4, the proposed repetitive model predictive controller has zero phases characteristic. Theoretically, full frequency range learning can be implemented. However, a low pass filter is still needed to guarantee error contraction from being violated at high frequency range, where unknown system dynamics might exist. The suitable cut-off frequency of the designed control system will be investigated through experiment in later section.

4.5 Experimental Results

To study the effectiveness of the proposed control scheme, various experiments have been conducted. As the most significant friction disturbance occurs at the speed reversal point, sinusoidal and triangle wave trajectories are used in this study for the performance evaluation.

4.5.1 Dynamic Response

Fig. 4-10(a) shows the experimental results of the tracking error history with the proposed control approach. The experiment is implemented in the way as shown in Fig 4.1. In which, $G_f(z)$ is obtained directly from equation (4.7). With the cut-off frequency set as 200Hz, a 25 terms (m = 12) Q filter is obtained by using equation (4.4) and (4.5). The system with nominal load is required to track a sinusoidal motion with 1cm amplitude and 0.5Hz frequency. Due to the nonlinear friction disturbances, the conventional MPC can not track the profile perfectly. This can be observed from the first run of the tasks in Fig. 4-10(a), and the corresponding tracking error in Fig. 4-10(b). There are mainly two error components. One is caused by the phase delay, and the other is caused by the friction force at velocity reversal point. From the results of second and subsequent runs shown in Fig. 4-10(a) and Fig. 4-10(b), it is observed that the proposed RMPC algorithm suppressed most of these tracking errors after the first few runs. On the other hand, the tracking error due to stand still caused by the nonlinear friction at velocity reversal point can only be attenuated gradually.

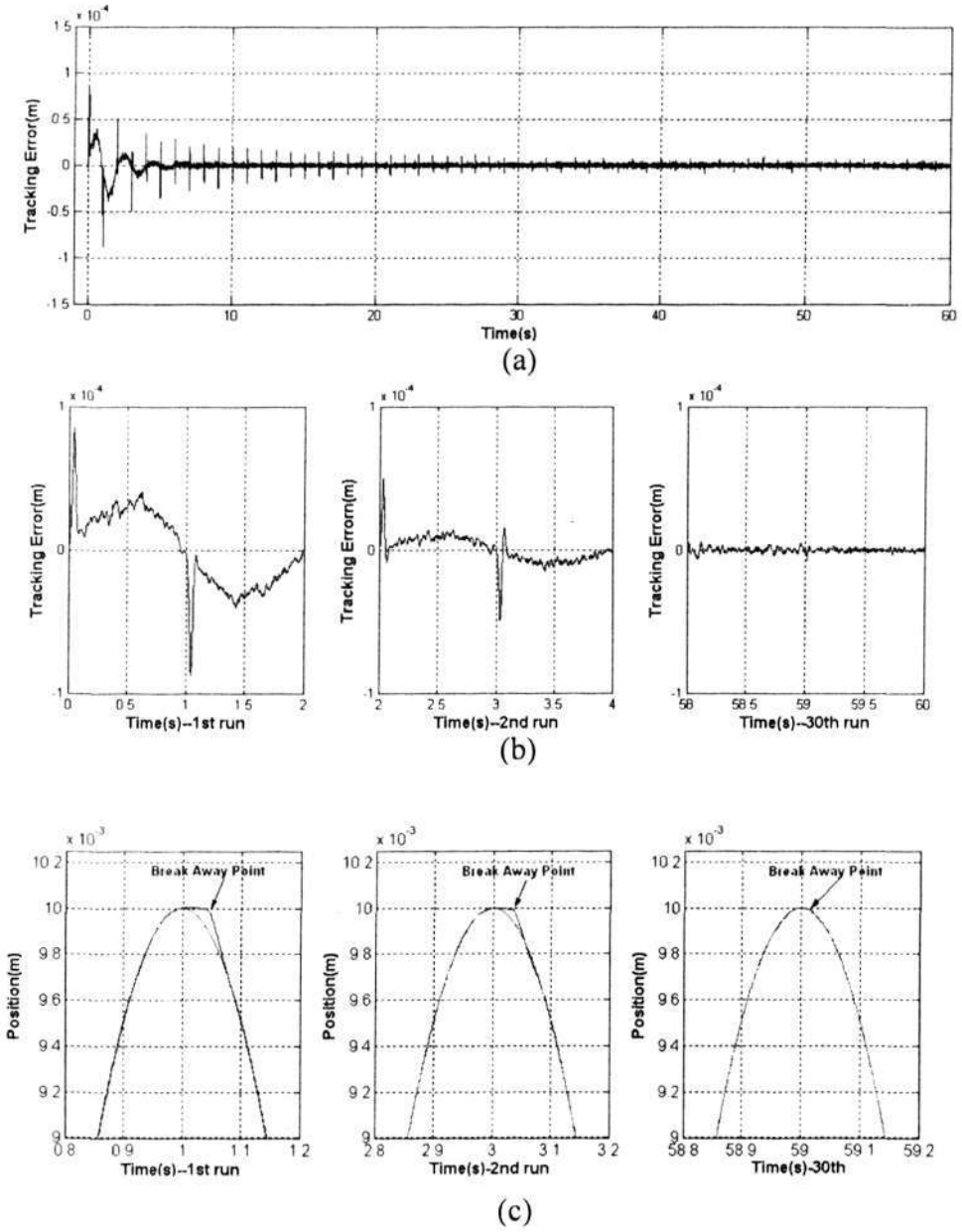

Fig. 4-10 (a)Experimental result of tracking error of RMPC with sinusoidal trajectory (b)Zoom in View of tracking error at 1st, 2nd and 30th run.(c) Zoom in View of position reference and result at 1st, 2nd and 30th run.

Fig. 4-10(b) shows the tracking errors for the 1st, 2nd and 30th runs. From the results, it is clear that the proposed approach successfully suppresses the tracking error. The corresponding close up view of the reference and actual responses are shown in Fig. 4-10(c).The first figure of Fig. 4-10(b) and Fig. 4-10(c) show the initial run of the motor. It can be observed that when the system experiences a velocity reversal at the position

boundary whereby the Coulomb friction dominates, the output has a large tracking error due to the significant changes in the friction force. As shown in Fig. 4-10(b) and Fig. 4-10(c) for the second and 30th run, the tracking error will be attenuated to a negligible level after several runs with the repetitive control action.

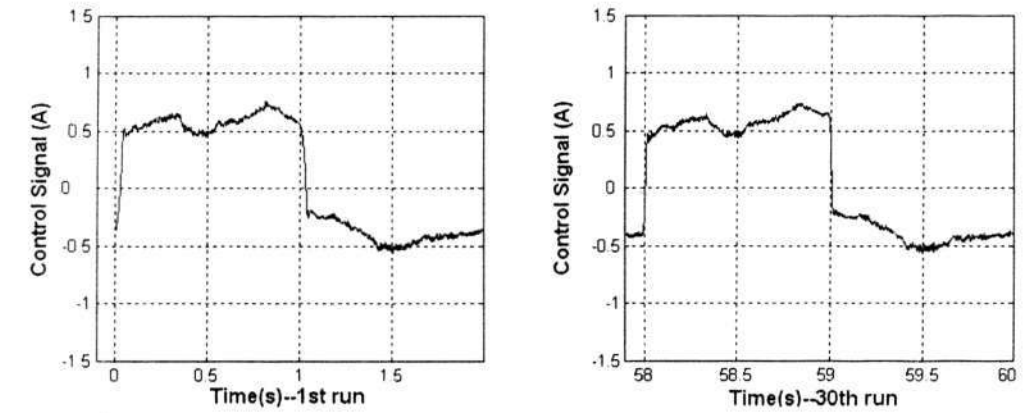

(a)

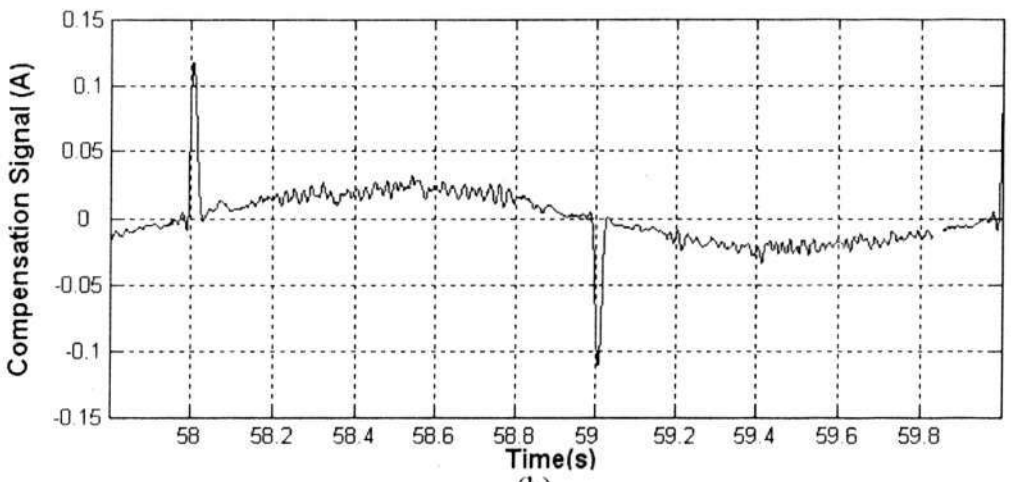

(b)

Fig. 4-11(a) Control signal at 1st run and 30th run (b) Compensation signal at 30th run

The control signal at 1st run and 30th run are shown in Fig. 4-11 (a) and the compensation signal at 30th run is shown in Fig. 4-11 (b). From the figure, it is observed that a large compensation signal is obtained at the velocity reversal point after learning.

To further examine the effectiveness of the proposed controller, a different reference trajectory is used. The dynamic response of the prototype system with a triangle reference

waveform of 1mm amplitude and 0.5Hz frequency is next investigated. The experimental results are shown in Fig. 4-12. As shown in Fig. 4-12(b) and Fig. 4-12(c), the system is suffered from severe friction influence at the velocity reversal point. Because of the sudden change in the speed direction, the linear motor drive can not follow the desired trajectory immediately. A spike with $80\mu m$ amplitude is observed in the tracking error history in the first run. After several learning cycles, the maximum tracking error contracts to around $10\mu m$. It has been significantly reduced from its original value. As the feed-forward part of a MPC controller has a low-pass filter effect on the desired trajectory. The high frequency part of the triangle part is filtered out. The Average RMS tracking error is around 1um for the whole tracking process. Considering the nature of MPC controller and real application needs, it is a satisfactory result.

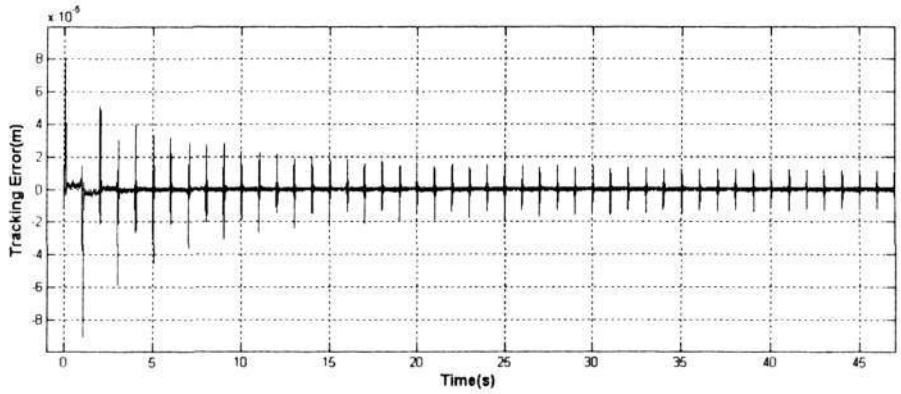

(a)

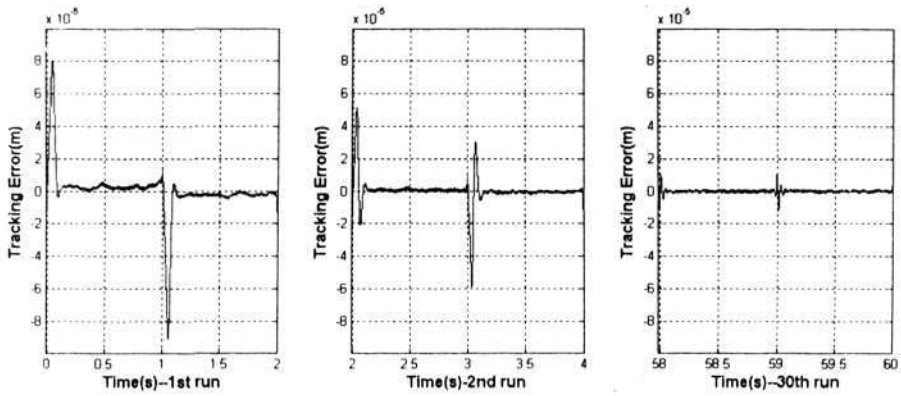

(b)

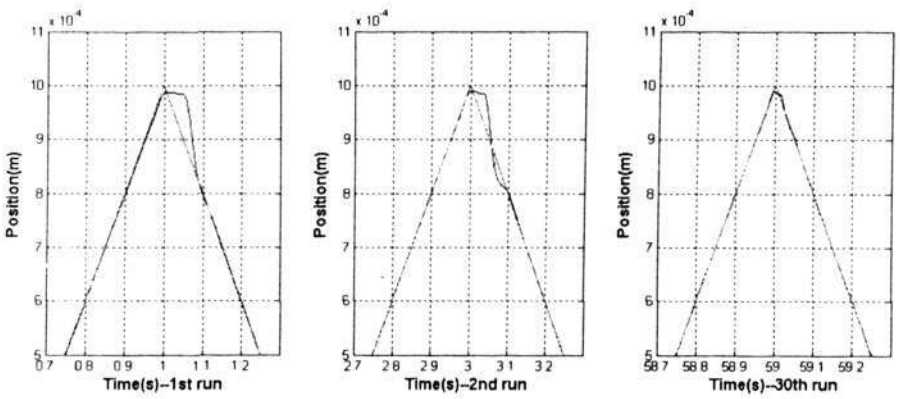

(c)

Fig. 4-12 (a)Experimental result of tracking error of RMPC with Triangle Waveform (b) Zoom in View of tracking error at 1st, 2nd and 30th run. (c) Zoom in View of position reference and result at 1st, 2nd and 30th run.

4.5.2 Effects of Filter Cutoff Frequencies on Tracking Performance

As mentioned in the robustness analysis in section 4.4, a low pass filter is needed to guarantee error contraction from being violated at high frequency range, where unknown system dynamics might exist. With a suitably designed filter, the long term stability of the repetitive controller can be guaranteed. On the other hand, the repetitive controller only minimizes the frequency components of the tracking error that are located in the pass band of the filter. Selection of a wider bandwidth will potentially provide better tracking performance. In this section, the influence of the filter on the learning efficiency is investigated.

Fig. 4-13 (a) and Fig. 4-13 (b) show the tracking performance of the proposed control approach with different cut off frequencies of the low pass filter Q in (4.5). As shown in Fig. 4-13, the maximum and RMS tracking errors are monotonic. While the RMS tracking error remains almost the same, the maximum tracking error has more deviation and improves with increase filter bandwidth from 50Hz to 400Hz. From the results, it is also observed that the system yields no significant improvement when the bandwidth is larger than 200Hz. To reduce the effect of noise sensitivity on the system, 200Hz is selected for the system. As can be observed from Fig. 4-13 (a), the maximum error is reduced to less than 10 μm after 20 runs. This is well below the initial error of 90 μm at the first run. Similarly, the rms tracking error also decreases rapidly during the first few runs and reaches a steady state value of 1 μm after 20 runs.

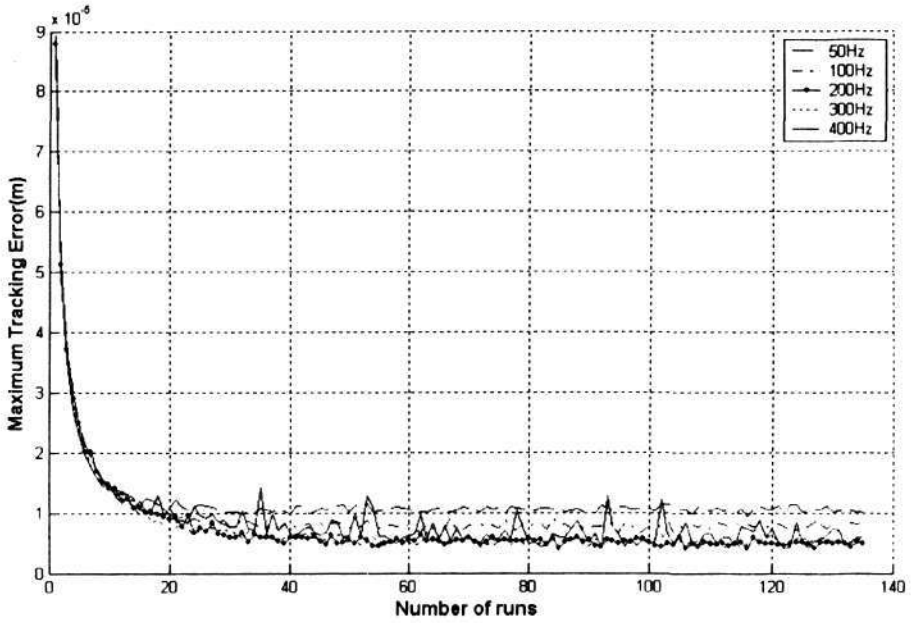

(a)

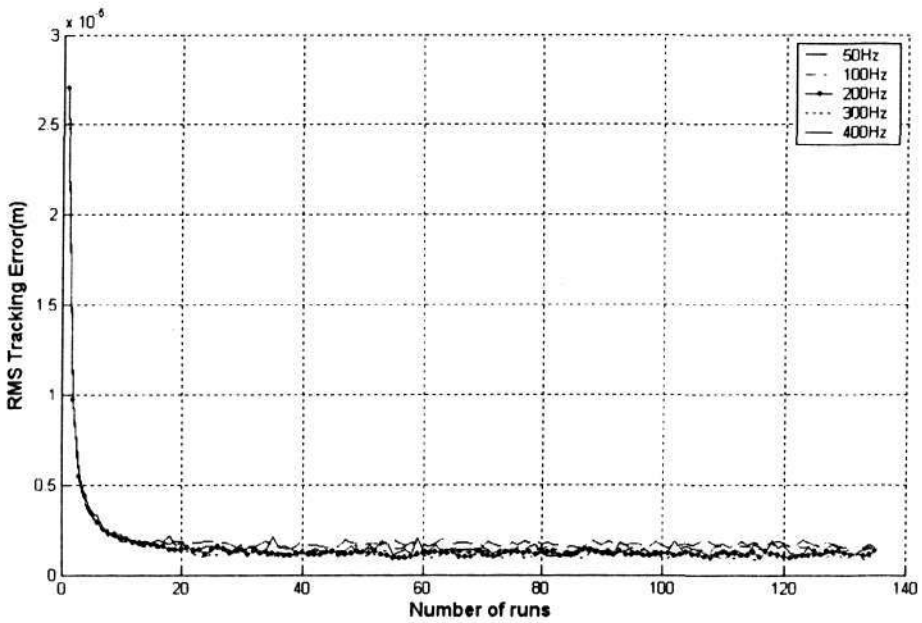

(b)

Fig. 4-13 Experimental result of (a)Maximum tracking Error and (b) RMS tracking error

4.5.3 Comparison with P-type Repetitive controller

P-type learning controller has been extensively studied and used for performance comparison in the literature [137-139]. In the experiment, the performance of the proposed controller is compared with P-type repetitive controller through learning efficiency study. The tracking error history without phase compensation is combined with the desired trajectory. Similarly, the DC gain of the repetitive controller is chosen as 0.7. As shown in Fig. 4-14, the p-type repetitive controller achieves best performance at 50Hz. The stability condition (equation 4.12) of the system will be violated if a cut off frequency of 100Hz is chosen. As shown in the figure, the tracking performance starts to deteriorate after certain runs. The tracking error will diverge with time passes.

Comparing the experimental results in Fig. 4-13 and Fig. 4-14, it is clear that the proposed controller can provide larger learning frequency range, which in turn gives the learning control system a higher tracking accuracy. If the best results from both methods are compared, the proposed controller has about 50% improvement over the P-type repetitive controller in terms of maximum tracking error. For RMS tracking error, it also provides around 30% improvement. This finding agrees with the frequency analysis in previous section.

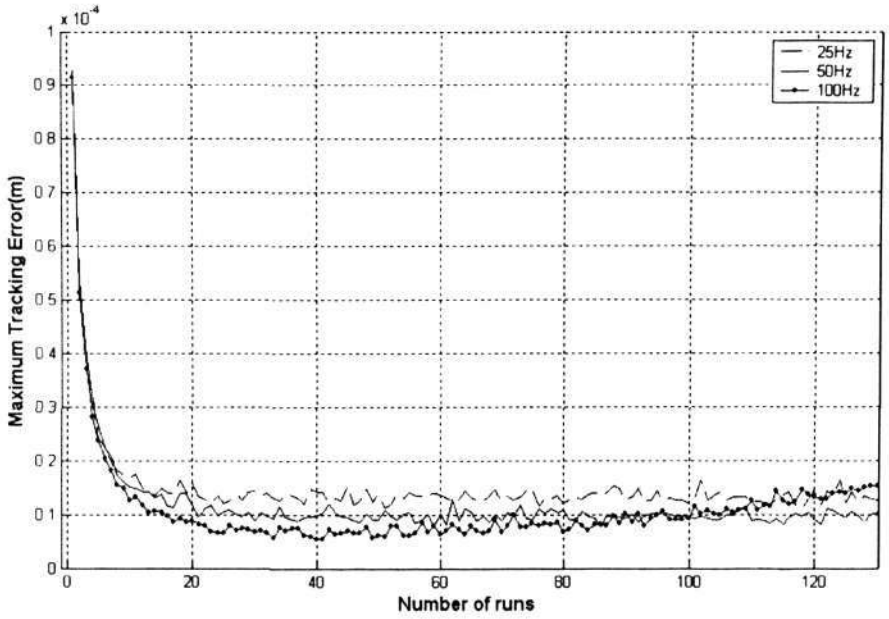

(a)

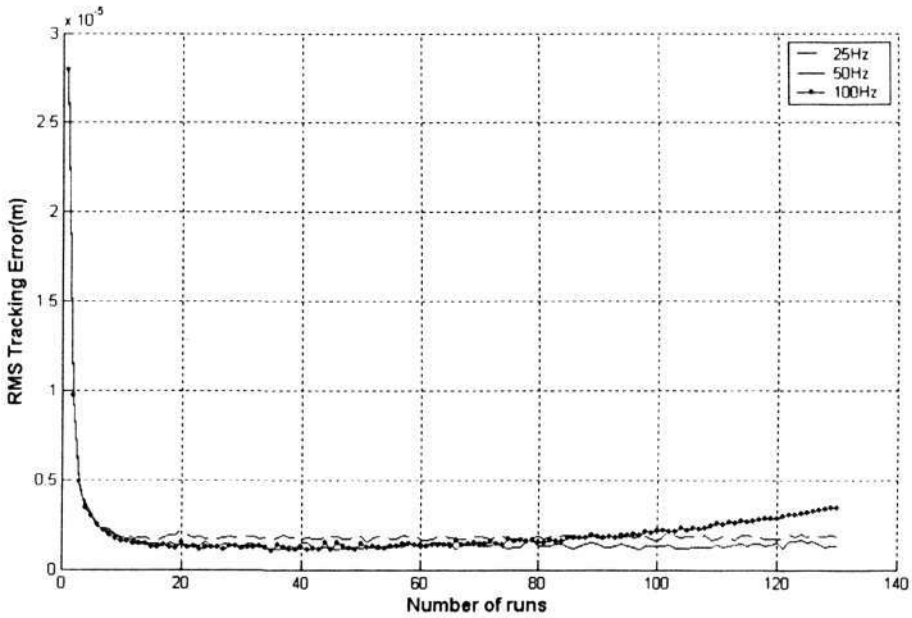

(b)

Fig. 4-14 Experimental result of P-type repetitive controller (a) Maximum tracking error and (b) RMS tracking error

4.5.4 Tracking Performance under Different Loadings

To investigate the robustness of the proposed approach, the tracking performance of the system under different constant loading conditions is studied. For the experiment, the sinusoidal profile has been used with a constant loading of nominal load (i.e 100%). The

maximum and RMS tracking errors for each run are recorded. Subsequently, the load is changed to 200% and 300%. The experimental results for the three tests are shown in Fig. 4-15. From the results, it is observed that the system has good robustness and shown little performance degradation with load increased from 100% to 300%. The maximum error is about $7\,\mu m$ and the RMS error is about $2\mu m$ in the steady state. The increase in the error is observed to be less than $1\mu m$ when the load increased to 300%.

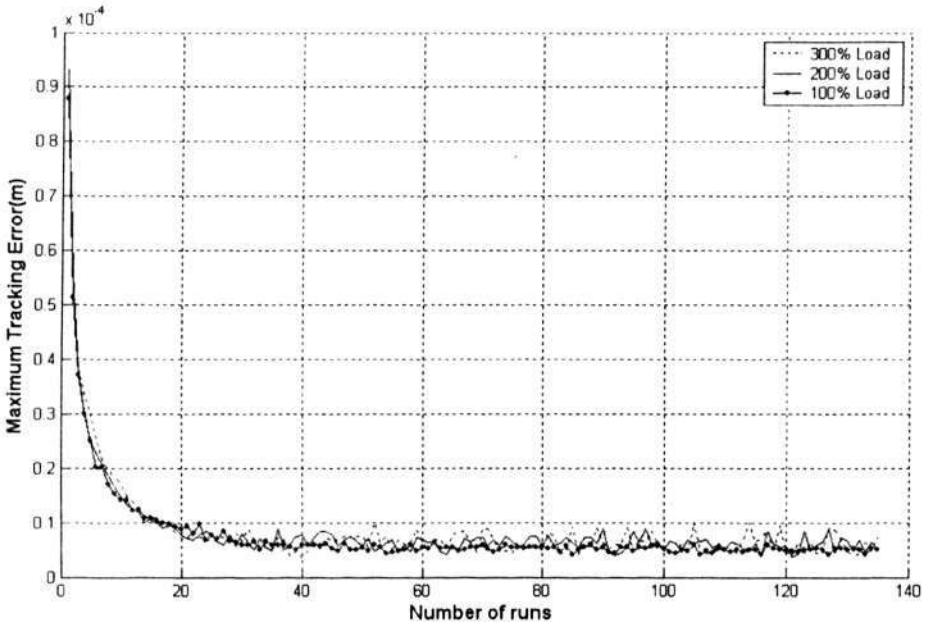

(a)

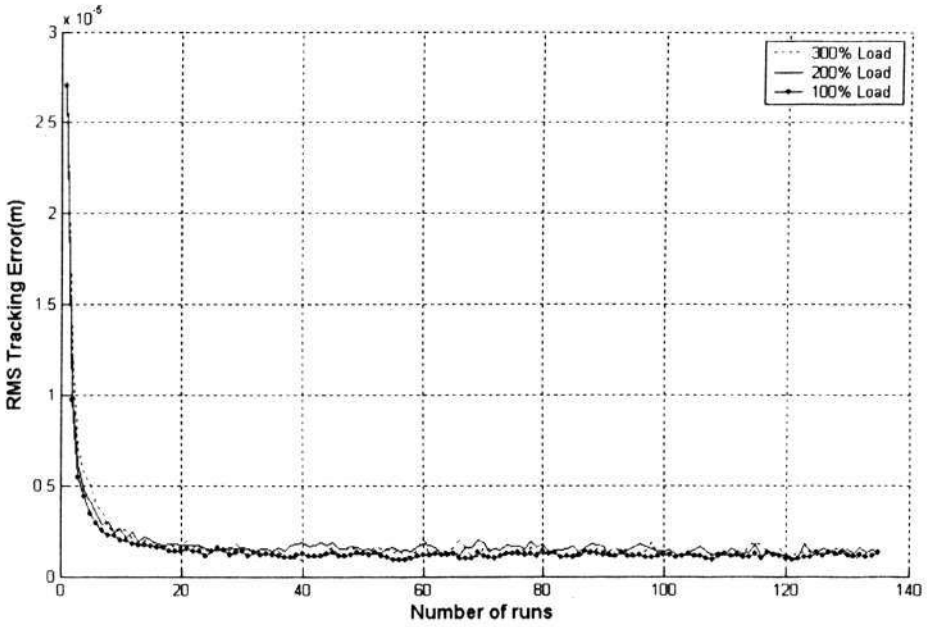

(b)

Fig. 4-15 Experimental result with 100% to 300% load variation (a) maximum tracking error (b) rms tracking error

4.5.5 Effects of Different Reference Trajectories on Tracking Performance

Fig. 4-16 shows the experimental results with the reference sinusoidal trajectory's frequency varied from 0.25 to 2 Hz while the reference amplitude remains the same at 1 cm. For ease of comparison, the tracking error normalized to its initial value before learning is used. It is observed that the percentage of RMS tracking error reduced is smaller for lower reference frequencies. When the trajectory frequency increases, the corresponding speed of the motor will also increase. At higher speed, the breakaway point resulting from the friction moves towards the peak speed at the reversal point. Consequently, the controller requires less time to mitigate the tracking error and it results in a faster convergent to the steady state error.

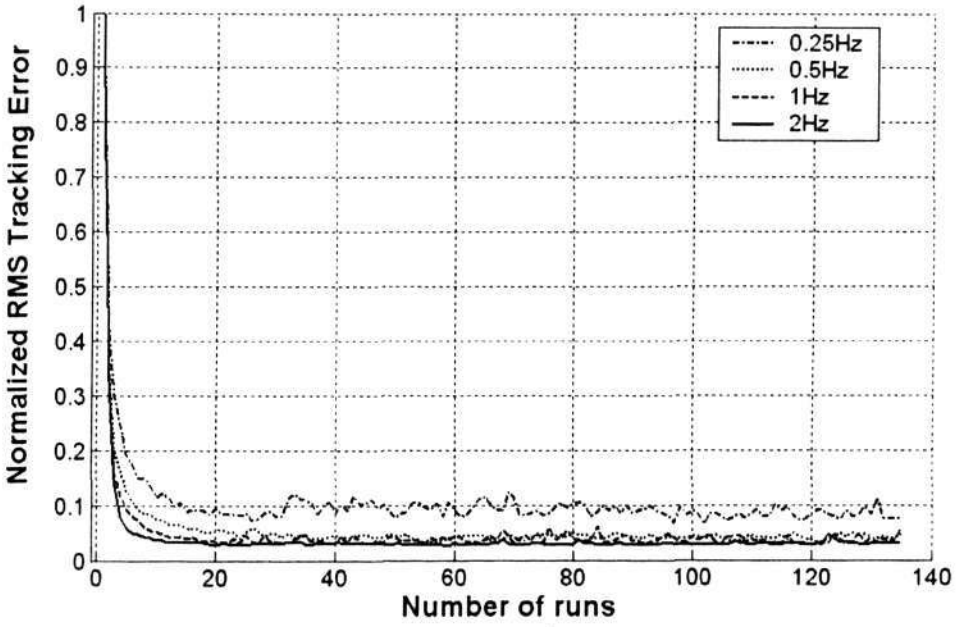

Fig. 4-16 Tracking performance under different reference frequencies

The experimental results of different trajectory amplitudes with the same frequency of 0.5Hz are shown in Fig. 4-17. For ease of comparison, the tracking error normalized to its initial value before learning is used. From Fig. 4-17, it is observed that the convergence rate is dependent on the reference amplitude. Larger amplitude leads to faster convergent to the steady state error. For example, when the reference amplitude is 100 μm, it takes about 40 runs to reach the steady state. If the amplitude is increased to 5 cm, it takes only 5 runs. It may be observed that with a larger reference amplitude, the speed of the motion will be increased. This result agrees with the earlier observation in Fig. 4-16, i.e. the influence of friction force at speed reversal will be less severe at high speed than low speed. Moreover, there is a limit on the speed of the profile. As shown in Fig. 4-17, when 50um amplitude is applied, the repetitive controller will diverge after a few runs. In this case, the stick-slip phenomenon dominates the whole learning process. This leads to an ineffective learning.

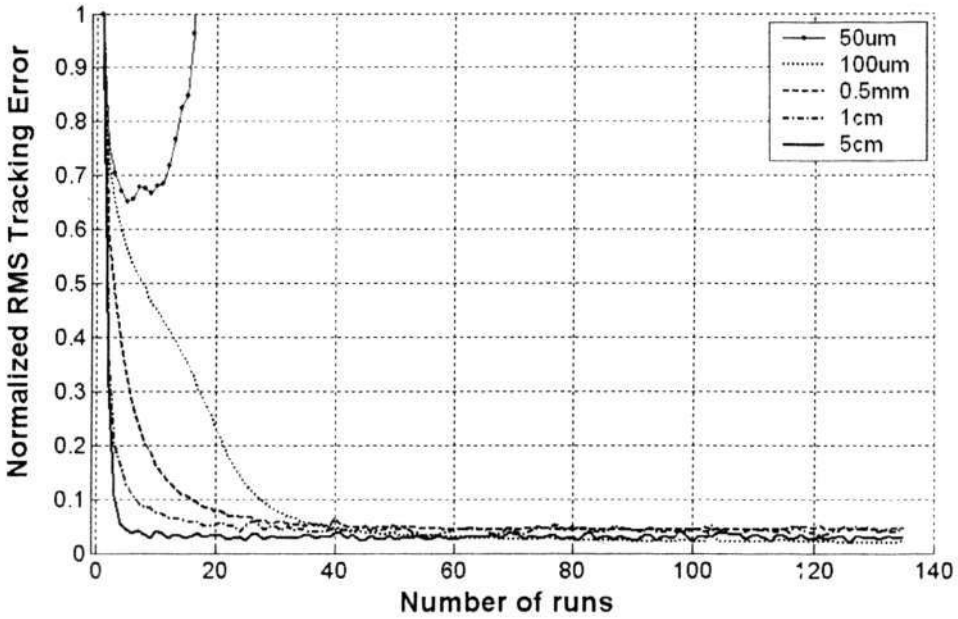

(b)

Fig. 4-17 Normalized converging rate comparison under different reference amplitudes

The tracking performance with a sinusoidal profile of 100um amplitude is demonstrated in Fig. 4-18. In this figure, it is found that the break away point is relatively farther from the peak of the sinusoidal wave. Before the break away point arrives, the object will move certain distance. The spring-like effect before gross-sliding is studied in [140]. This kind of microscopic motion is usually called pre-sliding motion. The transition between sticking and sliding has been addressed in [141]. This type of dynamics becomes more significant at micro-meter level. Thus, comparing Fig. 4-18 with Fig. 4-10, the pre-sliding motion is more obvious when smaller amplitude is applied. As the friction force at the beginning of the motion has a relationship with the displacement, the changing rate of control signal in Fig. 4-18 at velocity reversal point changes is slower than that in Fig. 4-11 after learning. This can also be explained by the pre-sliding motion.

As mentioned earlier, there is a limit on the lower speed of the system. If at the start of the learning process, the torque is not big enough, the motor will get stuck at zero velocity and fails to reach the desired position. The controller will increase the torque in the next run, and at some position in the dead zone, the torque is large enough to successfully pass through zero velocity. But then the final position is on the other side of the jump and the position has moved too far, larger than the original tracking error. As the same type of process in the opposite direction, the tracking error will diverge. For example, the repetitive controller will diverge after a few runs when the 50um amplitude sinusoidal wave is applied as shown in Fig. 4-17. To investigate this situation in greater detail, the tracking performance history with are depicted in Fig. 4-19. As shown in the Fig. 4-19, the tracking error will not converge as desired. Although the pre-sliding effect is also obvious in Fig. 4-18, the corrected torque didn't move the motor too far on the opposition direction. However, as shown in Fig. 4-19, the tracking error becomes larger due to the stick-slip phenomenon. The experimental results show that the pre-sliding motion becomes more obvious, and the occurrence of break away point becomes more uncertain. In this low speed situation, the stick-slip phenomenon dominates the whole learning process, and makes the learning impossible.

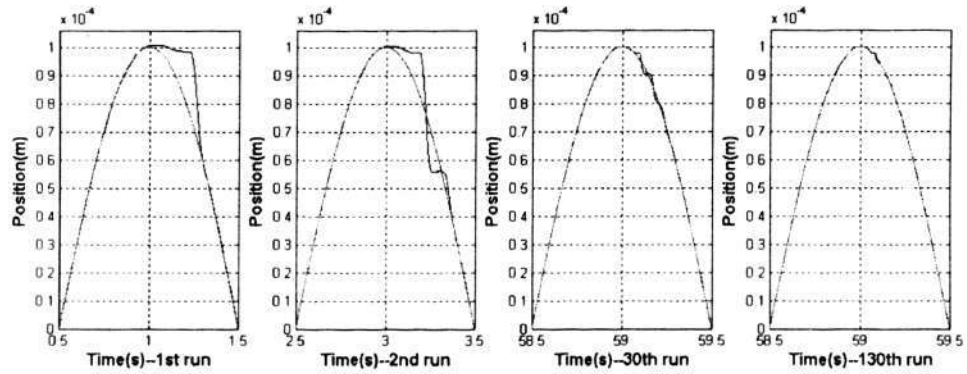

(a)

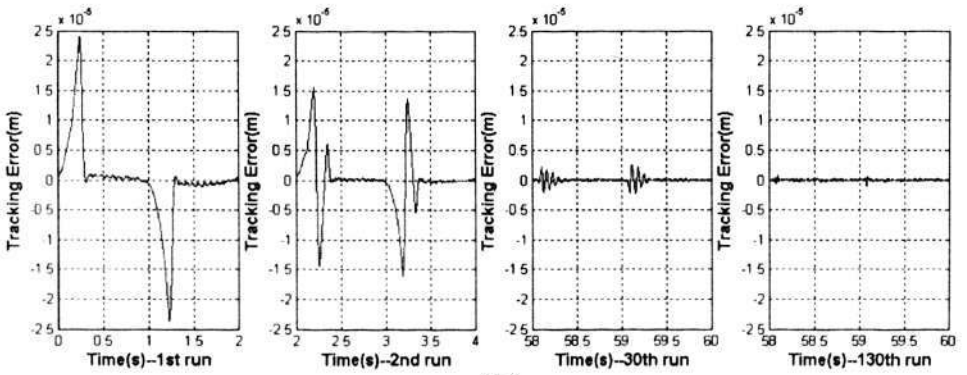

(b)

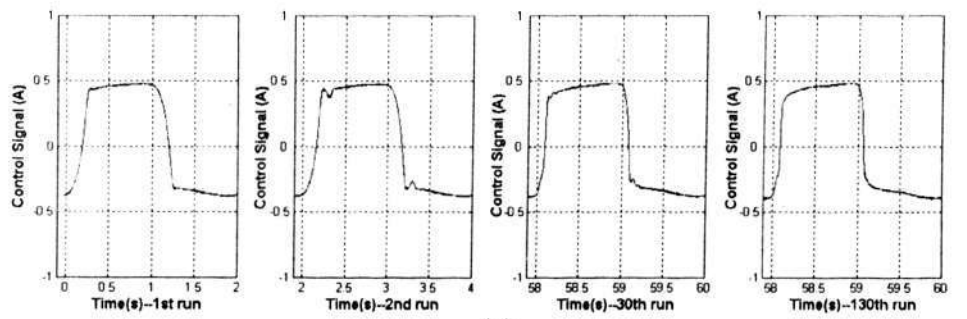

(c)

Fig. 4-18 Tracking performance of 100um amplitude sine wave (a) position tracking response (b) tracking error history (c) Control signal

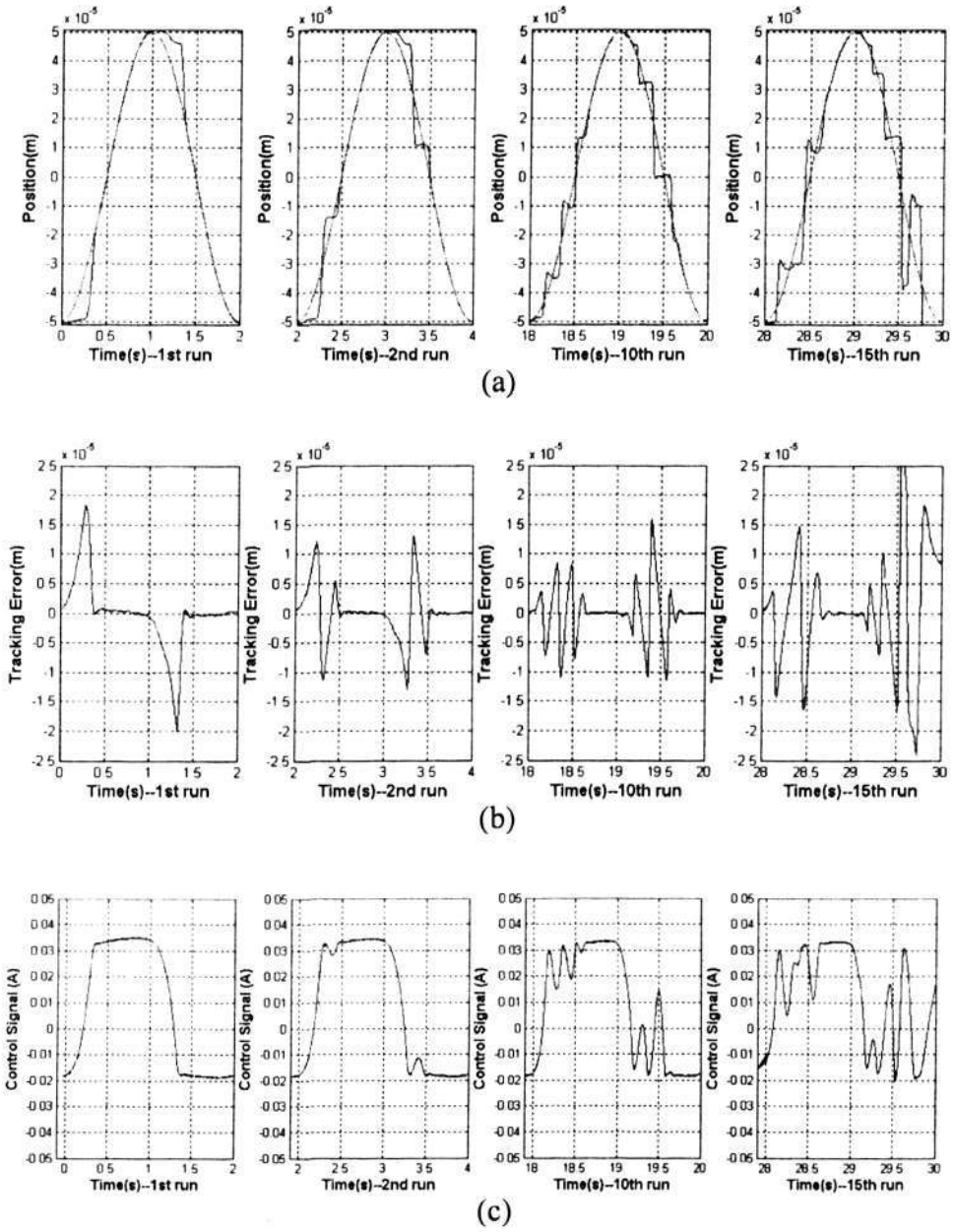

Fig. 4-19 Tracking performance of 50um amplitude sine wave (a) position tracking response (b)tracking error history(c)control signal

4.6 Conclusions

In this chapter, an advanced tracking algorithm is proposed for the motion control system to minimize tracking error for repetitive tasks. Better tracking performance is achieved by learning and compensating the disturbance forces over a series of runs adaptively. The repetitive model predictive control algorithm has zero phase learning property, which provides wider learning frequency range. A new trajectory generation mechanism, which combines the predicted disturbance and desired trajectory, is adopted for the MPC algorithm. Experimental results have demonstrated that the proposed approach has good performance in minimizing the influence of phase delay and the friction effect. Moreover, it is robust against load and parameter variations under varying operating conditions. Through the experimental study, the limit of the learning algorithm has been investigated. The study has shown that the proposed approach yields good performance for trajectories with wide velocity range.

Chapter 5

Model Predictive Control for Parallel Connected Inverters system

5.1 Introduction

As introduced in Chapter 1, there are mainly two control objectives for the parallel connected inverters system. One is tracking the voltage reference; the other is sharing the current equally among the inverters. The modelling and design become more complex when the number of inverter increases. In this thesis, a new scheme for parallel operation of inverters is introduced. Different from most methods that design the controller based on the transfer function approach, a state space model based MPC controller is designed in this chapter to systematically control the current and voltage. In [66], the use of the model predictive control (MPC) scheme to control an inverter is reported. In this thesis, we further develop the approach to control multiple inverters connected in parallel for an UPS. Different from previously reported works on MPC based single inverter [66] and motion control system [142] that are single input and single output (SISO) systems, the system under consideration is formulated as multi-input multi-output (MIMO) system with multiple optimization objectives. The effectiveness of the proposed algorithm for controlling the system will be examined in this chapter. The dynamic performance and the robustness property will be demonstrated with experimental results based on a laboratory prototype.

5.2 Control law formulation

In chapter 2, a Multi-input and Multi-output (MIMO) prediction model for parallel connected inverters system has been developed. With this prediction model, a model predictive control algorithm will be developed in this section. For the parallel connected inverters system, the multivariable predictive controllers requires a number of tuning parameters, namely a prediction horizon N_y for each of the output variables and a control horizon N_u for each of the input variables, as well as performance weights for each output and input. To maintain the ease of tuning, the cost function is simplified as follows:

1. The prediction horizons for output voltage tracking and current sharing are chosen to be the same.
2. The control horizons for the individual inverter are set to be the same.
3. The control weighting factors for all inverters are chosen to be the same.

Based on these criterions, the simplified cost function is formulated as follows:

$$\begin{aligned} J = {} & \alpha \sum_{j=1}^{N_y} \left\| V_0^*(kT+jT) - \hat{V}_0(kT+jT|kT) \right\|^2 \\ & + \beta \sum_{j=1}^{N_y} \left(\sum_{l=1}^{n-1} \left\| i_l(kT+jT) - i_{l+1}(kT+jT) \right\|^2 + \left\| i_n(kT+jT) - i_1(kT+jT) \right\|^2 \right) \\ & + \lambda \sum_{j=1}^{Nu} \left\| \Delta \mathbf{u}(kT+jT-T) \right\|^2 \end{aligned} \tag{5.1}$$

which is subjected to the constraints,

$$\Delta \mathbf{u}(kT+jT-T) = \mathbf{0}_{n\times 1} \qquad \forall\, j > N_u. \tag{5.2}$$

where n is the number of inverters, $\hat{V}_o$ is the prediction of output voltage of the system, α, β and λ are the weighting factors.

The cost function (5.1) comprises of three parts: the voltage tracking error; the inverter circulation current; and the quadratic measure of the control effort to limit large control signal variation. In (5.1), the current sharing optimization is formulated as the difference between adjacent inverters. The last term $i_n - i_1$ in the second objective of (5.1) is introduced to place the same weighting on i_1 and i_n as the rest. When these objectives are optimized together, the net effect is that each inverter is compared with the nominal average current $\frac{1}{n} I_0$.

Let $\Delta \mathbf{U} = \left[\Delta \mathbf{u}(kT) \quad \cdots \quad \Delta \mathbf{u}(kT + N_u T - T)\right]$ and perform minimization of (5.1) with respect to $\Delta \mathbf{U}$. After some algebraic manipulation, it can be proved that

$$\begin{aligned}\Delta \mathbf{U} = &\left(\alpha \mathbf{M}^T \mathbf{R}^T \mathbf{W}_1^T \mathbf{W}_1 \mathbf{R} \mathbf{M} + \beta \sum_{l=1}^{n+1} \mathbf{M}^T \mathbf{R}^T \mathbf{W}_{l+1}^T \mathbf{W}_{l+1} \mathbf{R} \mathbf{M} + \lambda \mathbf{M}^T \mathbf{M} \right)^{-1} \\ &\times \left[\alpha \mathbf{M}^T \mathbf{R}^T \mathbf{W}_1^T \mathbf{V}^* (kT) - \left(\alpha \mathbf{M}^T \mathbf{R}^T \mathbf{W}_1^T \mathbf{W}_1 + \beta \sum_{l=1}^{n+1} \mathbf{M}^T \mathbf{R}^T \mathbf{W}_{l+1}^T \mathbf{W}_{l+1} \right) \mathbf{\Phi} \cdot \mathbf{X}(kT) \right]\end{aligned} \tag{5.3}$$

where

$$\mathbf{M} = \begin{bmatrix} \mathbf{1}_{n\times 1} & \mathbf{0}_{n\times 1} & \cdots & \mathbf{0}_{n\times 1} \\ \mathbf{0}_{n\times 1} & \mathbf{1}_{n\times 1} & & \mathbf{0}_{n\times 1} \\ \vdots & & \ddots & \vdots \\ \mathbf{0}_{n\times 1} & \cdots & \mathbf{0}_{n\times 1} & \mathbf{1}_{n\times 1} \\ \mathbf{0}_{n\times 1} & \cdots & \cdots & \mathbf{0}_{n\times 1} \\ \vdots & & & \vdots \\ \mathbf{0}_{n\times 1} & \cdots & \cdots & \mathbf{0}_{n\times 1} \end{bmatrix}_{N_y \times (n \cdot N_u)} \qquad \mathbf{W}_1 = \begin{bmatrix} 1 & \mathbf{0}_{1\times n} & 0 & \cdots & 0 & \mathbf{0}_{1\times n} \\ 0 & \mathbf{0}_{1\times n} & 1 & \mathbf{0}_{1\times n} & \vdots & \vdots \\ \vdots & \ddots & \ddots & \ddots & 0 & \vdots \\ 0 & \cdots & \cdots & \mathbf{0}_{1\times n} & 1 & \mathbf{0}_{1\times n} \end{bmatrix}_{N_y \times (n+1)N_y}$$

$$\mathbf{W}_{l+1} = \begin{bmatrix} \mathbf{0}_{1\times l} & 1 & \mathbf{0}_{1\times(n-2)} & \mathbf{0}_{1\times l} & 0 & \mathbf{0}_{1\times(n-2)} & \cdots & 0 & \mathbf{0}_{1\times(n-2)} \\ \mathbf{0}_{1\times l} & 0 & \mathbf{0}_{1\times(n-2)} & \mathbf{0}_{1\times l} & 1 & \mathbf{0}_{1\times(n-2)} & \ddots & \vdots & \vdots \\ \vdots & \ddots & \ddots & \ddots & \ddots & \ddots & \ddots & 0 & \vdots \\ \mathbf{0}_{1\times l} & \cdots & \cdots & \cdots & \cdots & \cdots & 0 & 1 & \mathbf{0}_{1\times(n-2)} \end{bmatrix}$$

As the control law uses the receding horizon scheme, the control signal uses only the first element of (5.3), i.e.

$$\Delta \mathbf{u}(kT) = \begin{bmatrix} \mathbf{1}_{n\times 1} & \mathbf{0} & \cdots & \mathbf{0} \end{bmatrix}_{n\times N_u} \Delta \mathbf{U} \tag{5.4}$$

By substituting (5.4) into (5.3), the state space predictive control law can be formulated as

$$\Delta \mathbf{u}(kT) = \mathbf{K}_1 \mathbf{V}^*(kT) + \mathbf{K}_2 \mathbf{X}(kT) \tag{5.5}$$

where

$$\mathbf{K} = \begin{bmatrix} 1 & 0 & \cdots & 0 \end{bmatrix}_{1\times N_u} \left(\alpha \mathbf{M}^T \mathbf{R}^T \mathbf{W}_1^T \mathbf{W}_1 \mathbf{R} \mathbf{M} + \beta \sum_{l=1}^{n+1} \mathbf{M}^T \mathbf{R}^T \mathbf{W}_{l+1}^T \mathbf{W}_{l+1} + \lambda \mathbf{M}^T \mathbf{M} \right)^{-1}$$

$$\mathbf{K}_1 = \mathbf{K} \left(\alpha \mathbf{M}^T \mathbf{R}^T \mathbf{W}_1^T \right)$$

$$\mathbf{K}_2 = -\mathbf{K} \left(\alpha \mathbf{M}^T \mathbf{R}^T \mathbf{W}_1^T \mathbf{W}_1 + \beta \sum_{l=1}^{n+1} \mathbf{M}^T \mathbf{R}^T \mathbf{W}_{l+1}^T \mathbf{W}_{l+1} \right) \mathbf{\Phi}$$

5.3 Performance Analysis

As mentioned in section 5.2, the control objective is simplified to have the same prediction horizon, control horizon and weighting factors. Consequently, the general tuning rules for the multivariable MPC follows the tuning guidelines as in single objective MPC. In (5.1), there are three weighting factors α, β and λ. Hence, there is a trade-off among the different objectives. As their ratios can be determined by any two weighting factors, we let $\lambda = 1$ and adjust α, β in the sequel. The internal stability of the system can be examined by ensuring the poles of the characteristic equation

$$\left| z\mathbf{I} - (\mathbf{G} + \mathbf{H}\mathbf{K}_2) \right| = 0 \tag{5.6}$$

lie within the unit circle. In the experimental system, the parameters are tuned as $N_1 = 5$, $N_u = 2$, $\lambda = 1$, $\alpha = 4$, $\beta = 30$. Fig. 5-1(a) shows the movement of the pole when one of the weighting factors (i.e α or β) is varied. In this figure, the poles of the nominal system with the experimental parameters are denoted as "X". From Fig. 5-1(a), it is

observed that there are five nominal poles. Moreover, it is observed that the poles are located within the unit circle. The arrow in Fig. 5-1(a) shows the movement of the system poles when α changes from 0.0001 to 1000. The poles can be separated into two groups. One group is influenced by the voltage-tracking objective as α is varied; and the other is influenced by the current sharing objective as β is varied. As can be observed from Fig. 5-1(a), three of the poles are changing as α varies. Moreover, they approach the origin when α increases but move towards the stability boundary when α decreases yielding a slow responding system. If the weighting factor β is varied while α is fixed, similar conclusion can be drawn for current sharing performance as shown in Fig. 5-1 (b). The two poles that are stationary in Fig. 5-1(a) are now affected and move towards the origin while β changes from 0.0001 to 1000. With larger β, it leads to better regulated current sharing.

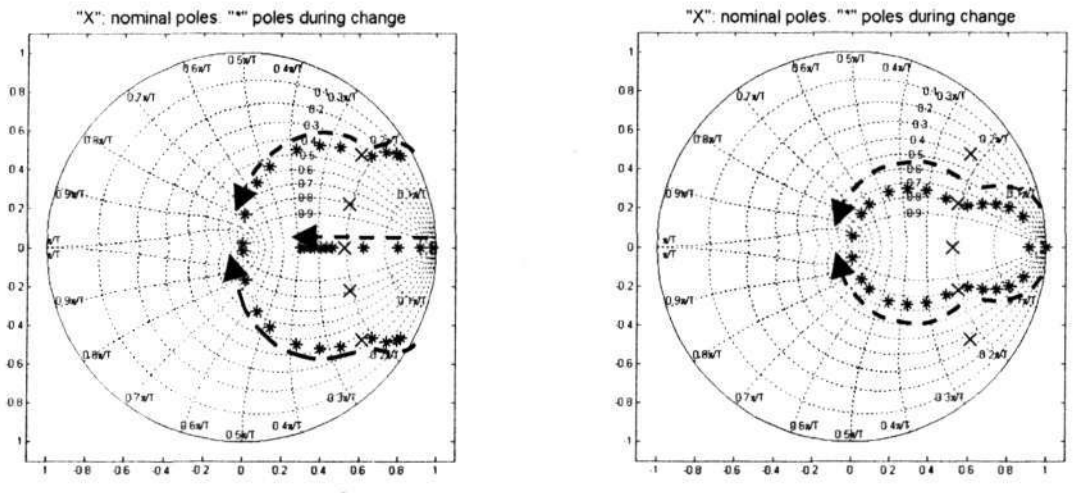

(a) (b)

Fig. 5-1 Closed-loop poles distribution (a) with α changes from 0.0001 to 1000. (b) with β changes from 0.0001 to 1000

Besides the feedback gain $\mathbf{K}_2$, the MPC controller also has a feed-forward gain matrix $\mathbf{K}_1$. This feed-forward gain matrix serves as a phase lead filter to correct the phase error that is inherent in the state feedback control. The bode plot of the control system with and without $\mathbf{K}_1$ is shown in Fig. 5-2(a). From the results, it is noted that the MPC controller performs better than state feedback controller as it achieves near zero phase tracking performance for a wider bandwidth.

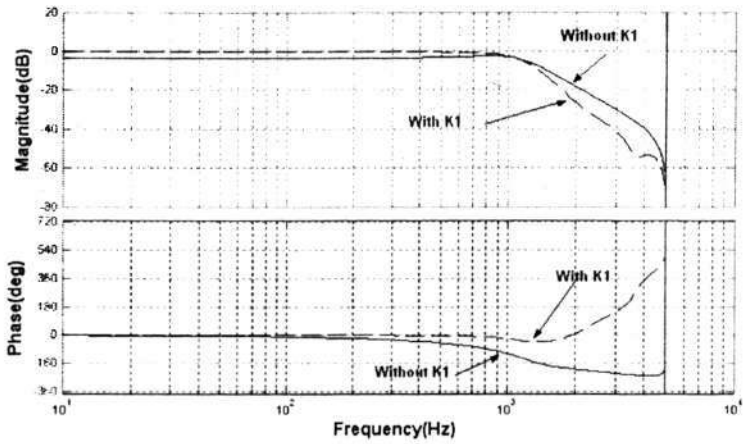

(a)

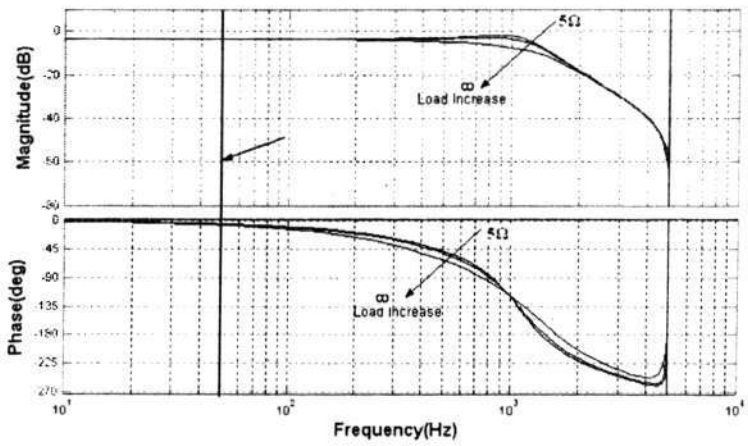

(b)

Fig. 5-2 Bode plots of the system (a) with and without feed-forward gain (b) under load variation

The influence of load variation on the system is demonstrated in Fig. 5-2(b). When the load changes from ∞ to $5\,\Omega$, the magnitude at the critical frequency 50Hz remains almost the same. Thus, the system will maintain same voltage amplitude when the load changes. Thus, it is concluded that the system is robust to load variation.

5.4 Hot Swap Design and Its Robustness Analysis

The objective of using parallel connected inverters system is to provide greater flexibility and fault tolerant capability. The ability to perform hot-swap operation is also highly desirable. When fault occurs, the faulty inverter needs to be replaced without shutting down the system that will affect the system's normal operation. Under this situation, the order of the system model changes. To make the controller suitable for the implementation, the controller structure needs to be modified. As we assumed that all the parameters for the inverters are the same, with equal effort on the feedback, it is expected to have identical rows of $\mathbf{K}_1 = [\mathbf{K}_{11} \quad \mathbf{K}_{12} \quad \cdots \quad \mathbf{K}_{1n}]^T$, i.e. $\mathbf{K}_{11} = \mathbf{K}_{12} = \cdots = \mathbf{K}_{1n}$. With the same reference voltage, the control signal from the reference has the same impact on individual inverter. Thus, only one row is needed as the common controller gain as shown in Fig. 5-3.

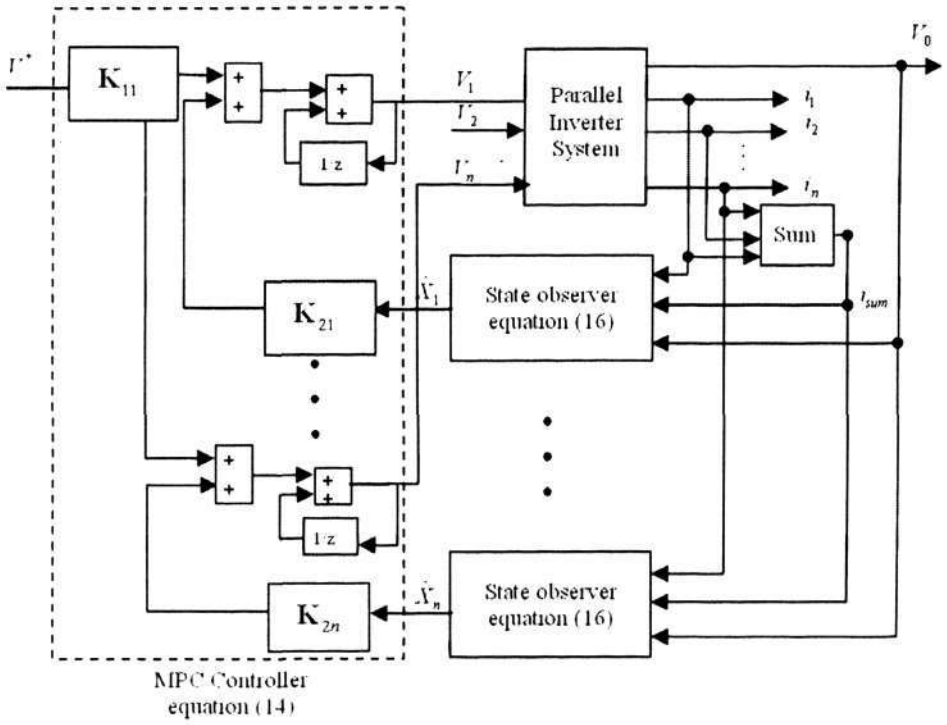

Fig. 5-3 Block diagram of the control system

For n-inverters system, the original state variable vector is defined as

$$\hat{\mathbf{X}} = \left[\Delta V_o(kT) \;\; \Delta i_1(kT) \;\; \cdots \;\; \Delta i_n(kT) \;\; V_o(kT-T) \;\; i_1(kT-T)-i_2(kT-T) \;\; \cdots \;\; i_{n-1}(kT-T)-i_n(kT-T)\right]^T \tag{5.7}$$

For the controller gain $\mathbf{K_2}$, it can be formulated more compactly by combining the individual inverter currents into a sum. This would result in the following modified state vector:

$$\hat{\mathbf{X}}_l = \left[\Delta V_o(kT) \;\; \Delta i_l(kT) \;\; \sum_{j=1}^{n}\Delta i_j(kT) \;\; V_o(kT-T) \;\; i_l(kT-T) \;\; \sum_{j=1}^{n} i_j(kT-T)\right]^T \tag{5.8}$$

where $l = 1, 2, ...n$ is the index for the inverter and n is the total number of inverters connected in parallel. With this modification, the order of the state vector can be maintained as 6 and is independent on the number of inverters in the system. Consequently, the same controller structure can be used for variable number of inverters. The structure and complexity will not increase with changes in inverter's number.

As the parameters of inverters are assumed to be the same, the impact of other inverters on the controlled inverter is the same. If we take row one $\mathbf{K}_{21}$ of the original $\mathbf{K}_2$ as example, where $k_1, k_2, \ldots$ are the original row elements of the vector $\mathbf{K}_{21}$. Let $\mathbf{K}_{2l}$ be the l row vector of modified $\mathbf{K}_2$ for the simplified state vector (5.8). The control vectors on $\Delta i_j(kT)$ $(j = 1 \cdots n)$ can be arranged in the form for the simplified state (5.8) as

$$\mathbf{K}_{2l}(2) = k_2 - k_3 \tag{5.9}$$

$$\mathbf{K}_{2l}(3) = k_3 = k_4 = \cdots = k_{n+1} \tag{5.10}$$

Form the relationship in (5.7), the control vector on $i_j(kT - T)$ $(j = 1 \cdots n)$ can be arranged as $\begin{bmatrix} k_{n+3} & k_{n+4} - k_{n+3} & k_{n+5} - k_{n+4} & \cdots & -k_{2n+1} \end{bmatrix}$. When arranged in the form of (5.8), we the gains on other inverters' current to inverter 1 are the same. So the corresponding feedback gain for (5.5) with the simplified state vector (5.8) can be derived as

$$\mathbf{K}_{2l}(5) = k_{n+3} - k_{2n+1} \tag{5.11}$$

$$\mathbf{K}_{2l}(6) = k_{n+4} - k_{n+3} = k_{n+5} - k_{n+4} = \cdots = -k_{2n+1} \tag{5.12}$$

With the equation (5.12), we have

$$k_{n+3} = -(n-1)k_{2n+1} \tag{5.13}$$

Thus the equation (5.11) can be simplified as following

$$\mathbf{K}_{2l}(5) = \frac{n}{n-1} k_{n+3} \tag{5.14}$$

Thus the corresponding feedback gain $\mathbf{K}_{2l}$ for (5.5) with the simplified state vector (5.8) can be summarized as

$$\mathbf{K}_{2l} = \begin{bmatrix} k_1 & k_2 - k_3 & k_3 & k_{n+2} & \dfrac{n}{n-1} k_{n+3} & -k_{2n+1} \end{bmatrix} \tag{5.15}$$

As shown in Fig. 5-3, the required states can be reconstructed with the feedback signals from the system. The output voltage of the inverter system and the current of individual inverter are measured. The individual inverter currents are then combined to form the total current i_{sum}. By comparing these three variables with their values at previous sampling interval, the first three incremental states in (5.8) can be obtained. These three incremental states are then combined with the three measured signals at previous sampling interval to form the new states for each inverter. Whenever an inverter is removed/added to the system, its contribution to the system i_{sum} is automatically reflected in the state computation (5.8) for other inverters. The controller will then adjust the control action accordingly based on (5.5).

During operation, the number of inverters could be changed in real time when one inverter becomes faulty. In some situations, when the system power rating is insufficient for the load, additional inverters are added to boost the capacity. For these varying operations, the stability and robustness of the system need to be ensured.

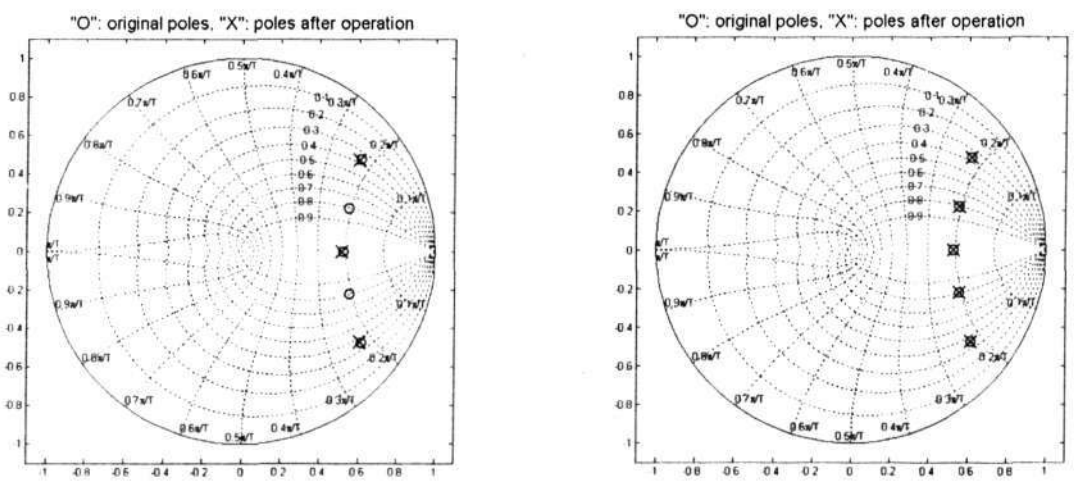

(a) (b)

Fig. 5-4 Poles distribution when the inverter number changes. (a) One inverter removed from the nominal system (b) extra inverter added to the system.

The stability for the hot-swap operation could be determined by analyzing the closed-loop poles distribution. Consider the case of two inverter systems. When one inverter is removed from the system, the two poles related to current sharing disappear as shown in Fig. 5-4(a). The system remains a stable single inverter system. In the Fig. 5-4(b), one more inverter is added into the two inverters system. It shows that there are two pairs of duplicated poles related to the current sharing when the new inverter is added to the system. In both situations, the pole positions only changes slightly.

5.5 Simulation Result

To investigate the system performance of the proposed approach, simulation studies have been carried out and the results are presented in this section. The parameters of the experimental system used in this study are summarized in the Table 5.1.

Input Voltage V_{in}	75 Vdc
Output Voltage V_o	50 Vac
Output Voltage Frequency f	50 Hz
Input Inductor L_1	2 mH
Input Inductor L_2	1 mH
Equivalent series resistor r_1	3.4 Ω
Equivalent series resistor r_2	1.7 Ω
Output Capacitor C_1	4.7μH
Output Capacitor C_2	9.4 μH
Nominal Load R	50 Ω

Table 5-1 Parameters of the parallel connected inverters systems

We first investigate the robustness of the system with respect to the parameter variation. For this simulation study, one of the output filters of the inverter is set to 200% of the other inverter. This arbitrarily changes the symmetry of the output filter characteristics. Fig. 5-5(a) shows the simulation result of the output voltage and current waveforms without current sharing control. In the simulation, the desired output voltage is set at 100 Volt (pp) with a fixed frequency of 50 Hz. A constant resistive load has been connected to the output such that an output current of 2A (pp) is drawn. It is observed that the parameter variation causes different output currents and this will induce a circulating current to the system.

Fig. 5-5(b) shows the system performance when the proposed method is used. The current waveforms clearly show that the inverters share equal contribution of the required load current. Similar result is also obtained when the load increases to 200% of the nominal value. This is shown in Fig. 5-5(c). Thus, the system using the proposed approach has good robustness with respect to load changes.

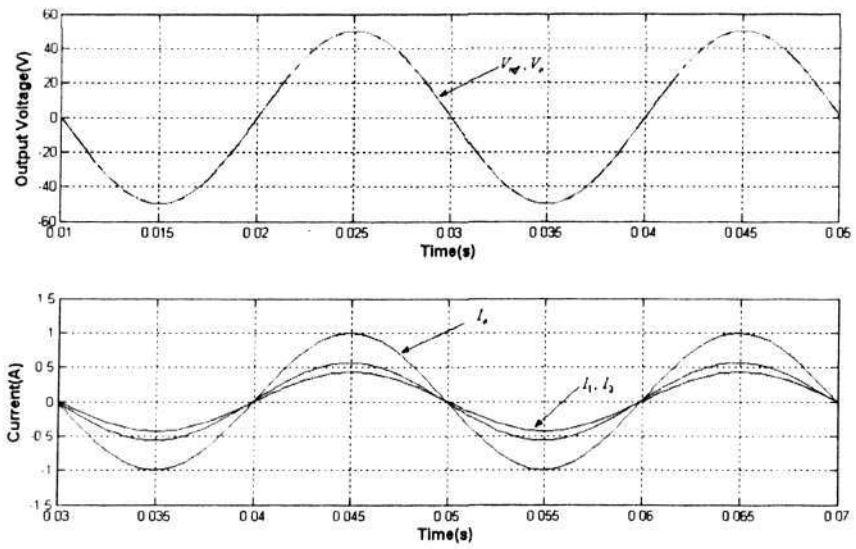

(a)

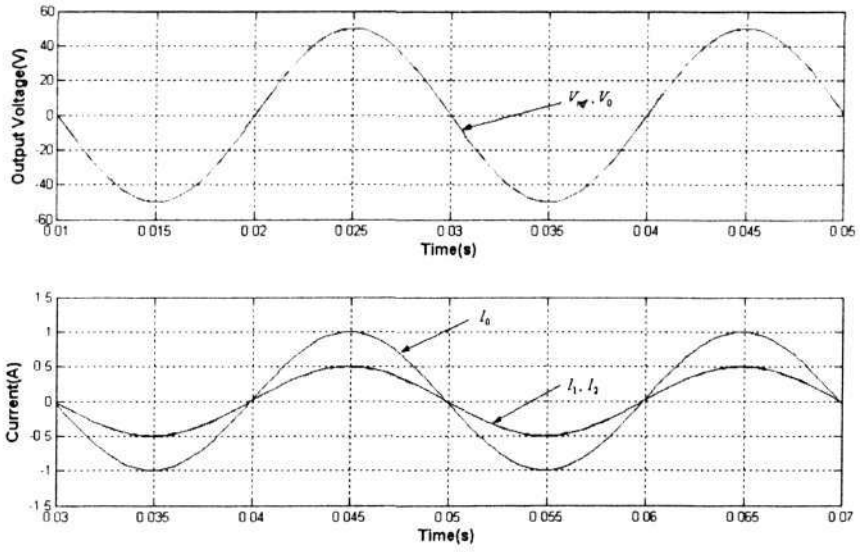

(b)

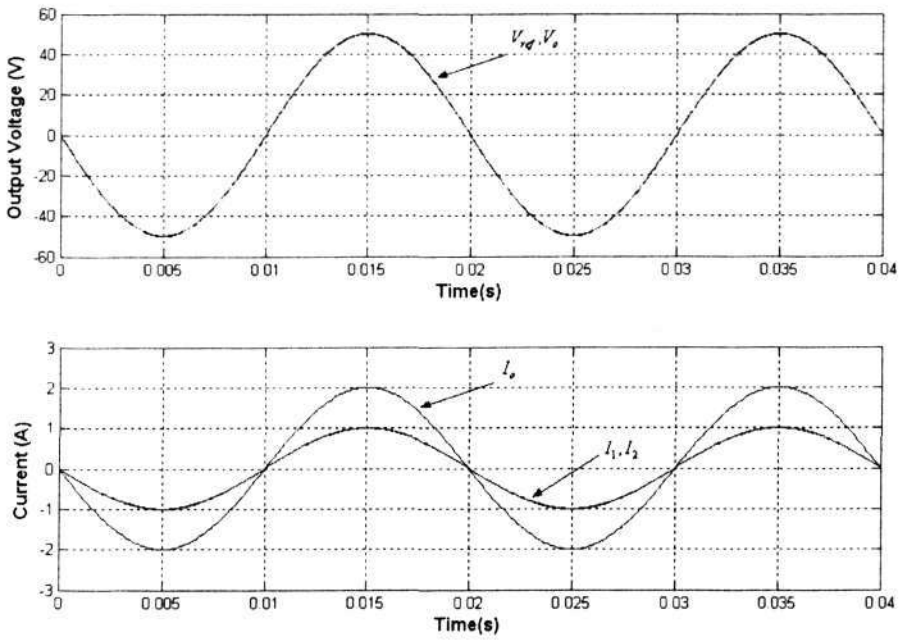

(c)

Fig. 5-5 (a)Two inverters in operation without current sharing control (b) Performance of the proposed multi-objective MPC controller(c) Performance of the proposed multi-objective MPC controller with 200% of the nominal load

Fig. 5-6(a) shows the simulation result of the system with triac load. The firing angles are set at 60° and 180° for positive and negative cycles. Fig. 5-6(b) shows the simulation result of the system with rectifier load. A 50Ω resistor load and 1500μF capacitor is

used. From both simulation results, it is observed that the output current is equally distributed between the inverters regardless of the types of loads.

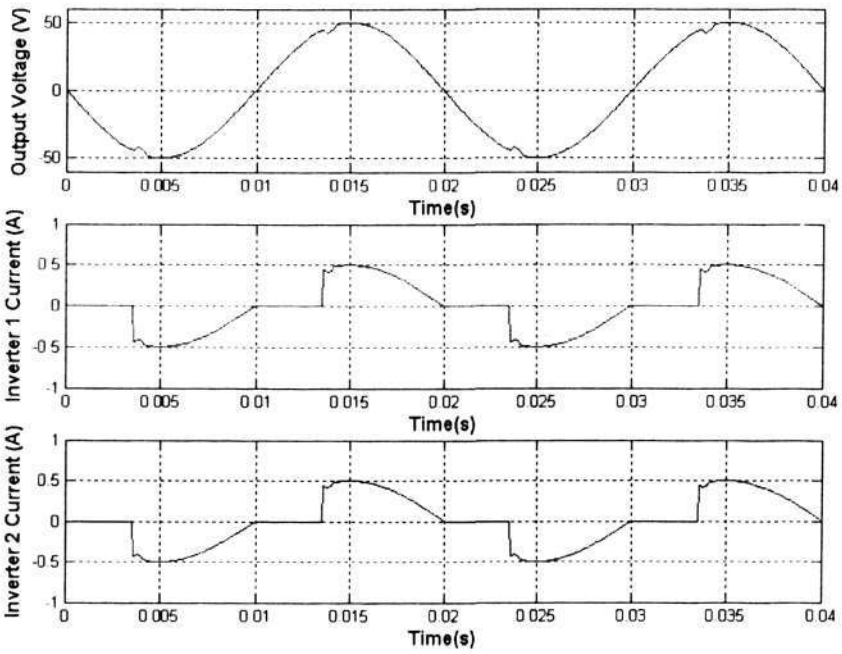

(a)

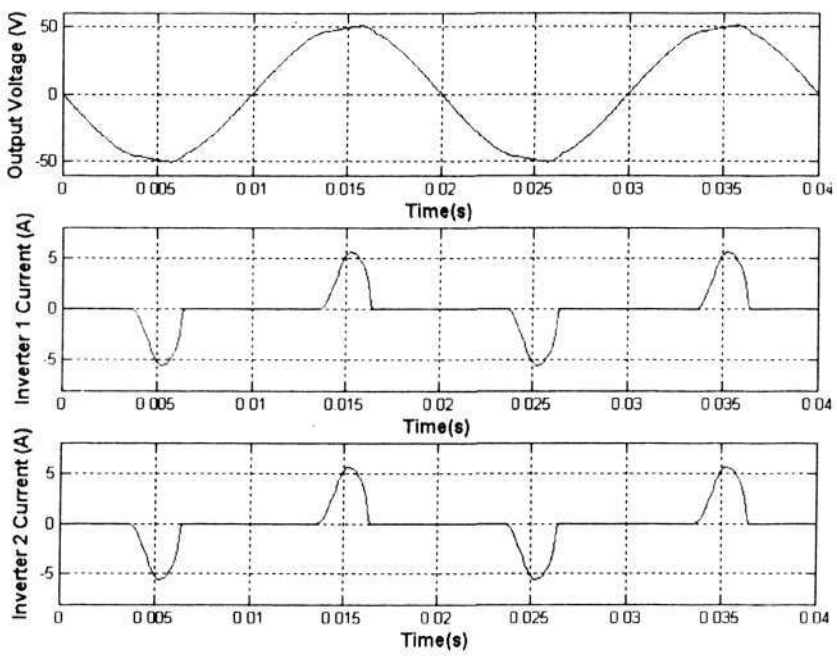

(b)

Fig. 5-6 Simulation results of the system under(a) triac load (b) rectifier load

To compare the performance of the proposed scheme with other current sharing inverter system, we consider the instantaneous droop method [52] [143]. It is a time-domain method for controlling voltage and frequency using parallel connected inverters. A finite output impedance voltage source is imitated, by controlling the current flowing through virtual impedance as a result of the voltage difference between inverters [143]. For this method, the system is constructed with two separately controlled voltage inverters, in which SISO MPC controller is used. The equivalent system is demonstrated in Fig. 5-7. Here, it is assumed that the virtual impedance is purely resistive. The output voltage reference drops proportionally to corresponding output current.

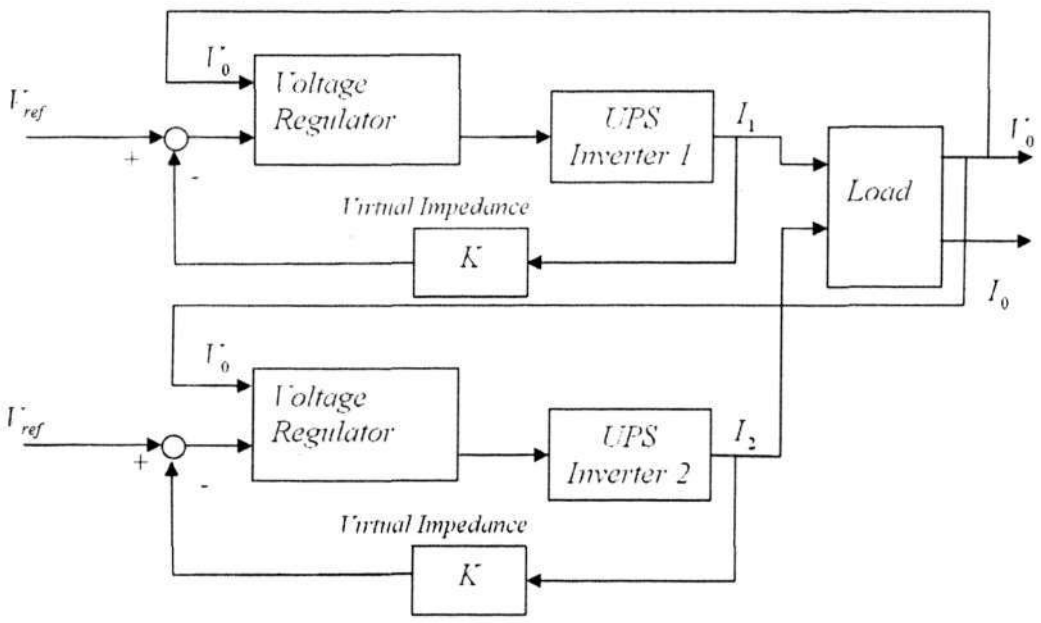

Fig. 5-7 control diagram of the voltage droop method

Suppose the original equivalent output impedance of a single inverter is Z_t.

$$V_{ref} - V_0 = Z_t \cdot I_t \tag{5.16}$$

With the virtual impedance K, the relationship becomes

$$(V_{ref} - K \cdot I_t) - V_0 = Z_t \cdot I_t \tag{5.17}$$

(5.17) can be rewritten as

$$V_{ref} - V_0 = (Z_t + K) \cdot I_t \tag{5.18}$$

Thus, it is equivalent to increasing the equivalent thevenin impedance from Z_t to $Z_t + k$. This will lower the current sensitivity to the actual thevenin impedance Z_t. A better current distribution performance can be expected.

In the simulation, the parameter K is tuned to achieve a current sharing performance as in Fig. 5-7. The virtual impedance K is selected as $10\,\Omega$. The simulation result of the voltage droop method is shown in Fig. 5-8(a). As can be observed from the figure, the current sharing performance is greatly improved. However, the voltage tracking performance is slightly influenced. The sensitivity of voltage tracking accuracy with respect to load changes will increase. For a constant load, the voltage reference might be tuned according to the output current to have a more accurate voltage tracking performance. However, the voltage tracking accuracy will still be influenced when the load changes. As shown in Fig. 5-8(b), the voltage tracking accuracy will decrease when 200% of the nominal load is used.

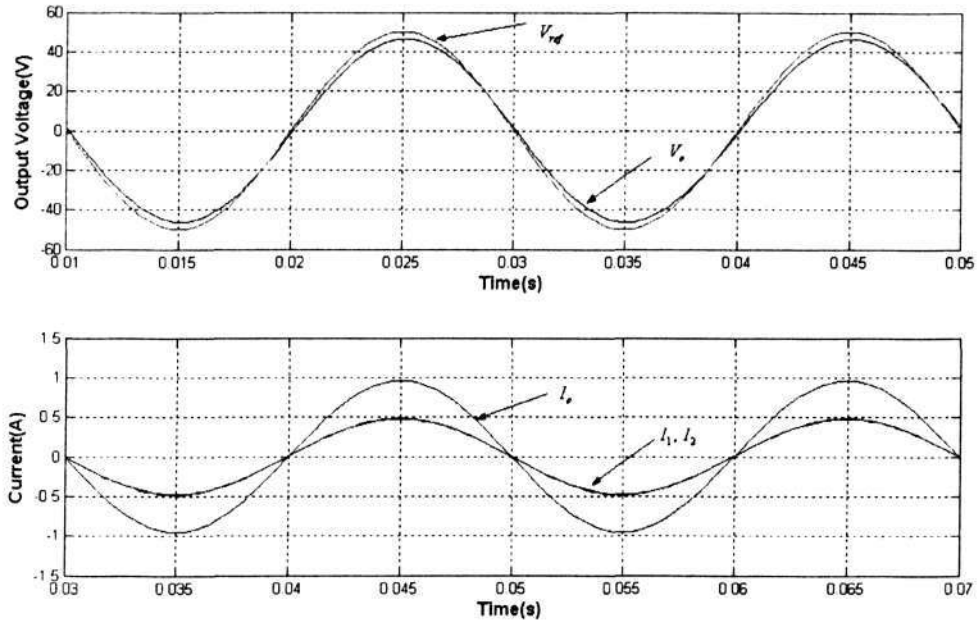

(a)

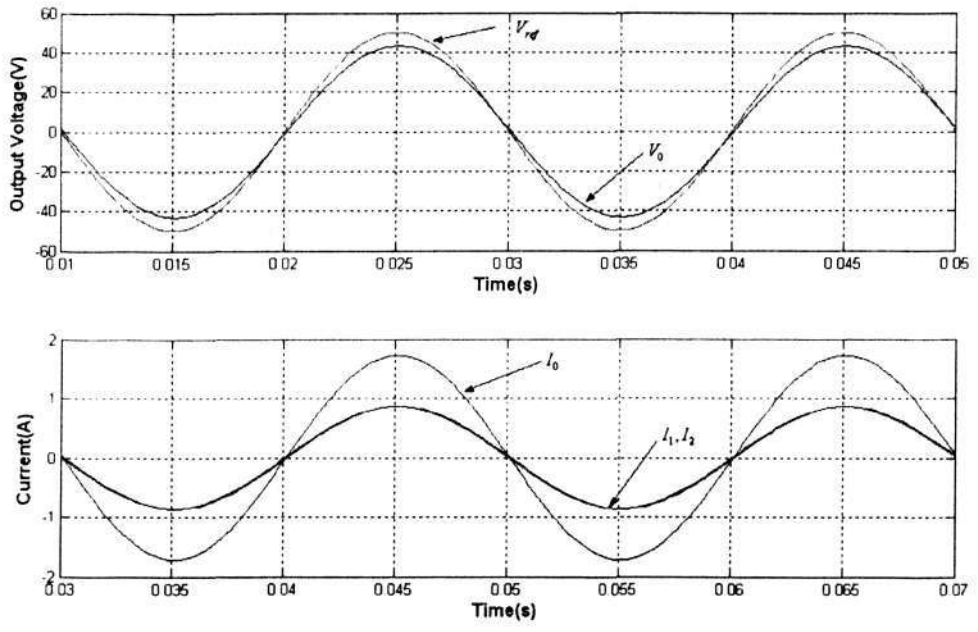

(b)

Fig. 5-8 Two inverters in operation with virtual impedance method (a) nominal load condition (b) 200% load condition

For ease of comparison, the simulation results are summarized in the Table 5-2.

Simulation Condition	Voltage tracking error (%)	Circulating Current (%)
Voltage tracking control without currer sharing	0.05%	13.3%
Voltage tracking control with virtual impedance method (Nominal Load)	7.6%	0.34%
Voltage tracking control with virtual impedance method (200% load)	15.4%	0.53%
Multi-objective model predictive controller	0.05%	0.32%
Multi-objective model predictive controller (200% load)	0.3%	0.34%

Table 5-2 Simulation result comparison with different operating conditions

From Table 5-2, it is clear that the proposed multi-objective model predictive controller has greatly minimized the current difference between the inverters. The difference is only 0.32% of the individual inverter output current. For the same operating conditions, the virtual impedance method would have a voltage tracking error of 7%. In contrast, the proposed approach is only 0.05%. Increasing the virtual impedance equals to decreasing the magnitude of system's equivalent reference voltage. Consequently, the voltage tracking accuracy of each inverter will be affected.

5.6 Experimental Results

The proposed approach has been realized with a laboratory setup using a TMS320C31 based DSP board. The DSP board uses a slave processor TMS320P14 to generate the PWM waveform at a switching frequency of 25 kHz. The digital controller and the observer are coded in C program. A sampling period of 40 μs has been used in the experiment. For the parallel connected inverters system, each inverter consists of four insulated gate bipolar transistors (IGBT) IXGH16N60C2D1 connected as a H-bridge. The IGBT is driven by a driver integrated circuit IXDD414 with opto-coupler HCPL316J. In the setup, two similar inverters with different parameters as shown in Table 5.1 are used and connected in parallel to verify the effectiveness of the proposed control scheme. The LC low past filters of all the inverters are designed to have the same cutoff frequency of 1.8 kHz (Fig. 2-7). The output voltage and inverter currents are measured using hall-effect voltage sensors (LV25-P) and current sensors (LEM-HEME FB50P) during each interrupt. They are feedback to the DSP after converted to digital signals via 12-bit ADCs. For the recording of experimental results, high voltage differential probes (Tektronix P5200) and current probes with amplifier (Tektronix A6302 & AM503) are used and the waveforms recorded using an oscilloscope (Agilent Infiniium 54852A).

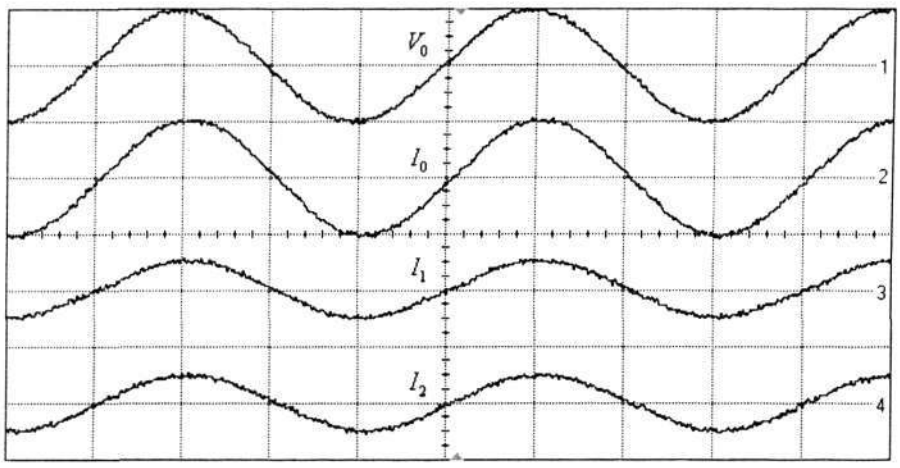

(50V/div, 1A/div, 5ms /div)
(a)

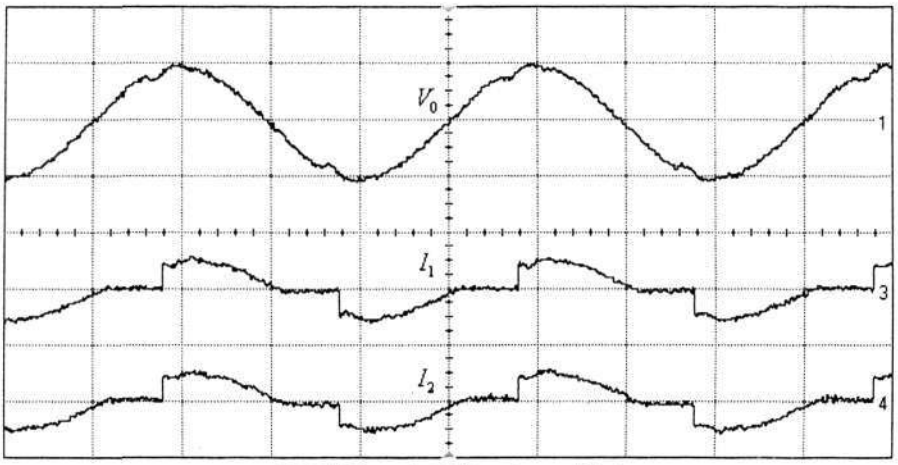

(50V/div, 1A/div, 5ms /div)
(b)

Fig. 5-9 Experimental results of the system under (a) 50 Ω load (b)triac load

Fig. 5-9 shows the performance of the parallel connected inverters system under both static and dynamic loads based on the constant resistive load and the triac load respectively. For the triac load, the firing angles are set at 72° and 252° for positive and negative cycles. From the results, it is observed that the output voltage is sinusoidal. Although there is imbalance between inverters (Table 5.1), the circulating current is well maintained as reported in the experimental results. The designed system can share

various kinds of the load equally. Moreover, the output current is equally distributed between the inverters regardless of the types of loads.

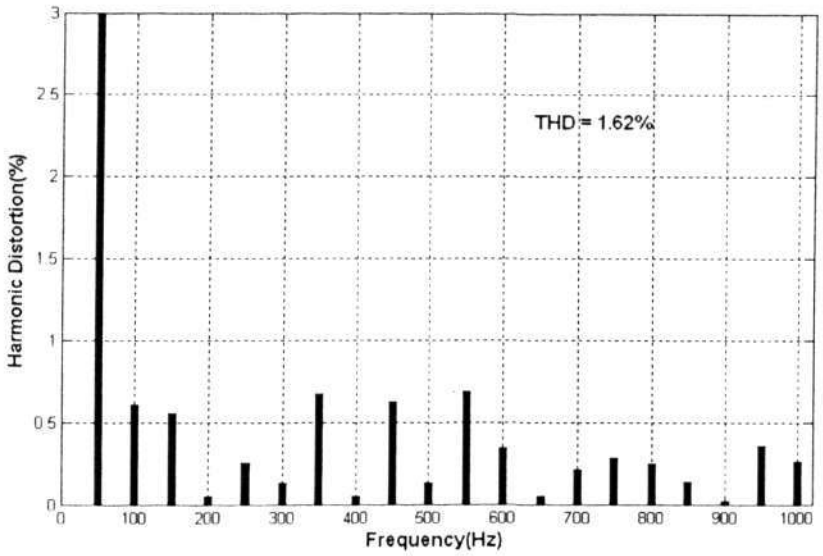

(a)

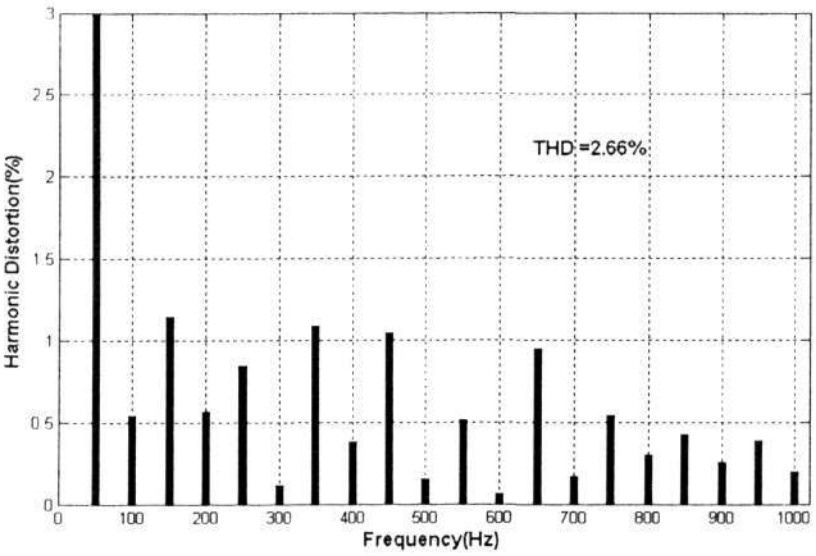

(b)

Fig. 5-10 Harmonic distortion of the output voltage (a) 50 Ω load (b)triac load

The corresponding total harmonic distortion (THD) and harmonics of the output voltage under both operating conditions are summarized in Fig. 5-10 (a) and Fig. 5-10(b). The result show that the THD for the resistive and triac loads are 1.62% and 2.66% respectively.

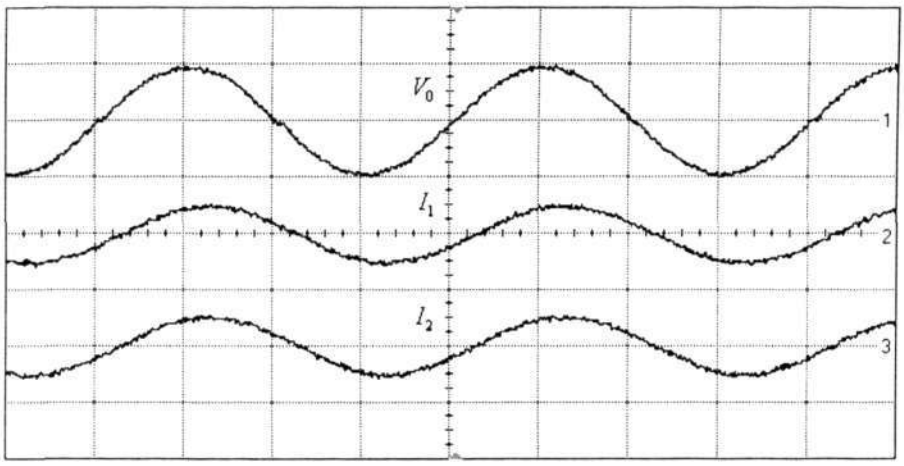

(50V/div, 1A/div, 5ms /div)

Fig. 5-11 Experimental results of the system under R-L load

Fig. 5-11 shows the performance of the parallel connected inverters system under R-L load. For this experiment, a 65mH inductor is placed in series with a 50Ω load resistor. From the results, it is observed that the current is distributed equally by the two inverters. Because of the inductive characteristics of the load, the current lags the voltage around 30°.

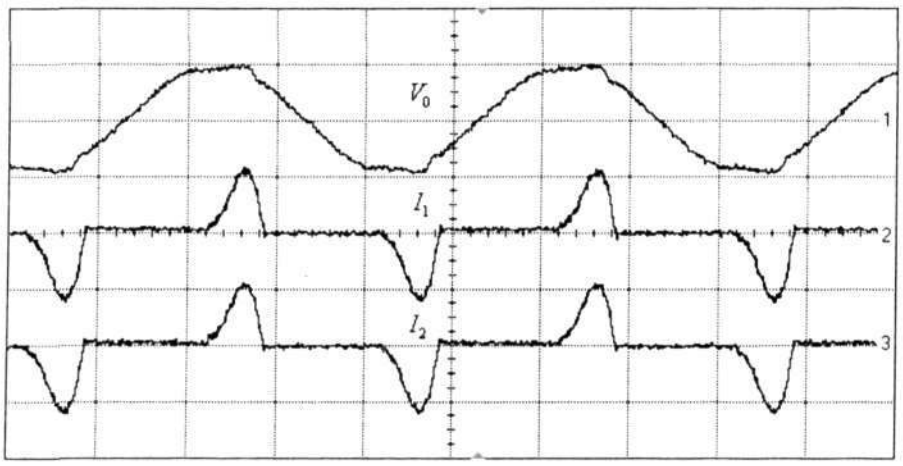

(50V/div, 4A/div, 5ms /div)

Fig. 5-12 Experimental results of the system under rectifier load

Fig. 5-12 shows the experimental result with a rectifier load. In this case, a $1800\mu F$ capacitor is placed in parallel with a 50Ω load resistor. As shown in this figure, the voltage waveform is only slightly distorted, although the current has high spikes. Moreover, the current sharing between the two inverters is well maintained.

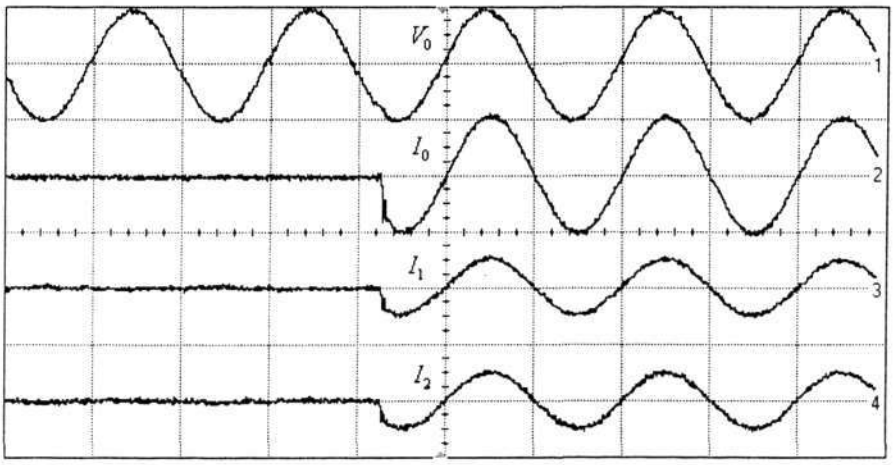

(50V/div, 1A/div, 10ms /div)
(a)

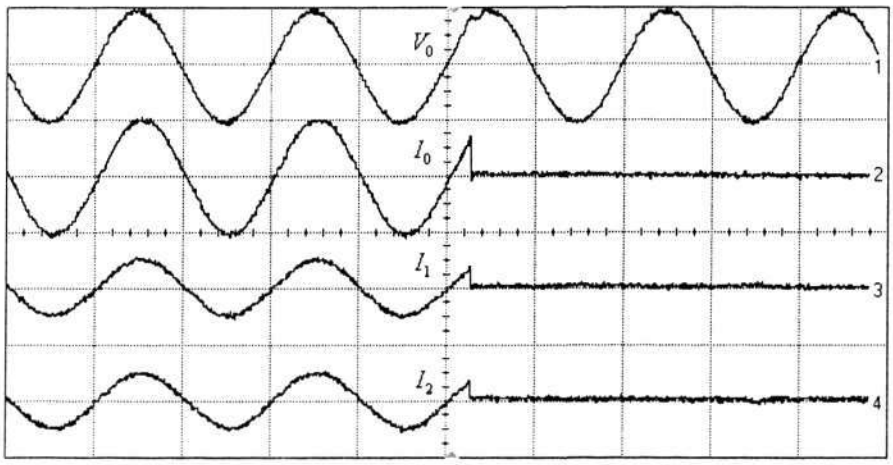

(50V/div, 1A/div, 10ms /div)
(b)

Fig. 5-13 Dynamic experimental response (a) load changes from null to full (b) load changes from full to null

Fig. 5-13 (a) shows the dynamic response of the system when the load changes from no load to a 50 Ω load. From the results, it is observed that the load current is equally shared by the inverters even during the switching transient. Fig. 5-13 (b) shows the response of the system when the load changes form the nominal load to no load. According to the analysis in Fig. 5-2(b), the load variation should have negligible influence on the voltage tracking performance. The experimental results show that the output voltage amplitude is well maintained, under the dynamic loading condition. In both figures, it can be observed that the current sharing is well maintained during no load condition and the switching transient.

Fig. 5-14(a) shows the response when inverter 2 is isolated from the system due to fault condition. It is shown that the inverter 1 takes over the full load immediately, supplying 200% of its nominal load. The quality of the output voltage and current waveforms are very well maintained despite the switching. Fig. 5-14(b) shows the response when a new inverter is added back into the system. Initially, the load is supplied only by the inverter 1. Then the inverter 2 is connected to the system later on. The results show that the influence on the output voltage and current waveforms is insignificant. Good output quality is sustained during both switching transients.

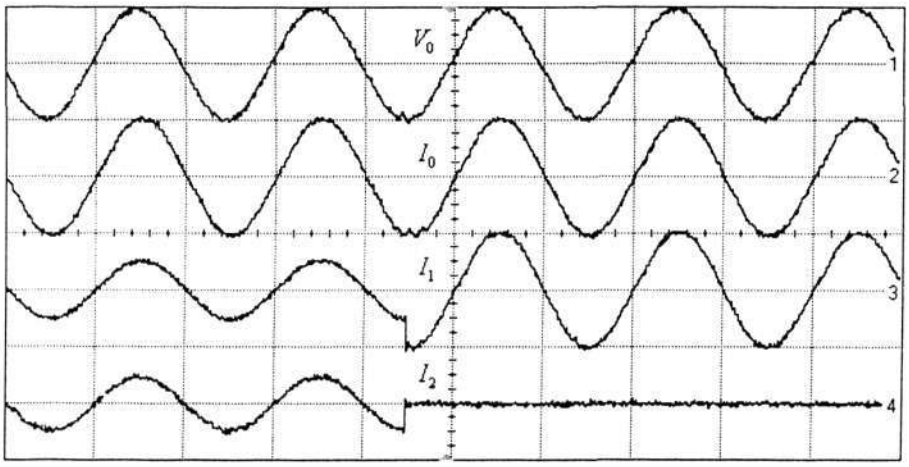

(50V/div, 1Adiv, 10ms /div)
(a)

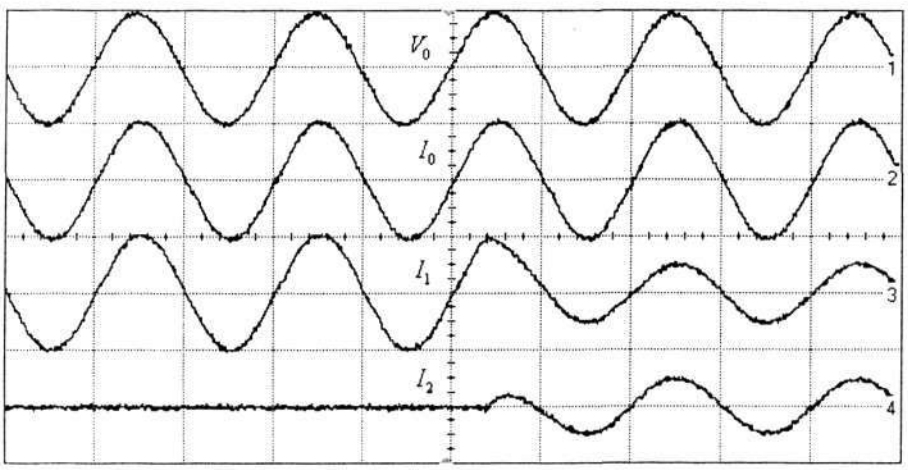

(50V/div, 1Adiv, 10ms /div)
(b)

Fig. 5-14 Experimental result of output voltage and current waveforms (a) Inverter 2 is isolated from the system (b) Inverter 2 is plugged into the system

5.7 Conclusions

In this chapter, a novel control scheme utilizing multi-objective model predictive control theory has been developed to control the parallel connected inverters of an UPS for tight closed loop control. The proposed control scheme achieves good performance on both voltage reference tracking and current sharing. In designing the system, the proposed approach has taken modularity into consideration such that it could function well for systems with a variable number of parallel connected inverters. To verify the proposed scheme, a laboratory prototype has been setup. The experimental results have shown that the proposed approach yields good performance under both static and dynamic loading conditions as well as hot-swap operations.

Chapter 6

Conclusions and Recommendations

6.1 Conclusions

This dissertation presents the research on model predictive control technique for the control of linear motor drive and parallel connected inverters. For the linear motor drive, the focus is on improving the tracking precision by introducing repetitive control technique. For the parallel connected inverters, the focus is on the load sharing. In summary, some results have been obtained in this study are highlighted as follows:

- A new repetitive model predictive control (RMPC) algorithm has been developed for the linear motion control system. The motor drive is able to track the desired trajectory accurately under unmodeled disturbances and parameter uncertainties. In contrast to conventional friction compensation design, the RMPC provide a simple and efficient way to achieve superior tracking accuracy without the need to determine the friction model.

- The RMPC algorithm combines the merits of model predictive control (MPC) and repetitive control (RC), so that the system can take the advantage of the regulation ability of MPC and the learning ability of RC. The tracking error caused by inaccurate system parameters, disturbances, and nonlinear friction force are asymptotically minimized by the proposed RMPC algorithm.

- The RMPC presented in this thesis is based on phase compensation method. By passing the tracking error history through a non-causal FIR filter with reversed system phase, an overall system phase of near zero is obtained. When compared with the P-type repetitive controller, the proposed method provides a wider learnable frequency range.

- A MPC control algorithm has been developed for a parallel inverter system. The system is modeled as a multi-input multi-output (MIMO) system. By combining two control objectives: voltage tracking and current sharing into a cost function, the control law is obtained. The stability and robustness of the parallel inverter system is verified in simulation and experiment.

- A laboratory prototype has been constructed for performance evaluation of the single phase parallel connected inverters. The experimental results have shown that the proposed approach yields good performance under both static and dynamic loading conditions as well as hot-swap operations. The advantages of the proposed approach include easy design and simple hardware implementation.

6.2 Recommendations for Further Research

1) Extend the learning range of the RMPC controller

Friction force at low velocity has high nonlinearity. As demonstrated in Chapter 4, the proposed repetitive model predictive controller has a physical limit in making the learning process effective at very low velocity. As the stick-slip phenomenon is unavoidable, this phenomenon needs to be further studied to determine the condition for effective learning. By considering the conditions in the controller design, the learning range of the designed linear motion system will be extended.

2) Development of the proposed controller for three-phase UPS system

The UPS is a backup power supply system. As the power level increases beyond 10kVA, it becomes advantageous to use a three-phase inverter. The control of three-phase inverter is more complicated than the single-phase. Besides the control of each phase output, the balance among the three phases should also be considered. To introduce the proposed MPC controller for the three-phase UPS system, it is necessary to investigate the characteristics of the entire system. Moreover, the repetitive model predictive control algorithm for linear motor drive can be used to improve the tracking performance of the inverters. For the parallel connected inverters system, the proposed algorithm needs to be extended for the MIMO system operation.

Publications

Journal Papers:

1. **A Repetitive Model Predictive Control Approach for Precision Tracking of a Linear Motion system**
   R. Z. Cao and K. S. Low, IEEE Trans. Industrial Electronics, Special Issue on Predictive Control in Power Electronics and Drives, Vol.56, No. 6, June 2009, pp. 1955-1962.

2. **Model Predictive Control of Parallel Connected Inverters for Uninterruptible Power Supplies**
   K. S. Low and R. Z. Cao, IEEE Trans. Industrial Electronics, Special Issue on Uninterruptible Power Supply (UPS) Systems, Vol. 55, N0. 8, Aug 2008, pp. 2884-2893.

Conference papers:

1. **Repetitive Model Predictive Control of a Precision Linear Motor Drive**
   R. Cao, and K. S. Low, IEEE Industrial Electronics, Control and Instrumentation Conference (IECON '07), 7 November- 10 November 2007, Taipei, Taiwan, pp. 1132 - 1137.

2. **Model Predictive Control of Parallel Connected Inverters for Uninterruptible Power Supplies**
   K. S. Low, and RZ Cao, 37th IEEE Power Electronics Specialists Conference (PESC '06), 18 June- 22 June 2006, Jeju, Korea, pp. 2158-2163.

3. **A MEMS based variable optical attenuator**
   R. Z. Cao, K. S. Low, A. Q. Liu and C. Hong, IEEE Industrial Electronics, Control and Instrumentation Conference (IECON '04), 2 November- 6 November 2004, Busan, Korea, 1945-1950.

References

[1] G. C. Onwubolu, "Mechatronics: Principles and Applications," Elsevier, 2005.

[2] S. Dejimaa, W. Gaoa, K. Katakuraa, S. Kiyonoa, and Y. Tomitab, "Dynamic modeling, controller design and experimental validation of a planar motion stage for precision positioning " Precision Engineering vol. 29, pp. 263-271, 2005.

[3] D. Sun, "Adaptive coupling control of two working operations in CNC integrated machines," Journal of Dynamic Systems Measurement and Control-Transactions of the Asme, vol. 125, pp. 662-665, 2003.

[4] S. Refaat, J. M. Herve, S. Nahavandi, and H. Trinh, "High-Precision Five-Axis Machine for High-Speed Material Processing Using Linear Motors and Parallel-Serial Kinematics," IEEE Conference on Emerging Technologies and Factory Automation, pp. 501-506, 2006.

[5] S. Gordon and M. T. Hillery, "Development of a high-speed CNC cutting machine using linear motors " Journal of Materials Processing Technology vol. 166, pp. 321-329, 2005.

[6] J. Li, Y. Liu, L. Sun, and D. Jie, "Mechanism and control of linear positioning for IC wire bonders," 6th International Conference on Electronic Packaging Technology 2005, pp. 171-174, 2005.

[7] J. van Amerongen, "Mechatronic design," Mechatronics, vol. 13, pp. 1045-1066, 2003.

[8] S. A. Nasar and I. Boldea, Linear motion electric machines: Wiley, 1976.

[9] J. F. Cieras and Z. J. Piech, Linear Synchronous Motors: CRC PRESS, 2000.

[10] I. Boldea and S. A. Nasar, Linear Electric Actuators and Generators: Cambridge University Press, 1997.

[11] I. Boldea, Linear Motion Electromagnetic Devices Taylor & Francis, 2002.

[12] H. Yousefi, M. Hirvonen, H. Handroos, and A. Soleymani, "Application of neural network in suppressing mechanical vibration of a permanent magnet linear motor," Control Engineering Practice, vol. 16, pp. 787-797, 2008.

[13] D. L. Zhang, Y. P. Chen, W. Ai, and Z. Zhou, "Precision motion control of permanent magnet linear motors," International Journal of Advanced Manufacturing Technology, vol. 35, pp. 301-308, 2007.

[14] J. Q. Gong and B. Yao, "Neural network adaptive robust control with application to precision motion control of linear motors," International Journal of Adaptive Control and Signal Processing, vol. 15, pp. 837-864, 2001.

[15] D. L. Zhang, Y. P. Chen, Z. D. Zhou, W. Ai, and X. D. Li, "Robust adaptive motion control of permanent magnet linear motors based on disturbance compensation," IET Electric Power Applications, vol. 1, pp. 543-548, 2007.

[16] W. T. Su and C. M. Liaw, "Adaptive positioning control for a LPMSM drive based on adapted inverse model and robust disturbance observer," IEEE Transactions on Power Electronics, vol. 21, pp. 505-517, 2006.

[17] S. J. Qin and T. A. Badgwell, "A survey of industrial model predictive control technology," Control Engineering Practice, vol. 11, pp. 733-764, 2003.

[18] S. G. Tzafestas and E. J. Kyriannakis, "Regulation of GMA welding thermal characteristics via a hierarchical MIMO predictive control scheme assuring stability," IEEE Transaction on Industrial Electronics, vol. 3, 2000.

[19] J. G. VanAntwerp and R. D. Braatz, "Fast model predictive control of sheet and film processes," IEEE Trans. Control Systems Technology, vol. 8, 2000.

[20] K. S. Low and H. L. Zhuang, "Robust model predictive control and observer for direct drive applications," IEEE Trans. on Power Electron., vol. 15, pp. 1018-1028, 2000.

[21] A. Linder and R. Kennel, "Direct Model Predictive Control-a new direct predictive Control strategy for electric drives," European conference on Power Electronics and Applications, pp. 101-108, 2005.

[22] K. S. Low, "A DSP-based single-phase AC power source," IEEE Trans. Ind. Electron., vol. 46, pp. 936-941, 1999.

[23] R. Vargas, P. Cortes, P. U. Ammann, J. Rodriguez, and J. Pontt, "Predictive Control of a Three-Phase Neutral-Point-Clamped Inverter," IEEE Trans. Ind. Electron., vol. 54, pp. 2697-2705, 2007.

[24] R. Ginhoux, J. Gangloff, M. de Mathelin, L. Soler, M. M. A. Sanchez, and J. Marescaux, "Active filtering of physiological motion in robotized surgery using predictive control," IEEE Transactions on Robotics, vol. 21, pp. 67-79, 2005.

[25] B. Armstronghelouvry, P. Dupont, and C. C. Dewit, "A Survey of Models, Analysis Tools and Compensation Methods for the Control of Machines with Friction," Automatica, vol. 30, pp. 1083-1138, 1994.

[26] J. Amin, B. Friedland, and A. Harnoy, "Implementation of a friction estimation and compensation technique," IEEE Control system Magazine, vol. 42, pp. 71-76, 1997.

[27] S. W. Lee and J. H. Kim, "Robust adaptive friction compensation," IEEE Industrial Electronics magazine, vol. 42, pp. 474-479, 1995.

[28] K. S. Low and M. T. Keck, "Advanced precision linear stage for industrial automation applications," IEEE Transactions on Instrumentation and Measurement, vol. 52, pp. 785-789, 2003.

[29] M. K. Ciliz and M. Tomizuka, "Neural network based friction compensation in motion control," Electronics Letters, vol. 40, pp. 752-753, 2004.

[30] H. Du and S. S. Nair, "Low velocity friction compensation," IEEE Control system Magazine, vol. 18, pp. 61-69, 1998.

[31] E. D. Tung, G.Anwar, and M.Tomizuka, "Low velocity friction compensation and feedforward solution based repetitive control," ASME J. Dynanic Syst., Meas. Contr., vol. 115, pp. 279-284, 1993.

[32] R. W. Longman, "Iterative learning control and repetitive control for engineering practice," International Journal of Control, vol. 73, pp. 930-954, 2000.

[33] E. Tung, G. Anwar, and M. Tomizuka, "Low velocity friction compensation and feedforward solution based on repetitive control," Proceedings of the American Control Conference, vol. 3, pp. 2615-2620, 1991.

[34] K. Kaneko and R. Horowitz, "Repetitive and adaptive control of robot manipulators with velocity estimation," IEEE Transactions on Robotics and Automation, vol. 13, pp. 204-217, 1997.

[35] D. Sun and J. K. Mills, "Performance improvement of industrial robot trajectory tracking using adaptive-learning scheme," Journal of Dynamic Systems Measurement and Control-Transactions of the Asme, vol. 121, pp. 285-292, 1999.

[36] D. Sun, X. L. Shi, and Y. H. Liu, "Adaptive learning control for cooperation of two robots manipulating a rigid object with model uncertainties," Robotica, vol. 14, pp. 365-373, 1996.

[37] G. Hillerström, "Adaptive Suppression of Vibrations—A Repetitive Control Approach," IEEE Transactions on Control System Technology, vol. 4, pp. 72-78, 1996.

[38] S. Hattori, M. Ishida, and T. Hori, "Vibration suppresion control method for PMSM utilizing repetitive control with auto-tuning function and Fourier transfrom," IECON'01. 27th Annual Conference of the IEEE Industrial Electronics Society vol. 3, pp. 1673-1679, 2001.

[39] S. Rhim, A. Hu, N. Sadegh, and W. Book, "Combining a multirate repetitive learning controller with command shaping for improved flexible manipulator control," Journal of Dynamic Systems Measurement and Control-Transactions of the ASME, vol. 123, pp. 385-390 2001.

[40] R. F. Fung, J. S. Huang, C. G. Chien, and Y. C. Wang, "Design and application of a continuous repetitive controller for rotating mechanisms," International Journal of Mechanical Sciences, vol. Volume 42, pp. 1805-1819, 2000.

[41] R. D. Hanson and T. C. Tsao, "Periodic sampling interval repetitive control and its application to variable spindle speed noncircular turning process," Journal of Dynamic Systems Measurement and Control-Transactions of the ASME, vol. 122, pp. 560-566, 2000.

[42] C. Kempf, W. Messner, M. Tomizuka, and R. Horowitz, "Comparison of four discrete-time repetitive control algorithms," Proceedings of the IEEE Conference on Decision and Control, vol. 3, pp. 2700-2704, 1992.

[43] C. Smith and M. Tomizuka, "Cost effective repetitive controller and its design," Proceedings of the American Control Conference, vol. 2, pp. 1169-1174, 2000.

[44] Y. P. Hsin and R. W. Longman, "Repetitive control to eliminate periodic measurement disturbances: application to disk drives," Advances in the Astronautical Sciences, vol. 114, pp. 135-150, 2003.

[45] K. Zhou, D. Wang, and K. S. Low, "Periodic errors elimination in CVCFPWM DC/AC converter systems: Repetitive control approach," IEE Proceedings-Control Theory and Applications, vol. 147, pp. 694-700, 2000.

[46] R. Costa-Castello, R. Grino, and E. Fossas, "Odd-harmonic digital repetitive control of a single-phase current active filter," IEEE Transactions on Power Electronics, vol. 19, pp. 1060-1068, 2004.

[47] C. Rech, H. Pinheiro, H. A. Grundling, H. L. Hey, and J. R. Pinheiro, "Comparison of digital control techniques with repetitive integral action for low cost PWM inverters," IEEE Transactions on Power Electronics, vol. 18, pp. 401-410, 2003.

[48] B. Roberts and J. McDowall, "Commercial successes in power storage " IEEE Power and Energy Magzine, vol. 3, pp. 24-30, 2005.

[49] J. M. Guerrero, L. GarciadeVicuna, J. Matas, M. Castilla, and J. Miret, "Output Impedance Design of Parallel-Connected UPS Inverters With Wireless Load-Sharing Control," IEEE Transactions on Industrial Electronics, vol. 52, pp. 1126-1135, 2005.

[50] J. M. Guerrero, J. Matas, L. G. d. Vicuna, M. Castilla, and J. Miret, "Decentralized Control for Parallel Operation of Distributed Generation Inverters Using Resistive Output Impedance," IEEE Transactions on Industrial Electronics, vol. 54, pp. 994-1004, 2007.

[51] T. F. Wu, H. M. Hsieh, Y. E. Wu, and Y. K. Chen, "Parallel-Inverter System With Failure Isolation and Hot-Swap Features," IEEE Transactions on Industry Applications, vol. 43, pp. 1329-1340, 2007.

[52] B. Shi and G. Venkataramanan, "Parallel operation of voltage source inverters with minimal intermodule reactors," Industry Applications Conference, 2004. 39th IAS Annual Meeting, vol. 1, 2004.

[53] X. Sun, Y. S. Lee, and D. H. Xu, "Modeling, analysis, and implementation of parallel multi-inverter systems with instantaneous average-current-sharing scheme," IEEE Transactions on Power Electronics, vol. 18, pp. 844-856, 2003.

[54] Z. H. Ye, D. Boroyevich, J. Y. Choi, and F. C. Lee, "Control of circulating current in two parallel three-phase boost rectifiers," IEEE Transactions on Power Electronics, vol. 17, pp. 609-615, 2002.

[55] C. X. Chen, D. Xu, E. S. W. Kong, and Y. F. Zhang, "Multichannel carbon-nanotube FETs and complementary logic gates with nanowelded contacts," IEEE Electron Device Letters, vol. 27, pp. 852-855, 2006.

[56] Z. M. Ye, P. K. Jain, and P. C. Sen, "Circulating current minimization in high-frequency ac power distribution architecture with multiple inverter modules operated in parallel " IEEE TRANSACTIONS ON INDUSTRIAL ELECTRONICS, vol. 54, pp. 2673-2687 2007.

[57] F. J. Chen, C. L. Chu, and C. L. Huang, "Parallel-connections of pulse width modualtd inverters using current sharing reactors," IEEE Transaction on Power Electronics vol. 10, pp. 673-679, 1995.

[58] J. M. Guerrero, L. G. de Vicuna, J. Matas, M. Castilla, and J. Miret, "A wireless controller to enhance dynamic performance of parallel inverters in distributed generation systems," IEEE Transactions on Power Electronics, vol. 19, pp. 1205-1213, 2004.

[59] C.-C. Hua, K.-A. Liao, and J.-R. Lin, "Parallel operation of inverters for distributed photovoltaic power supply system," IEEE Power Electronics Specialists Conference, pp. 1979 - 1983, 2002.

[60] K. B. De Brabandere, B.; Van den Keybus, J.; Woyte, A.; Driesen, J.; Belmans, R.; Leuven, K.U.;, "A voltage and frequency droop control method for parallel inverters," Power Electronics Specialists Conference, vol. 4, pp. 2501 - 2507, June 2004.

[61] A. Tuladhar, H. Jin, T. Unger, and K. Mauch, "Control of parallel inverters in distributed AC power systems with consideration of line impedance effect," IEEE Transactions on Industry Applications, vol. 36, pp. 131-138, 2000.

[62] Y. Pei, G. Jiang, X. Yang, and Z. Wang, "Auto-master-slave control technique of parallel inverters in distributed AC power systems and UPS," Power Electronics Specialists Conference, vol. 3, pp. 2050 – 2053, June 2004.

[63] J. F. Chen and C. L. Chu, "Combination Voltage-Controlled and Current-Controlled Pwm Inverters for Ups Parallel Operation," IEEE Transactions on Power Electronics, vol. 10, pp. 547-558, 1995.

[64] T. F. Wu, Y. K. Chen, and Y. H. Huang, "3C strategy for inverters in parallel operation achieving an equal current distribution," IEEE Transactions on Industrial Electronics, vol. 47, pp. 273-281, 2000.

[65] Y. K. Chen, Y. E. Wu, T. F. Wu, and C. P. Ku, "ACSS for paralleled multi-inverter systems with DSP-based robust controls," IEEE Transactions on Aerospace and Electronic Systems, vol. 39, pp. 1002-1015, 2003.

[66] K. S. Low, "A digital control technique for a single-phase PWM inverter," IEEE Transactions on Industrial Electronics, vol. 45, pp. 672-674, 1998.

[67] Linear Actuators & Motors
http://www.copleycontrols.com/motion/motors/ServoTube/.

[68] Renishaw RGH22: www.renishaw.com/.

[69] DS1104 R&D Controller Board:
www.dspaceinc.com/ww/en/inc/home/products/hw/singbord/ds1104.cfm

[70] J. A. Santisteban and R. M. Stephan, "Vector control methods for induction machines: an overview " IEEE Transactions on Education, vol. 44, 2001.

[71] M. F. Rahman, L. Zhong, E. Haque, and M. A. Rahman, "A direct torque-controlled interior permanent-magnet synchronous motor drive without a speed sensor," IEEE Transactions on Energy Conversion, vol. 18, pp. 17-22, 2003.

[72] H. A. Toliyat and G. B. Kliman, Handbook of Electric Motors CRC Press, 2004.

[73] L. Zhong, M. F. Rahman, W. Y. Hu, K. W. Lim, and M. A. Rahman, "A direct torque controller for permanent magnet synchronous motor drives," IEEE Transactions on Energy Conversion, vol. 14, pp. 637-642, 1999.

[74] J. N. Chiasson, Modeling and high-performance control of electric machines John Wiley, 2005.

[75] L. X. Tang, L. M. Zhong, M. F. Rahman, and Y. W. Hu, "A novel direct torque control for interior permanent-magnet synchronous machine drive with low ripple in torque and flux - A speed-sensorless approach," IEEE Transactions on Industry Applications, vol. 39, pp. 1748-1756, 2003.

[76] A. O'Dwyer, Handbook of Pi and Pid Controller Tuning Rules: Imperial College Press, 2003.

[77] K. J. Lee, H. P. Ko, C. Y. Kang, H. J. Kim, S. J. Yoon, and S. Nahm, "A study on the friction and thrust force of the shaft and mobile element in the impact typed piezoelectric ultrasonic linear motor," Journal of Electroceramics, vol. 17, pp. 499-503, 2006.

[78] J. S. Chen, K. C. Chen, Z. C. Lai, and Y. K. Huang, "Friction characterization and compensation of a linear-motor rolling-guide stage," International Journal of Machine Tools & Manufacture, vol. 43, pp. 905-915, 2003.

[79] G. D. Kim and C. N. Chu, "Indirect cutting force measurement considering frictional behaviour in a machining centre using feed motor current," International Journal of Advanced Manufacturing Technology, vol. 15, pp. 478-484, 1999.

[80] M. Feng and T. Kenjo, "Friction and wear of spindle motor hydrodynamic bearings for information storage systems during startup and shutdown," Microsystem Technologies-Micro-and Nanosystems-Information Storage and Processing Systems, vol. 13, pp. 987-997, 2007.

[81] S. Cong, "Two adaptive friction compensations for DC servomotors," Proceedings of The IEEE International Conference on Industrial Technology, pp. 113-117, 1996.

[82] L. R. Ray and J. S. Remine, "Machine friction estimation for modeling, diagnostics, and control," Proceedings of the American Control Conference, vol. 5, pp. 2737-2741, 1998.

[83] C. I. Huang and L. C. Fu, "Adaptive approach to motion controller of linear induction motor with friction compensation," IEEE-ASME Transactions on Mechatronics, vol. 12, pp. 480-490, 2007.

[84] D. Stajic, N. Peric, and J. Deur, "Friction compensation methods in position and speed control systems," Proceedings of the IEEE International Symposium on Industrial Electronics, vol. 3, pp. 1261-1266, 1999.

[85] R. Furlan, F. A. Cuzzol, and T. Parisini, "Friction compensation in the interstand looper of hot strip mills: A sliding-mode control approach," Control Engineering Practice, vol. 16, pp. 214-224, 2008.

[86] T. Tjahjowidodo, F. Al-Bender, H. Van Brussel, and W. Symens, "Friction characterization and compensation in electro-mechanical systems," Journal of Sound and Vibration, vol. 308, pp. 632-646, 2007.

[87] R. Stribeck, "Die wesentlichen Eigenschaften der Gleit- und Rollenlager," The key qualities of sliding and roller bearings. Zeitschrift des Vereines Seutscher Ingenieure, pp. 1342–1348, 1902.

[88] H. Olsson, "Describing function analysis of a system with friction," Proceedings of the 4th IEEE Conference on Control Applications, pp. 310-315, 1995.

[89] "Curve fitting toolbox," Mathworks.

[90] P. J. Hor, Z. Q. Zhu, D. Howe, and J. Rees-Jones, "Minimization of cogging force in a linear permanent magnet motor," IEEE Transaction on Magnetics, vol. 34, pp. 3544-3547, 1998.

[91] M. Platen and G. Henneberger, "Examination of leakage and end effects in a linear synchronous motor for vertical transportation by means of finite element computation," IEEE Transaction on Magnetics, vol. 37, pp. 3640-3643, 2001.

[92] J. S. Lai, L. Leslie, J. Ferrell, and T. Nergaard, "Characterization of HV-IGBT for high-power inverter applications," Industry Applications Conference, 2005, pp. 863-868, 2005.

[93] F. Blaabjerg, Z. Chen, and S. B. Kjaer, "Power electronics as efficient interface in dispersed power generation systems," IEEE Transactions on Power Electronics, vol. 19, pp. 1184-1194, 2004.

[94] O. A. Eno and D. S. Thompson, "Digital Control of Two Stage High Power Inverter," Power Electronics and Motion Control Conference, pp. 863-868, 2006.

[95] W. C. Lee, S. H. Lee, K. H. Kim, and D. S. Hyun, "Novel control strategy for parallel operation of UPS system," Power Electronics and Motion Control Conference, IPEMC 2004, vol. 2, pp. 983 - 988, 2004.

[96] Z. M. Ye, P. K. Jain, and P. C. Sen, "Circulating current minimization in high-frequency ac power distribution architecture with multiple inverter modules operated in parallel," IEEE Transactions on Industrial Electronics, vol. 54, pp. 2673-2687, 2007.

[97] E. F. Camacho and C. Bordons, Model Predictive Control: Springer, 2004.

[98] J. Richalet, A. Rault, J. L. Testud, and J. Papon, "Model predictive heuristic control: applications to industrial process " Automatica, vol. 14, pp. 413-428, 1978.

[99] C. R. Cutler and B. L. Ramaker, "Dynamic matrix control- a computer control algorithm," Proceedings of American Control Conference, 1980.

[100] D. W. Clarke, C. Mahtadi, and P. S. Tuffs, "Generalized predictive cotnrol, Parts1 and 2," Automatica, vol. 23, pp. 137-160, 1987.

[101] C. E. Garcia and M. Morari, "A unified review and some new results," I & EC Process Design and Development vol. 21, pp. 308-323, 1982.

[102] D. Q. Mayne and H. Michalska, "Receding horizon control of nonlinear systems," IEEE Transactions on Automatic Control, vol. 35, pp. 814-824, 1990.

[103] J. B. Rawlings, "Tutorial overview of model predictive control.," IEEE Control Systems Magazine, vol. 20, pp. 38-52, 2000.

[104] M. Morari and J. H. Lee, "Model predictive control: past, present and future," Computers & Chemical Engineering, vol. 23, pp. 667-682, 1999.

[105] D. Q. Mayne, J. B. Rawlings, C. V. Rao, and P. O. M. Scokaert, "Constrained Model Predictive control: stability and optimality " Automatica, vol. 36, pp. 789-814, 2000.

[106] J. A. Rossiter, Model Base Predictive Control: A Practical Approach: CRC Press, 2003.

[107] W. H. Kwon and S. Han, Receding Horizon Control: Model Predictive Control for State Models: Springer, 2005.

[108] J. M. Maciejowski, Predictive control with constraints Prentice-Hall, 2002.

[109] K. R. Muske and J. B. Rawlings, "Receding horizon recursive state estimation," Proceedings of American Control Conference, pp. 900-904, 1993.

[110] R. C. Dorf and R. H. Bishop, Modern Control Systems: Prentice Hall, 2001.

[111] K. V. Ling and K. W. Lim, "Receding horizon recursive state estimation," IEEE Transactions on Automatic Control, vol. 44, pp. 1750-1753, 1999.

[112] C. V. Rao, J. B. Rawlings, and J. H. Lee, "Stability of constrained linear moving horizon estimation," Proceedings of American Control Conference, vol. 5, pp. 3387-3391, 1999.

[113] D. W. Clarke and C. Mohtadi, "Properties of generalized predictive control," Automatica, vol. 26, pp. 859-875, 1989.

[114] H. Demircloglu and E. Karasu, "Generalized predictive control: A practical application and comparision of discrete and continuous time versions," IEEE Control Systems Magazine, vol. 20, pp. 161-175, 2000.

[115] R. K. R. Krishnan, Electric Motor Drives: Modeling, Analysis, and Control: Prentice Hall, 2001.

[116] Z. P. Jiang and H. Nijmejer, "Tracking Control of Mobile Robots: A Case Study in Backstepping " Automatica, vol. 33, 1997.

[117] P. Ge and M. Jouaneh, "Tracking control of a piezoceramic actuator " IEEE Transactions on Control Systems Technology, , 1996.

[118] S. Saito, H. Miyazaki, and T. Sato, "Pick and place operation of a micro-object with high reliabilityand precision based on micro-physics," 1999 IEEE International Conference on Robotics and Automation vol. 4, 1999.

[119] H. S. Lee and M. Tomizuka, "Robust motion controller design for high-accuracy positioning systems " IEEE Transactions on Industrial Electronics, vol. 43, pp. 48-55.

[120] G. M. Bone, "A Novel Iterative Learning Control Formulation of Generalized Predictive Control," Automatica, vol. 31, pp. 1483-1487, 1995.

[121] J. Gangloff, R. Ginhoux, M. de Mathelin, L. Soler, and J. Marescaux, "Model predictive control for compensation of cyclic organ motions in teleoperated laparoscopic surgery," IEEE Transactions on Control Systems Technology, vol. 14, pp. 235-246, 2006.

[122] K. S. Lee and J. H. Lee, "Model predictive control for nonlinear batch processes with asymptotically perfect tracking," Computers & Chemical Engineering, vol. 21, pp. S873-S879, 1997.

[123] K. S. Lee, I. S. Chin, H. J. Lee, and J. H. Lee, "Model predictive control technique combined with iterative learning for batch processes," Aiche Journal, vol. 45, pp. 2175-2187, 1999.

[124] S. Natarajan and J. H. Lee, "Repetitive model predictive control applied to a simulated moving bed chromatography system," Computers & Chemical Engineering, vol. 24, pp. 1127-1133, 2000.

[125] J. H. Lee, S. Natarajan, and K. S. Lee, "A model-based predictive control approach to repetitive control of continuous processes with periodic operations," Journal of Process Control, vol. 11, pp. 195-207, 2001.

[126] M. Gupta and J. H. Lee, "Period-robust repetitive model predictive control," Journal of Process Control, vol. 16, pp. 545-555, 2006.

[127] K. L. Zhou, K. S. Low, D. Wang, F. L. Luo, B. Zhang, and Y. Wang, "Zero-phase odd-harmonic repetitive controller for a single-phase PWM inverter," IEEE Trans. on Power Electronics, vol. 21, pp. 193-201, 2006.

[128] H. Elci, R. W. Longman, M. Q. Phan, J. N. Juang, and R. Ugoletti, "Simple learning control made practical by zero-phase filtering: Applications to robotics," IEEE Transactions on Circuits and Systems I-Fundamental Theory and Applications, vol. 49, pp. 753-767, 2002.

[129] A. Ambardar, Analog and Digital Signal Processing. Boston: PWS Publishing Company, 1995.

[130] A. V. Oppenheim, R. W. Schafer, and J. R. Buck, Discrete-time Signal Processing: Prentice Hall, 1999.

[131] M. Tomizuka, T. C. Tsao, and K. K. Chew, "Discrete-time domain analysis and synthesis of repetitive controllers," Proceedings of the American Control Conference, vol. 88, pp. 860-866, 1988.

[132] T. Inoue, "Practical repetitive control system design," Proceedings of the IEEE Conference on Decision and Control, vol. 3, pp. 1673-1678, 1990.

[133] F. R. Shaw and K. Srinivasan, "Discrete-time repetitive control system design using regeneration spectrum," Proceedings of the 1991 ACC, vol. 3, pp. 2628-2633, 1991.

[134] K. SRINIVASAN and F. R. SHAW, "Analysis and Design of Repetitive Control- Systems Using the Regeneration Spectrum," Journal of Dynamic Systems Measurement and Control-Transactions of the ASME, vol. 113, pp. 216-222, 1991.

[135] H. Elci, R. W. Longman, M. Phan, J. N. Juang, and R. Ugoletti, "Automated learning control through Model Updating for Precision motion control," Adaptive Structures and Composite Materials: Analysis and Applications, vol. 45, pp. 299-314, 1994.

[136] R. W. Longman and T. Kwon, "Obtaining good transients in iterative learning control using step response data," Proceedings of the 2002 AIAA/AAS Astrodynamics Specialist Conference and Exhibit, pp. 4981-4990, 2002.

[137] W. M. C Kempf, M Tomizuka, R Horowitz, "A comparison of four discrete-time repetitive control algorithms," American Control Conference, vol. 13, pp. 48-54, 1993.

[138] D. Wang, "On D-type and P-type ILC designs and anticipatory approach," International Journal of Control, vol. 73, pp. 890-901, 2000.

[139] G. Hillerström and K. Walgama, "Repetitive control theory and applications-A survey," Proceedings of the 13th triennial world congress of IFAC, vol. D, pp. 1-6, 1996.

[140] J. C. Pratt and E. Eisner, "The effect of a tangential force on the contact of metallic bodies," Proceedings of the Royal Society, vol. 238, pp. 529-550, 1957.

[141] E. Rabinowicz, Friction and wear of materials.: Wiley, 1995.

[142] K. S. Low, K. Y. Chiun, and K. V. Ling, "Evaluating generalized predictive control for a brushless DC drive," IEEE Transactions on Power Electronics, vol. 13, pp. 1191-1198, 1998.

[143] K. D. Brabandere, B. Bolsens, J. V. Keybus, A. W. J. Driesen, and R. Belmans, "A Voltage and Frequency Droop Control Method for Parallel Inverters " IEEE Trans. on Power Electronics, vol. 22, pp. 1107-1112, 2007.